UNIVERSITY OF CALIFORNIA, SAN DIEGO

Histone demethylase LSD1: Connecting developmental signals, chromatin, and cell response

A dissertation submitted in partial satisfaction of the requirements for the degree of Doctor of Philosophy

in

Biomedical Sciences

by

Nicholas Kyle Vinckier

Committee in charge:

Professor Maike Sander, Chair
Professor Sylvia Evans
Professor Lawrence Goldstein
Professor Karl Willert
Professor Eugene Yeo

2017

The Dissertation of Nicholas Kyle Vinckier is approved, and it is acceptable in quality and form for publication on microfilm and electronically:

_____

_____

_____

_____

_____

Chair

University of California, San Diego

2017

DEDICATION

I would first like to dedicate this dissertation to my incredible wife, Gwendolyn, who has been impossibly patient during my studies and in all aspects of our lives together. I truly would not have been able to do this without your unwavering support. Thank you for believing in me, especially when my confidence faltered.

You are my world.

To Mom and Dad, thank you for raising me to be a scientist and for always letting me ask questions, even when it annoyed you, you hid it well.
To my sister, Erin, the first Dr. Vinckier, thank you for putting up with me growing up and for the awesome nephew and niece. I hope science helps make the world better for Joey and Sami.

To all my friends, thank you for keeping me grounded and helping me balance work and play; and to my crazy dog, Moose, whose smile never failed to brighten my day.

And to Dan, whose infectious love of science instilled within me a renewed passion for research.
We miss you, buddy.

TABLE OF CONTENTS

LIST OF ABBREVIATIONS

AA	Activin A
Cre	Cre-recombinase
CreER^{TM}	Cre-recombinase-Estrogen receptor fusion protein
DE	Definitive endoderm
DNA	Deoxyribonucleic acid
LSD1iearly	Early LSD1 inhibition
PP1	Early pancreatic progenitors
EN	Endocrine cell stage
EGF	Epidermal growth factor
FSC-A	Forward scatter area
GFP	Green fluorescent protein
HOXA1	Homeobox A1
HOXB1	Homeobox B1
HOXC4	Homeobox C4
hESC	Human embryonic stem cell
hPSC	Human pluripotent stem cell
ITS	Insulin-transferrin-selenium
KGF	Keratinocyte growth factor
LSD1ilate	Late LSD1 inhibition
PP2	Late pancreatic progenitors
LSD1	Lysine-specific demethylase 1
NGN3	Neurogenin-3
NKX6.1	NKX homeobox 1
ncRNA	Non-coding RNA
PDX1	Pancreatic and duodenal homeobox 1
PGK	Phosphoglycerate kinase

GT	Primitive gut tube
RA	Retinoic acid
RAR	Retinoic acid receptor
RARB	Retinoic acid receptor β
RXR	Retinoid X receptor
RNA	Ribonucleic acid
shRNA	Short-hairpin RNA
SOX9	SRY-Box 9
TGFBi	TGFβ R1 kinase inhibitor
TTS	Transcription termination site
UTR	Untranslated region

LIST OF FIGURES

LIST OF TABLES

LIST OF SUPPLEMENTAL FILES

vinckier_supplemental_tables.xlsx

Table S1.

Table S2.

Table S3.

Table S4.

Table S5.

Table S6.

ACKNOWLEDGEMENTS

I would first like to thank my doctoral advisor, Dr. Maike Sander, for her support and guidance during my dissertation studies. I am also extremely grateful for the encouragement I received from the rest of the Sander Lab. In particular, I want to thank Dr. Allen Wang for his superb mentorship, Fenfen Liu for her impressive lab management skills, we would all be lost without you, and Tommy Harper, M.S., for the scientific discussions during early morning surf sessions. I would also like to thank my advancement and dissertation committee: Dr. Sylvia Evans, Dr. Lawrence Goldstein, Dr. Karl Willert, Dr. Eugene Yeo. Thank you all for your time, suggestions and advice; I greatly appreciate all your help. I also thank the professors and administration of Biomedical Sciences Graduate Program.

Chapter 1 includes material that is currently being prepared for submission for publication, Vinckier, Nicholas; Patel, Nisha; Wang, Allen; Wang, Jinzhao; Carrano, Andrea; Benner, Christopher and Sander, Maike. “LSD1-mediated Decommissioning of Developmental Enhancers is Required for Proper Pancreatic Endocrine Formation”. The dissertation author was the primary investigator and author of this material. This work was supported by funds granted to MS from the National Institutes of Health, Pediatrics Diabetes Research Consortium and the California Institute for Regenerative Medicine.

Chapter 2 includes material of which the dissertation author was the primary investigator and author. This work was supported by funds granted to MS from the National Institutes of Health, Pediatrics Diabetes Research Consortium and the California Institute for Regenerative Medicine. In addition to these sources, NKV was also supported, in part, by the UCSD institutional Cancer Cell Biology training grant, from the National Institutes of Health.

Appendix, in full, is a reprint of material as it appears in Vinckier, Nicholas; Jinzhao, Wang and Sander, Maike. "Pancreatic Differentiation from Human Pluripotent Stem Cells." *Working with Stem Cells*. Ed. Henning Ulrich, Ed. Priscilla Davidson Negraes. Switzerland: Springer International Publishing, 2016. 257-275. The dissertation author was the primary investigator and author of this material.

VITA

EDUCATION

2010 – 2017. *University of California at San Diego*
- Doctor of Philosophy, Biomedical Sciences Graduate Program

2003 – 2008. *University of California at Santa Barbara*
- Bachelor of Science, Biochemistry with Honors
- Spanish Minor

WORK EXPERIENCE

September 2010 – Present. *Graduate Student Researcher, Dr. Maike Sander, UC San Diego*
- Dissecting the role of the chromatin modifying enzyme LSD1 during human pancreatic endocrine development using in vitro differentiation of human pluripotent stem cells to pancreatic lineages.
- Investigation of the spatial and temporal role of neurogenin3 in proper pancreatic endocrine development.
- Utilization of in vitro pancreatic differentiation protocols to manipulate gene expression and timing during pancreatic differentiation of hPSCs.

August 2009 – September 2010. *Research Assistant, Dr. Stanley M. Parsons, UC Santa Barbara*
- Characterization of γ-hydroxybutyrate dehydrogenase (GHB-DH) for development of simple test for presence of γ-hydroxybutyrate (GHB).
- Isolation of enzyme from over-expressing *E. coli* cell cultures using affinity chromatography.
- Perform initial velocity and enzyme kinetics studies via UV/Vis Spectroscopy and computer analysis of data including nonlinear regression.
- Perform metal ion analysis of enzyme isolations via ICP spectroscopy.
- Perform ^{3}H based radiometric assays measuring acetylcholine uptake in vesicular acetylcholine transporter.

June 2008 – July 2009. *Laboratory Assistant, UC Santa Barbara*
- Maintained chemical and laboratory supplies and general cleanliness of the laboratory.
- Assisted graduate students in research by maintaining stocks of necessary chemicals, solutions, and various growth media.
- Performed monthly radiation tests and cleanings to ensure laboratory complied with University Radiation Safety requirements.

June 2009 – August 2009. *Summer Research Mentor, UC Santa Barbara*
- Taught high school students research techniques, data collection and analysis procedures.
- Assisted students in the writing of research papers, and presentation of findings to an audience.
- Engaged students in learning about chemistry and biochemistry.

PUBLICATIONS

- Vinckier, N. et al. "Pancreatic Differentiation from Human Pluripotent Stem Cells." *Working with Stem Cells*. Ed. Henning Ulrich, Ed. Priscilla Davidson Negraes. Switzerland: Springer International Publishing, 2016. 257-275.
- Vinckier N. K., Chworos A., Parsons S. M. (2011). Improved isolation of proteins tagged with glutathione *S*-transferase. Protein Expr. Purif. 75 161–164 10.1016/j.pep.2010.09.006.

LABORATORY SKILLS

- Chromatin immunoprecipitation of DNA-associated proteins for deep sequencing (ChIP-seq).
- Computational analysis of next generation sequencing data generated from ChIP-seq and RNA-seq.
- Human embryonic and induced pluripotent stem cell culture and differentiation, human cell genome editing using TALEN and CRISPR/Cas systems, DNA plasmid and siRNA transfection and electroporation
- Generation of lentiviral vectors for gene misexpression and knockdown in human cells.
- Isolation and analysis of specific cell types using FACS, immunofluorescent cytochemistry, qRT-PCR.
- Bacterial cell culture, chromatographic enzyme isolation, Bradford assay, SDS-PAGE, UV/Vis, IR, ^{1}H-NMR, and Inductively Coupled Plasma (ICP) spectroscopy.
- DNA and Protein isolation and characterization using 1D and 2D gel electrophoresis, Western blot, DNA mutation and amplification using PCR and restriction digests.

COMPUTER EXPERIENCE

- Skilled in operating Microsoft Windows (Windows 98 through Windows 10) and UNIX based operating systems including Mac OS X, Ubuntu Linux and Cygwin for Windows.
- Proficient in bash shell, R/R-studio, Excel, Word, PowerPoint and OneNote, Adobe Photoshop and Illustrator CS5.1.
- Skilled in various bioinformatics software tools and modules including: HOMER, Bedtools, MACS, Bowtie2, STAR, diffReps and DESeq.
- Basic understanding of Python programming language.

AWARDS & HONORS

- Awarded graduate student travel grant for the 2013 Beta Cell Biology Consortium Investigator Retreat.
- Phi Lambda Upsilon National Honorary Chemical Society. *UC Santa Barbara Department of Chemistry & Biochemistry* (2008-2009).
- Phi Beta Kappa

REFERENCES *(Contact information available upon request)*

- Sander, Maike M.D. – Thesis Advisor. Professor, Depts. of Pediatrics and Cellular & Molecular Medicine. *UC San Diego*
- Wang, Allen Ph.D. – Graduate research mentor. Postdoctoral researcher, Dept of Pediatrics. *UC San Diego*
- Lawrence S.B. Goldstein Ph.D. – Professor, Dept. of Cellular & Molecular Medicine. *UC San Diego*
- Parsons, Stanley Ph.D. – Professor, Dept. of Chemistry and Biochemistry. *UC Santa Barbara*

ABSTRACT OF THE DISSERTATION

Histone demethylase LSD1: Connecting developmental signals, chromatin, and cell response

by

Nicholas Kyle Vinckier

Doctor of Philosophy in Biomedical Sciences

University of California, San Diego, 2017

Professor Maike Sander, Chair

Over the course of development, regulation of gene transcription is the main mechanism by which pluripotent stem cells become restricted to the various distinct cell types found in the mature organism. Among the many different processes that regulate gene transcription, is the control of physical access to DNA and the genes for which it codes. DNA wound around histone proteins forms chromatin and the enzymes that modify the landscape of that chromatin control which regulatory elements, like promoters and enhancers, are active. This process confers different developmental competencies in cells, enabling them to respond uniquely to similar environmental and developmental signals, regulating gene transcription in turn. The study of these processes during in vitro differentiation of stem cells has enabled us and others to draw links between

chromatin remodelers, transcription factors and cellular response to inductive cues during human development.

In Chapter 1, I explore the role of the lysine-specific demethylase (LSD1) during human pancreatic development using an in vitro system to differentiate human embryonic stem cells (hESCs) to the pancreatic endocrine lineage. Removal of LSD1 activity during a specific early time window of pancreatic development prevents endocrine formation. Investigation into enhancer regions occupied by LSD1 during this critical time window provided results that support a model in which LSD1-mediated decommissioning renders these enhancers insensitive to activation by external retinoic acid signaling.

In Chapter 2, I report my previous work dissecting the role of the transcription factor neurogenin-3 (NGN3) during human pancreatic development. Using the aforementioned hESC-based in vitro differentiation system, gain and loss-of-function studies showed that NGN3 is both necessary and sufficient to induce endocrine formation in human cells.

A final supplemental chapter provides an example of a hESC-based pancreatic differentiation protocol similar to the one employed for the studies outlined in Chapters 1 and 2 and discusses the importance of such model systems in dissecting the myriad mechanisms of human disease and development.

INTRODUCTION

The human genome is vast, both in the seemingly infinite versions of various traits for which it codes, and its cumulative physical length. Each copy of the human genome contains over three billion base pairs coding for over 19,000 genes (Morton 1991, Kent, Sugnet et al. 2002, Annunziato 2008). The sequences coding for these genes are interspersed throughout the genome, separated by non-coding intra- and intergenic regions. Many of the non-coding regions contain regulatory sequences that recruit various proteins and function to promote, inhibit, insulate and enhance transcription of protein coding genes (Wolffe and Pruss 1996). The highly complex string of DNA bases contained within a single cell, if arranged end-to-end, would cover a distance of 2 meters (Annunziato 2008). To accommodate this great length within the nucleus of a cell, chromosomal DNA is coiled around histone protein complexes forming units called nucleosomes. These repeating nucleosome units form a “beads on a string” structure that tightly condenses the DNA inside the cell nucleus. Nucleosome complexes of histones and DNA and other associated proteins are commonly referred to as chromatin (Wolffe and Pruss 1996, Wolffe 2000, Annunziato 2008). In addition to tightly packaging the genome into the cell nucleus, this chromatin plays an important role in regulating gene expression by controlling the physical accessibility of genes and their regulatory sequences to transcriptional machinery (Lee, Hayes et al. 1993, Garcia-Ramirez, Rocchini et al. 1995, Wolffe and Pruss 1996, Koch, Andrews et al. 2007, Rossetto, Avvakumov et al. 2012, Thurman, Rynes et al. 2012). Rearrangement of histones along a DNA strand can regulate transcription of genes by exposing or sequestering these regulatory regions and actual gene coding sequences as well (Rossetto, Avvakumov et al. 2012, Shen, Yue et al. 2012). These rearrangements are facilitated by covalent post-translation modifications on the tails of histones (Garcia-Ramirez, Rocchini et al. 1995, Wolffe and Pruss 1996, Ernst, Kheradpour et al. 2011, Tan, Luo et al. 2011). A classic example of this process is the acetylation of lysine 27 on histone H3 (H3K27ac). The H3K27ac modification is associated with active regulatory elements such as promotors and gene-distal regulatory elements called enhancers (Wolffe and Pruss 1996, Creyghton, Cheng et al. 2010, Ernst, Kheradpour et al. 2011). At enhancers, the H3K27ac

modification aids in driving transcription of target genes by making DNA accessible to TFs and other DNA-binding protein complexes involved in gene transcription (Wolffe and Pruss 1996, Grunstein 1997, Koch, Andrews et al. 2007, Shlyueva, Stampfel et al. 2014). Increasingly, research demonstrates the importance of regulatory regions like enhancers and their chromatin state and the vital roles they play in proper cell differentiation and function (Rada-Iglesias, Bajpai et al. 2011, Whyte, Bilodeau et al. 2012, Xie, Everett et al. 2013, Wang, Yue et al. 2015).

CHAPTER 1 - THE ROLE OF LSD1 IN CONNECTING TRANSIENT DEVELOPMENTAL SIGNALS AND CELL RESPONSE VIA CHROMATIN REMODELING

ABSTRACT

The question of how pluripotent stem cells with identical genomes can develop into the various different cell types within a mature organism remains largely unanswered. Many methods of gene regulation exist, which ensure proper differentiation of stem cells to their respective cell fates. The role of chromatin and the enzymes that remodel it have been increasingly implicated in controlling how cells respond to developmental signals and the downstream effect on gene transcription during development. The lysine-specific demethylase (LSD1) is one such chromatin remodeling enzyme that has been shown to play a vital role in stem cell maintenance and differentiation. Here, we investigate the role of LSD1 during human pancreatic development using an in vitro system to differentiate human embryonic stem cells (hESCs) to the pancreatic endocrine lineage. We find that removal of LSD1 activity during a specific early time window of pancreatic development prevents endocrine formation in both humans and mice. Exploration into the genomic regions where LSD1 acts during this time window provided evidence for a mechanism wherein LSD1 decommissions retinoic acid (RA)-induced enhancers, rendering them insensitive to further activation by RA signals, ensuring proper timing of down-regulation of target genes. Here, we show the utility of in vitro differentiation systems in studying human development and provide data supporting a model in which the chromatin remodeler LSD1 reshapes the chromatin landscape altering the developmental competence of differentiating cells. These results provide an example of the crucial link between chromatin state and cellular response to developmental signals.

INTRODUCTION

For multicellular organisms, such as humans, to develop properly, stem cells must differentiate into multiple specialized cells. Stem cells by definition are capable of becoming any one of the many cell types of the human body (Jaenisch and Young 2008, Hanna, Saha et al. 2010,

Rada-Iglesias and Wysocka 2011). Each of the unique and highly specialized cell types within an individual contain identical genomic DNA sequences within their respective nuclei (Ernst, Kheradpour et al. 2011). This raises the question of how stem cells, indistinguishable from one another, can go down such divergent paths to become distinct cell types with completely different functional roles. Lineage-determining transcription factors (TFs) play a major role in controlling the fates of these multipotent cells by binding to regulatory elements such as gene promoters and distal regulatory elements called enhancers to promote target gene transcription (Jaenisch and Young 2008, Heinz, Benner et al. 2010, Ernst, Kheradpour et al. 2011, Shen, Yue et al. 2012). However, the presence of lineage-specific TFs alone cannot account for the various distinct cell types that emerge from a common multipotent progenitor pool. To give rise to the numerous types of terminally differentiated cells, stem cells, and the lineage intermediates stemming from them, must respond to a range of inductive cues throughout embryonic development (Schuldiner, Yanuka et al. 2000, Linker and Stern 2004, Heinz, Benner et al. 2010). The timing, duration and localization of TF activity and other inductive signals is crucial to proper differentiation, but is not enough to explain how and why cells can respond differently to those signals. Increasingly, research into this question implicates the chromatin landscape as a major gatekeeper capable of controlling cellular response to inductive cues (Shogren-Knaak, Ishii et al. 2006, Heintzman, Hon et al. 2009, Heinz and Glass 2012, Pham, Minderjahn et al. 2013, Xie, Everett et al. 2013, Heinz, Romanoski et al. 2015, Wang, Yue et al. 2015).

In addition to the aforementioned H3K27ac modification and its role in aiding transcription, another example of a histone modification that can modulate target gene expression is the mono-, di- and tri-methylation of lysine 4 on histone H3 (H3K4me1/me2/me3). Along with H3K27ac, the H3K4me3 modification is associated with active promoters (Bernstein, Mikkelsen et al. 2006, Kim and Shiekhattar 2015) whereas the H3K4me1 and H3K4me2 marks are more frequently associated with enhancers (Creyghton, Cheng et al. 2010, Heinz, Benner et al. 2010, Wang, Yue et al. 2015). Concurrent H3K27ac and H3K4me1/me2 marks are indicative of active enhancers (Heinz and Glass 2012, Whyte, Bilodeau et al. 2012, Wang, Yue et al. 2015), while enhancers presenting the

H3K4me1/me2 modifications alone, are said to be in a “poised” state, ready to be activated upon H3K27ac addition (Heinz, Benner et al. 2010, Whyte, Bilodeau et al. 2012, Wang, Yue et al. 2015). Histone modifications such as these are mediated by chromatin modifying enzymes that can add or remove acetyl groups, methyl groups, phosphates, and ubiquitin on histones (Ernst, Kheradpour et al. 2011, Tan, Luo et al. 2011, Thurman, Rynes et al. 2012). It is likely that these chromatin remodelers are critical to the cell’s acquisition of developmental competence, the ability of multipotent cells respond appropriately to inductive signals from their environment. One chromatin remodeling enzyme that has been shown to play an important role in embryonic development is the histone demethylase LSD1 (Wang, Hevi et al. 2009, Foster, Dovey et al. 2010, Nair, Ge et al. 2012, Whyte, Bilodeau et al. 2012, Wang, Yue et al. 2015). LSD1 is a lysine-specific demethylase capable of removing mono- and di-methylation modifications from histone H3 (Shi, Lan et al. 2004, Wang, Lu et al. 2011, Laurent, Ruitu et al. 2015). Knockout of *Lsd1* in mice results in embryonic lethality (Wang, Scully et al. 2007) and its activity has been shown to be vital for proper maintenance and differentiation of numerous pluripotent cells types from both mice and humans, including embryonic, neural, and hematopoietic stem cells (Forneris, Binda et al. 2006, Su, Ying et al. 2009, Sun, Alzayady et al. 2010, Zibetti, Adamo et al. 2010, Adamo, Sese et al. 2011, Nair, Ge et al. 2012, Whyte, Bilodeau et al. 2012, Kerenyi, Shao et al. 2013, Laurent, Ruitu et al. 2015).

Research into possible mechanisms through which LSD1 controls cell differentiation has identified several roles, including removal of repressive H3K9 mono- and di-methylation marks (Metzger, Wissmann et al. 2005, Sun, Alzayady et al. 2010) as well as removal of H3K4 mono- and di-methylation at certain enhancers, a process referred to as “decommissioning” (Whyte, Bilodeau et al. 2012, Kerenyi, Shao et al. 2013). Whyte and colleagues posited that LSD1-mediated decommissioning of certain enhancers, is required to fully suppress genes associated with those enhancers. Indeed, when LSD1 was inhibited in stem cells a retention of H3K4 mono- and di-methylation at LSD1-bound enhancers was observed, which coincided with a failure to fully downregulate expression of genes associated with those enhancers (Whyte, Bilodeau et al. 2012). The subsequent disruption of stem cell maintenance and differentiation was attributed to the failure

to decommission these enhancers as a result of LSD1 inhibition. These studies have demonstrated a clear link between LSD1-mediated modifications of the chromatin state within a variety of cell types, and the ability of those cells to properly function and differentiate. In addition, because LSD1 activity has been implicated in the proper differentiation of multiple cell lineages, including neurons, muscle, blood and adipocytes (Peng, Yerle et al. 2009, Li, Sun et al. 2012, Nair, Ge et al. 2012, Xiong, Wang et al. 2016) it is likely that LSD1 plays critical roles in other developmental contexts, such as pancreas development. It has been shown that lineage-specific chromatin states confer developmental competence in lineage intermediates during pancreatic endocrine differentiation (Wang, Yue et al. 2015). This process is critical for proper differentiation and is precisely controlled by myriad chromatin modifying enzymes. Previous research has suggested that, in addition to the activation and deactivation (addition and removal of H3K27ac) of enhancers, the poising and decommissioning (addition and removal of H3K4me1 and H3K4me2) of enhancers plays a vital role in ensuring lineage intermediates acquire the developmental competence to become properly differentiated cells (Mercer, Lin et al. 2011, Rada-Iglesias and Wysocka 2011, Kaikkonen, Spann et al. 2013, Heinz, Romanoski et al. 2015, Wang, Yue et al. 2015). Because LSD1 is known to decommission enhancers (Whyte, Bilodeau et al. 2012), and is important for development of a wide variety of cell types and tissues, it seemed likely that LSD1 could be one of the chromatin modifiers responsible for proper differentiation to the pancreatic endocrine fate. Here, we investigate the chromatin remodeling enzyme LSD1 and its role in reshaping the chromatin landscape during human pancreatic endocrine development.

In order to investigate the complexities of human development and disease, researchers have turned to the rapidly advancing field of in vitro differentiation of human pluripotent stem cells (hPSCs) (Avior, Sagi et al. 2016). With the ability to generate hPSCs from adult somatic cells, it is becoming commonplace to differentiate hPSCs derived from individuals with a particular disease and assess how those cells behave differently from hPSCs derived from unaffected individuals (Takahashi and Yamanaka 2006, Yamanaka 2007, Yamanaka and Blau 2010, Papp and Plath 2013). With the use of increasingly sophisticated gene editing technologies, researchers can now

correct mutations in diseased hPSCs and observe the reversal of the disease state (Xie, Ye et al. 2014, Hockemeyer and Jaenisch 2016, Zhang, Schmid et al. 2017). Moreover, mutations relevant to a disease can be introduced into healthy hESCs and those modified cells can then be differentiated to determine how a specific mutation contributes to a particular disease. Individuals afflicted by the disease diabetes mellitus stand to benefit greatly from such hPSC-based differentiation protocols. Diabetes is characterized by the inability to regulate blood glucose homeostasis and is caused by the loss or dysfunction of the insulin-secreting beta cell within the islets of Langerhans in the pancreas. Cadaveric islet transplantations have been shown to reverse diabetes (Shapiro, Ricordi et al. 2006), which, together with the fact that diabetes typically results from the dysfunction of a single cell type, makes the disease a prime candidate for cell-replacement therapies. clinical trials for which are currently ongoing (Motte, Szepessy et al. 2014, Schulz 2015). Although animal models of diabetes have proven invaluable resources for increasing our understanding of pancreas development and diabetes pathogenesis in vivo, hPSC-based in vitro pancreatic differentiation systems provide the unique ability to dissect the earliest stages of development and can provide virtually limitless material for analysis (Keller 2005). Moreover, the ability to generate functional beta cells from hESCs entirely in vitro (Russ, Sintov et al. 2011, Pagliuca, Millman et al. 2014, Rezania, Bruin et al. 2014), provides an ideal model system to study the proper differentiation and function of the human beta cell. In order to reap the many benefits promised by in vitro modeling of diseases like diabetes, it is necessary to first understand how healthy cells differentiate and function under normal conditions. The advent of robust hPSC-based in vitro differentiation systems has provided researchers with the tools necessary to study any number of human diseases and developmental processes entirely in vitro. These systems allow for extremely high-resolution spatiotemporal assays of the cell state, enabling the study of complex and intricate mechanisms of cellular differentiation on a scale not possible in any other model system. By employing one such system, capable of efficiently generating pancreatic endocrine cells from human embryonic stem cells (hESCs) (Schulz, Young et al. 2012, Xie, Everett et al. 2013, Wang, Yue et al. 2015), we investigated the role of LSD1 in the context of human pancreatic

endocrine development, and have begun to dissect the mechanisms by which LSD1 modulates developmental competence of cells through remodeling of the chromatin landscape.

RESULTS

Human Endocrine Cell Development Requires LSD1 Activity during a Narrow Time Window early in Pancreas Development

To investigate if LSD1 plays a role during human pancreatic endocrine development, we first determined whether LSD1 is expressed during normal human pancreas development. We observed high levels of LSD1 expression in human fetal donor (55 days post-conception; dpc) pancreatic progenitor cells identified by co-expression of SOX9 and PDX1 (Figure 1A). Additionally, co-expression of LSD1 and the endocrine cell marker chromogranin A (CHGA) was observed in both human fetal donor (94 dpc) endocrine progenitors and human adult donor (22 years old) islets of Langerhans (Figure 1A). LSD1 expression was also observed in multiple endocrine subtypes within human adult donor islets, including insulin (INS) expressing beta cells, glucagon (GCG) expressing alpha cells, and somatostatin (SST) expressing delta cells (Figure S1A). Using an in vitro system to differentiate human embryonic stem cells (hESCs) in a stepwise manner toward the pancreatic endocrine cell fate (Schulz, Young et al. 2012, Xie, Everett et al. 2013, Wang, Yue et al. 2015), we also observed robust LSD1 expression throughout all stages of pancreatic differentiation (Figure S1B-S1C).

Given our observation of LSD1 expression during pancreas development both in vivo and in vitro, and the known requirement for LSD1 in proper stem cell differentiation in other contexts (Sun, Alzayady et al. 2010, Zibetti, Adamo et al. 2010, Adamo, Sese et al. 2011, Wang, Lu et al. 2011, Li, Sun et al. 2012, Nair, Ge et al. 2012, Whyte, Bilodeau et al. 2012, Laurent, Ruitu et al. 2015, Duteil, Tosic et al. 2016), we hypothesized that LSD1 could play a critical role in human pancreatic endocrine formation. To assess this, we used the irreversible LSD1 inhibitor tranylcypromine (TCP) to block LSD1 activity during directed differentiation of hESCs to pancreatic endocrine cells (Figure 1B). Initial attempts to knockdown LSD1 at the ES stage prevented progression to the later stages and often resulted in cell death, precluding any study of the role(s) of LSD1 at later stages of endocrine differentiation (data not shown). Previous reports have similarly shown that LSD1 inhibition in stem cells prevents proper exit from the stem cell state (Sun,

Alzayady et al. 2010, Adamo, Sese et al. 2011, Nair, Ge et al. 2012, Whyte, Bilodeau et al. 2012). We were therefore prompted to disrupt LSD1 activity during the later stages of differentiation, particularly during the formation of pancreatic progenitor and endocrine cells. We first inhibited LSD1 during the transition from early (PP1) to late (PP2) pancreatic progenitor stages (LSD1i^{early}; Figure 1B) to determine whether LSD1 is required for proper formation of PP2. Expression of key progenitor marker proteins NKX6.1 and PDX1 were largely unaffected in LSD1i^{early} PP2 cells (Figure S1D-S1E). When LSD1i^{early} cells were further differentiated to the endocrine (EN) stage, NKX6.1 and PDX1 expression were again largely unaffected, however no hormone expression was observed (Figure 1C-1E), indicating that LSD1 inhibition at this early stage blocked formation of endocrine cells. Interestingly, later inhibition of LSD1 during the transition from PP2 to EN cells (LSD1i^{late}; Figure 1B) had no effect on EN cell formation, evidenced by the expression of the pancreatic hormones INS, GCG, and SST (Figure 1C-1E). The proteins NKX6.1 and PDX1, which continue to be expressed in cells past the progenitor stage and in mature beta cells, were also unaffected by the later LSD1 inhibition (LSD1i^{late}) (Figure 1C-1E). These data indicate that inhibition of LSD1 activity is required during the PP1 to PP2 transition to properly form endocrine cells, but its activity during the PP2 to EN transition is dispensable for endocrine formation. This suggests there is a critical time window in which LSD1 activity is required for generation of endocrine cells from hESCs.

LSD1 Inhibition Prevents Enhancer Decommissioning

To understand why endocrine cell formation requires LSD1 activity during the earlier PP1 to PP2 transition, but not the later PP2 to EN transition, we performed chromatin immunoprecipitation sequencing (ChIP-seq) for LSD1 at the PP1 stage to identify regions in the genome where LSD1 could be acting during this stage of differentiation. We identified 15,084 LSD1-bound peaks (Table S1) throughout the genome (Figure S2A). Of these, 3,285 were proximal (< 3 kb) to a transcription start site (TSS) and 11,799 were distal (> 3kb) to any TSS (Tables S2 and S3, respectively). Because LSD1 is known to associate with and modify enhancers (Whyte,

Bilodeau et al. 2012, Kerenyi, Shao et al. 2013) and cell type-specific enhancers are known to determine cell lineages (Heintzman, Hon et al. 2009, Heinz and Glass 2012, Heinz, Romanoski et al. 2015, Romanoski, Link et al. 2015, Wang, Yue et al. 2015), we investigated the distal regions bound by LSD1, which comprise the majority (~78%) of LSD1 peaks at the PP1 stage.

To begin to characterize the chromatin states during the PP1 to PP2 transition, we performed ChIP-seq for H3K27ac at the PP1 and PP2 stages. Because the H3K27ac modification has been widely shown to be a faithful indicator of active enhancers (Heintzman, Hon et al. 2009, Creyghton, Cheng et al. 2010, Zentner, Tesar et al. 2011, Zentner and Scacheri 2012), we used it here to categorize distal LSD1 peaks at PP1 into one of three enhancer groups (Figure 2A). The enhancer groups were defined as follows: Group 1 (G1) consists of LSD1-bound regions where H3K27ac decreases ≥ 2-fold from PP1 to PP2; Group 2 (G2) consists of LSD1-bound regions where H3K27ac does not change more than 2-fold (either increase or decrease) from PP1 to PP2; Group 3 (G3) consists of LSD1-bound regions where H3K27ac increases ≥ 2-fold from PP1 to PP2 (Figure 2A and Tables S4-S6). In essence, G1 enhancers deactivate from PP1 to PP2, G2 enhancers remain active from PP1 to PP2, and G3 enhancers become active from PP1 to PP2. LSD1 ChIP-seq revealed that LSD1 binding remains unchanged from PP1 to PP2 at G2 and G3 enhancer regions, but is largely decreased at G1 enhancers during this transition (Figure 2B). To further characterize the groups of LSD1-bound enhancers we next performed ChIP-seq for H3K4me1 and H3K4me2 at the PP1 and PP2 stages. Along with the H3K27ac mark, H3K4me1 and H3K4me2 are very often observed at active enhancers (Heinz and Glass 2012, Whyte, Bilodeau et al. 2012, Heinz, Romanoski et al. 2015, Wang, Yue et al. 2015). Enhancers that possess these marks, but lack H3K27ac are said to be in a “poised” state; ready to be activated following H3K27ac addition, or decommissioned through removal of methylation from H3K4 (Creyghton, Cheng et al. 2010, Rada-Iglesias, Bajpai et al. 2011, Whyte, Bilodeau et al. 2012, Wang, Yue et al. 2015). Furthermore, LSD1 is known to demethylate both H3K4me1 and H3K4me2, and although H3K9 mono- and di-methylation are substrates of LSD1 (Metzger, Wissmann et al. 2005, Wissmann, Yin et al. 2007, Zibetti, Adamo et al. 2010, Laurent, Ruitu et al. 2015), we observed no expression of

the transcript encoding the H3K9 demethylating isoform of LSD1 (LSD1+8a) (data not shown). We therefore specifically assayed for mono- and di-methylation of H3K4 and not H3K9. Both H3K4me1 and H3K4me2 levels are significantly decreased from PP1 to PP2 at G1 enhancers (Figure 2C), further evidence this group can be classified as “deactivating” during this transition. Similarly, changes in H3K4me1 and H3K4me2 from PP1 to PP2 at G2 and G3 enhancers support their classifications of “remaining active” and “activating”, respectively. To determine if the normal demethylation of H3K4 seen in G1 enhancers was dependent upon LSD1 activity, we next performed ChIP-seq for H3K4me1 and H3K4me2 in LSD1i^{early} PP2 cells. Indeed, when LSD1 was inhibited at PP1 there was a failure to remove both H3K4me1 and H3K4me2 marks in G1 (Figure 2D; compare blue and red plot lines). These data suggest that, during the PP1 to PP2 transition, LSD1 acts to decommission G1 enhancers, but not G2 and G3 enhancers, through removal of H3K4 mono- and di-methylation before vacating those regions. Interestingly, H3K27ac ChIP-seq in LSD1i^{early} PP2 cells revealed that the deactivation of G1 enhancers (H3K27ac removal) was not disrupted by LSD1 inhibition (Figure 2D), suggesting that the deactivation of these enhancers can be decoupled from their decommissioning. This evidence supports models from previous reports that proposed enhancer deactivation and decommissioning as two separate events, each with an important role in enhancer regulation (Koch, Andrews et al. 2007, Whyte, Bilodeau et al. 2012). A similar decoupling of H3K27ac and H3K4 methylation states was also seen in G2 and G3 enhancers (Figure S2B). All together these results suggest the existence of a set of LSD1-bound enhancers that are typically deactivated and decommissioned during the PP1 to PP2 transition under normal differentiation conditions (G1 enhancers). When LSD1 is inhibited during this transition the deactivation events still occur at G1 enhancers, but the subsequent decommissioning is blocked, leaving the enhancers in a poised state (Figure 2E). We therefore hypothesized that maintenance of G1 enhancers in a poised state at PP2 as a result of LSD1 inhibition at PP1 could affect the expression of genes associated with these enhancers.

LSD1 Represses Transiently Expressed, Retinoic Acid-Dependent Genes

To better comprehend the nature of G1 enhancers and their role in controlling target gene expression, we first annotated transcription factor (TF) binding motifs at LSD1 bound enhancers. Motif enrichment analysis was performed with HOMER (Heinz, Benner et al. 2010) using the combined set of G2 and G3 enhancers as the background over which enrichment was calculated. We found that the motif for retinoic acid receptor (RAR) and retinoid X receptor (RXR) heterodimer (RAR/RXR) was highly enriched in G1 enhancers (Figure 3A). When retinoic acid binds to RAR, the RAR/RXR heterodimer associates with coactivating proteins, which, in turn, effect RA-induced events within the nucleus, including transcription of target genes and enhancer activation (Mahony, Mazzoni et al. 2011, Rhinn and Dolle 2012, Cunningham and Duester 2015). Because there are multiple isoforms of RAR that can heterodimerize with multiple isoforms of RXR, we used a pan-RXR binding antibody to perform ChIP-seq for RXR in PP1 cells to identify all regions where RA might be able to elicit a response by binding to one of the various isoforms of RAR within a RAR/RXR heterodimer. We found that 45.5% of G1 enhancers were co-occupied by RXR (612/1345; compared to an expected 5.6% by random chance), within ± 10kb of the center of the corresponding LSD1 peak, at the PP1 stage (Figure 3B and Table 1). We also found overlapping RXR binding with G2 and G3 enhancers to be higher than expected by random chance; however, the amount of overlap with G1 enhancers was significantly higher than that observed in G2 and G3 enhancers (Figure S3A). We further analyzed the RXR-bound G1 enhancers and found that this subset of enhancers normally undergoes a sharp increase in H3K27ac during the gut tube (GT) to PP1 transition, followed by an equally abrupt decrease in H3K27ac from PP1 to PP2 (Figure 3C). This acute acetylation and deacetylation of RXR-bound G1 enhancers coincides precisely with the addition and removal of exogenous RA in the cell culture media, as part of the normal differentiation protocol (Figure 3C) (D'Amour, Bang et al. 2006, Kroon, Martinson et al. 2008, Schulz, Young et al. 2012). This suggests that these enhancers follow an RA-dependent activation pattern. Notably, the large decrease in H3K27ac from PP1 to PP2 also occurs when LSD1 is inhibited at PP1 (LSD1i^{early}) (Figure 3C) indicating this specific subset of G1 enhancers is still being deactivated during this transition, as was seen for G1 as a whole (Figure 2D). Additionally, as occurred at all

G1 enhancers, LSD1 inhibition likewise prevented removal of H3K4me1 and H3K4me2 at RXR-bound G1 enhancers (Figure S3B).

Our analysis identified 612 RXR-bound G1 enhancers, which we used with the Genomic Regions Enrichment of Annotations Tool (GREAT) (McLean, Bristor et al. 2010) to identify 634 potential target genes (Table 2). To better understand how these RXR-bound G1 enhancers might affect target gene expression we performed RNA-seq on GT, PP1, and PP2 control and LSD1i^{early} cells. The RNA-seq data was then analyzed to obtain normalized gene expression levels (fragments per kilobase per million mapped reads; FPKM) for each of the genes across the time course, from GT to PP1 to PP2 ± LSD1i^{early}. We next performed k-means cluster analysis on all 634 genes, based on their expression changes across the GT, PP1, and PP2 differentiation stages, to isolate groups of genes that share common expression patterns over this time course. This revealed several categories of genes including one group consisting of 95 genes with increased expression from GT to PP1 followed by a sharp decrease in expression from PP1 to PP2 (Figure 3D; yellow bounding box). This expression pattern showed a striking resemblance to the H3K27ac pattern observed for the 612 RXR-bound G1 enhancers, and included within it enhancers of several genes well-known to be induced by RA, such as *HOXA1, HOXB1, RARB,* and *DHRS3* (Balmer and Blomhoff 2002, Balmer and Blomhoff 2005, Kam, Shi et al. 2013). We then queried the entire set of 634 genes to identify all genes that exhibited this same RA-dependent expression pattern. Specifically, we selected genes with FPKM ≥ 1 at PP1, ≥ 2-fold increase from GT to PP1, and ≥ 2-fold decrease from PP1 to PP2. Of the 634 genes, 74 met all three criteria (Table 3) of which 74.3% (55 of 74) were also included in the group of 95 genes identified through cluster analysis. Interestingly, when LSD1 is inhibited at PP1 (LSD1i^{early}) there is a significant failure to down-regulate many of the 74 genes (Figure 3F), including several known to be induced by RA (Figure S3C). During the PP1 to PP2 transition, LSD1 inhibition does not disrupt the removal of H3K27ac from the RXR-bound G1 enhancers associated with these genes, including known RA-induced genes like *HOXA1*, *HOXC4*, *GATA4,* and *DHRS3* (Figures 3G and S3D), thus allowing deactivation of the enhancers. However, when LSD1 is inhibited removal of H3K4me2 is blocked, preventing

the decommissioning of these enhancers and leaving them in a poised state (Figures 3G and S3D). Taken together, these results suggest that LSD1-mediated decommissioning of RXR-bound G1 enhancers is required to fully repress expression of their target genes.

Prolonged Exposure of early Pancreatic Progenitors to Retinoic Acid Phenocopies LSD1 Inhibition

Our data indicate that LSD1 is required to convert RXR-bound G1 enhancers from a poised to a decommissioned state and that LSD1 inhibition during this transition (LSD1i^{early}) disrupts that process, allowing for continued expression of target genes. Because LSD1 inhibition locks these enhancers in a poised state, it is possible they remain receptive activating RA signals, which, in turn, could prevent repression of genes that must be silenced after PP1 for proper endocrine formation to occur. With this in mind, we hypothesized that prolonged exposure of differentiating cells to RA signaling through the PP1 stage (Figure 4A) would be sufficient to prevent repression of these same genes and ultimately prevent downstream endocrine formation, mimicking the LSD1i^{early} phenotype. The extended treatment of PP1 cells with RA (RA^{extended}) resulted in an overall failure to downregulate the 74 genes within the previously identified group associated with RXR-bound G1 enhancers. The significantly higher expression of these genes as a whole in RA^{extended} PP2 cells mimics the gene dysregulation observed in LSD1i^{early} PP2 cells. Of the 74 PP1-specific genes associated with RXR-bound G1 enhancers, 48 (~65%) failed to be repressed in PP2 cells when RA exposure was extended through the PP1 to PP2 transition (RA^{extended}), including several of the previously identified genes known to be induced by RA (Figure 4B, 4C and 4SA). Remarkably, when RA^{extended} cells were differentiated to the EN stage, almost no expression of pancreatic hormone proteins or mRNA was observed (Figures 4D, 4E and S4B). Protein expression of NKX6.1 and PDX1 at the EN stage were unaffected by extended RA treatment (Figure 4E and S4C). This phenotype was nearly identical to that observed when LSD1 was inhibited in early (PP1) pancreatic progenitors (LSD1i^{early}). The observed phenocopy of LSD1i^{early} as a result of extended RA treatment (RA^{extended}) and the identification of RXR-bound enhancers that are remodeled by LSD1, provide evidence in support of the existence of a link between LSD1-mediated

decommissioning of RXR-bound G1 enhancers and the cells ability to respond to external RA signals. Together, these results suggest the possibility that the mechanism by which LSD1i^{early} prevents the formation of endocrine cells could be mediated by the failure to decommission RXR-bound G1 enhancers, thus leaving them in a poised state in which they remain susceptible to RA signals. This, in turn, prevents the repression of target genes necessary for proper endocrine formation. However, there remains the possibility that aberrant RA signaling alone could disrupt endocrine formation, in a manner independent of the chromatin state at RXR-bound G1 enhancers.

LSD1 Prevents Aberrant Reactivation of Transient early Retinoic Acid-dependent Genes

To determine if cells in which G1 enhancers have already been decommissioned are still susceptible to RA-induced blockage of endocrine formation, we reintroduced RA into the differentiation media during the PP2 to EN transition (RA^{late}; Figure 5A). Unlike the phenotype observed in RA^{extended} EN cells, formation of pancreatic endocrine cells was unperturbed in RA^{late} EN cells (Figure 5B). Expression of NKX6.1 and PDX1 was also unaffected (Figures 5C and S5A), and although mRNA levels for the pancreatic hormones INS, GCG and SST decreased as a result of RA^{late} (Figure S5B), respective protein expression appeared similar to controls (Figures 5B and 5C). In contrast to the up-regulation of PP1-specific genes associated with RXR-bound G1 enhancers observed in LSD1i^{early} and RA^{extended} PP2 cells, no significant change was seen for these 74 genes in RA^{late} EN cells (Figures 5D and S5C). Surprisingly, several of the previously identified genes shown to be induced by RA remained unchanged in RA^{late} EN cells (Figure 5E). Moreover, some of the genes that were increased in RA^{extended} PP2 cells, including *DHRS3* and *SHH* were actually decreased in RA^{late} EN cells (Figure 5E). This indicates that whereas extended RA treatment through the PP1 to PP2 transition, the late addition of RA (RA^{late}) was not sufficient to induce the same upregulation of these genes. These data suggest that at different stages of differentiation cells respond differently to the same RA signaling molecule, signifying shifts in the cellular contexts as cells transition from one lineage intermediate to the next.

This change in developmental competence was further demonstrated when RA was reintroduced to LSD1i^{early} cells during the PP2 to EN transition (LSD1i^{early} + RA^{late}). In this case, many of the PP1-specific genes associated with RXR-bound G1 enhancers were up-regulated compared to LSD1i^{early} EN cells (Figure 5H and S5E/I). Perhaps unsurprisingly, late addition of RA to LSD1i^{early} PP2 cells (LSD1i^{early} + RA^{late}) resulted in a lack of endocrine cells at the EN stage, similar to LSD1i^{early} alone (Figure 5G). Interestingly, however, while LSD1i^{early} alone tended to result in upregulation of many of 74 PP1-specific genes associated with RXR-bound G1 enhancers, the late addition of RA in LSD1i^{early} PP2 cells (LSD1i^{early} + RA^{late}) caused even further upregulation of several of these genes (Figure 5E). These results indicate that late addition of RA to PP2 cells (RA^{late}) causes increased expression of many of the PP1-specific genes associated with RXR-bound G1 enhancers, if LSD1 has been previously inhibited during the transition from PP1 to PP2 (LSD1i^{early}). Without prior LSD1 inhibition, this same up-regulation of genes was not observed in RA^{late} EN cells. Together, these data suggest that LSD1 activity during the PP1 to PP2 transition is required to prevent reactivation of RA-dependent genes at later stages of differentiation.

Requirement for Lsd1 in Endocrine Cell Formation during a Short Window in early Pancreatic Development in mice

To confirm the phenotype observed during pancreatic differentiation of hESCs in an in vivo setting, we mimicked the removal of LSD1 activity using a genetic knockout approach in mice. To determine if Lsd1 plays a role in mouse pancreas development, similar to that observed in human differentiation, we first analyzed its expression pattern in the developing and adult mouse pancreas. We found that, as in humans, Lsd1 is expressed in the early multipotent pancreatic progenitors (marked by Pdx1/Sox9 co-expression) in the developing mouse embryo, as well as in embryonic and adult endocrine cells. (Figure S6A). Robust Lsd1 expression was also observed in multiple endocrine subtypes in adult mouse islets (Figure S6B). To explore the function of Lsd1 during mouse pancreas development, we selectively inactivated *Lsd1* in early pancreatic progenitor cells by generating *Pdx1Cre*;*Lsd1*$^{flox/flox}$ (*Lsd1*$^{\Delta pan}$) mice (Figure 6A). In *Lsd1*$^{\Delta pan}$ embryos, key aspects of

early pancreatic development, such as the induction of early pancreatic markers and outgrowth of the tissue buds, were unperturbed (Figure 6B, 6C and S6C). Furthermore, expression of acinar and ductal markers, and cell survival were unaffected by *Lsd1* deletion (Figure S6C and S6D). However, by embryonic day (e) 15.5, when widespread endocrine cell differentiation is evident in control mice, *Lsd1*$^{\Delta pan}$ embryos exhibited a complete lack of endocrine cells (Figure 6B), which remained apparent at birth (Figure 6D). These findings revealed that, as in humans, Lsd1 inactivation during pancreas development in mice prevents endocrine formation. This suggests that Lsd1 is required for endocrine lineage specification in mice.

To determine if a critical time window exists during which Lsd1 expression is critical for proper mouse pancreatic endocrine formation, as was observed during differentiation of hESCs, we crossed *Lsd1*$^{flox/flox}$ and *Pdx1CreER*^{TM} mice, allowing for time-specific inactivation of Lsd1 in pancreatic progenitors via tamoxifen administration (Figure 6E). Tamoxifen injection at e12.5 (*Lsd1*$^{\Delta late}$) targeted the multipotent pancreatic progenitor domain shortly before endocrine cell differentiation (Seymour and Sander 2011) and did not affect endocrine cell formation, as evidenced by the presence of LSD1-deficient hormone^{+} cell clusters in LSD1 (Figure 6F and S6E). By contrast, tamoxifen administration at e10.5 (*Lsd1*$^{\Delta early}$) resulted in almost complete loss of endocrine cells, phenocopying *Lsd1*$^{\Delta pan}$ mice (Figure 6F and S6E). Given the delay between tamoxifen administration and gene deletion (Nakamura, Nguyen et al. 2006), these results indicate a time window between e11 and e13 during which *Lsd1* deletion prevents endocrine formation. This suggests that Lsd1 activity is required during a specific early time window of mouse pancreas development, after which it is dispensable, for proper endocrine cell differentiation. These data provide in vivo confirmation of the phenotype observed when LSD1 is inhibited during in vitro differentiation of hESCs to the pancreatic endocrine lineage.

Of the 74 PP1-specific genes associated with RXR- bound enhancers identified in hESC-based LSD1 inhibition studies, 51 were expressed in either control or *Lsd1*$^{\Delta pan}$ mutant mice at e13.5. Overall, expression of these genes was increased in *Lsd1*$^{\Delta pan}$ compared to controls (Figure 6G and S6F). Among these 51 genes several showed significant up-regulation in *Lsd1*$^{\Delta pan}$

compared to control, including *Hoxa1 Hoxc4* and *Cadm3* (Figure 6H). All of these were similarly found to be up-regulated during LSD1 inhibition and induced by RA treatment in pancreatic differentiation of hESCs (Figures S3C, 4C and 5E/I). This indicates that, in addition to blocking endocrine formation, *Lsd1* knockout in early mouse embryos causes up-regulation of several genes previously shown to be induced by RA in during pancreatic differentiation of hESCs. This suggests that Lsd1 may act in a similar capacity during mouse pancreas development as it does during human pancreatic differentiation; wherein, Lsd1 deletion, prevents Lsd1-mediated decommissioning of associated RA-responsive enhancers. Without Lsd1 present to decommission these enhancers they remain susceptible to activation by circulating RA, which ultimately prevents the normal repression of target genes that is required for proper endocrine formation.

These results not only confirm the phenotype observed in hESCs, but also lend credence to the utility of hPSC-based in vitro systems in studying and dissecting processes of human development. With an in vitro differentiation system however, signaling factors such as RA can simply be withdrawn from the differentiation media at specific times to prevent further influence on the differentiating cells. In contrast, during in vivo development, many of these signaling molecules persist constitutively and the cellular response to these signals must be altered in precise spatiotemporal manner in order for multipotent progenitors to respond appropriately and differentiate into the correct cell types, thus ensuring proper development of fully functional organs. Altogether, these results support a model wherein LSD1-mediated decommissioning of enhancers functions to render cells insensitive to external developmental cues, effectively altering the developmental competence of the cells by reshaping the chromatin landscape.

DISCUSSION

Here, we have identified a specific time window during early pancreatic development in both human and mouse, in which LSD1 activity is required for pancreatic endocrine formation. We found that during this time window, LSD1 is localized to different classes of enhancers (Figure 2A). One of those LSD1-bound enhancers groups (G1) normally undergoes deactivation and decommissioning. Upon inhibition of LSD1 those enhancers are still deactivated (H3K27ac

removal), but decommissioning (H3K4me1/H3K4me2 removal) is disrupted (Figure 2D). Genomic regions within the G1 enhancer group were enriched for RXR binding motif; and indeed, nearly half of G1 enhancers were co-bound by RXR during this time window (Figure 3A). The inclusion of RA in the differentiation media during the transition prior to this critical time window is coincident with the activation of these enhancers (Figure 3D). Together these results indicate these enhancers may be responsive to the RA in the differentiation media and suggest they are first activated by RA, and later decommissioned by LSD1 when the enhancer needs to be fully repressed and prevented from future reactivation. Previous models of LSD1 control of enhancers suggest that LSD1-mediated demethylation of H3K4 at enhancers is required to properly decommission the enhancers and repress target genes (Whyte, Bilodeau et al. 2012). Consistent with this model, our results indicates LSD1 is required to convert these enhancers from a poised to a decommissioned state. This, along with the observed concomitant failure to down-regulate many of the genes associated with RXR-bound G1 enhancers, suggest that LSD1 inhibition during this transition (LSD1i^{early}) disrupts decommissioning of RA-activated enhancers and allows for continued expression of target genes.

Our findings provide evidence that suggests proper modulation of chromatin landscape is vital to ensuring cells respond appropriately to external inductive signals. The results presented here provide evidence in support of a model in which LSD1 occupies a group of RA-responsive enhancers that become active following exposure to RA during the GT to PP1 transition. During the transition to PP2 these enhancers are deactivated and LSD1 decommissions them, rendering them insensitive to external RA signals. This, in turn, allows for appropriate repression of target genes, even in the event the cells are re-exposed to RA. However, when LSD1-mediated decommissioning of these enhancers is blocked during the PP1 to PP2 transition these enhancers are left in a poised state. The poised enhancers remain susceptible to reactivation when exposed to RA signals, which, in turn, induces aberrant reactivation of target genes. A prime example of this was observed in the regulation of the gene *DUSP9*. During normal differentiation *DUSP9* expression increases from GT to PP1, where it peaks, before being downregulated in PP2. *DUSP9*

is known to be activated by RA (Simandi, Balint et al. 2010), but it was not up regulated in LSD1i^{early} PP2 cells. However, it is up-regulated at the EN stage when RA is added late (RA^{late}) to PP2 cells, but only if LSD1 was previously inhibited at the PP1 stage (LSD1i^{early}). This finding supports the model wherein the failure of LSD1 to decommission enhancers may not cause immediate up-regulation of potential target genes, but rather leaves the enhancers in a poised state, providing a permissive environment for enhancer reactivation. In fact, although LSD1i^{early} does not cause an upregulation of *DUSP9* at the PP2 stage, when measured at the later EN stage, *DUSP9* expression is elevated in LSD1i^{early} cells compared to EN controls. It is therefore possible that this gene, and others like it, are normally down-regulated after LSD1-mediated decommissioning of their associated enhancers; and, when those enhancers are not properly decommissioned, as a result of removal of LSD1 activity, they remain poised and susceptible to future reactivation, given the right inductive cues. The data shown here highlight the role of LSD1 as an important chromatin remodeler during development, and suggest that its ability to reshape the chromatin landscape of differentiating cells can alter the developmental competence of those cells, influencing their responses to developmental signals.

Developmental signals like RA are extremely important for development of a variety of tissues, including neurons, lung and pancreas (Durston, Timmermans et al. 1989, Avantaggiato, Acampora et al. 1996, Bibel, Richter et al. 2004, Plachta, Bibel et al. 2004, Mark, Ghyselinck et al. 2009). The importance of RA in pancreas development has been well established (Chen, Pan et al. 2004, Martin, Gallego-Llamas et al. 2005, Molotkov, Molotkova et al. 2005). These and other studies have demonstrated that for proper development to occur, different lineage intermediates must be exposed to RA at different times and concentrations and for different durations; and that each of these aspects are vary between, and are specific to each individual cell type. During in vitro differentiation of cells it is trivial to supply signaling factors at specific times and concentrations and durations, as needed. This is, in fact, one of the great benefits to these systems that allows for precise control of the signaling environment and the generation of highly pure populations consisting of a single cell type. However, during in vivo development many cells remain exposed

to these signaling factors before and after they must respond to them, raises the question of how these cells can modulate their responses to these developmental cues.

Using our in vitro model system, we gathered evidence that establishes a link between modification of the chromatin landscape by LSD1 during differentiation and the resulting changes in cellular response to external developmental signals. Here we have presented results that begin to explain one possible mechanism of how seemingly identical stem cells, with identical genomes, can respond to the same cues in very different ways and give rise to the wide variety of specialized cell types observed in the human body

METHODS

Chromatin immunoprecipitation followed by massively parallel multiplexed sequencing (ChIP-seq)

ChIP-seq was performed using the ChIP-IT High-Sensitivity kit (Active Motif) according to the manufacturer's instructions. Briefly, for each cell stage and condition analyzed, 5-10 x 10^6 cells were harvested and fixed for 15 min in an 11.1% formaldehyde solution. Cells were lysed and homogenized using a Dounce homogenizer and the lysate was sonicated in a Bioruptor® Plus (Diagenode), on high for 3 x 5 min (30 sec on, 30 sec off). Between 10 and 30 µg of the resulting sheared chromatin was used for each immunoprecipitation. Equal quantities of sheared chromatin from each sample were used for immunoprecipitations carried out at the same time. 4 µg of antibody against LSD1 (Abcam, ab17721), H3K4me1 (Abcam, ab8895), H3K4me2 (Millipore, 07-030), H3K27ac (Active Motif, 39133) and RXR (Santa Cruz, sc-831) were used for each respective ChIP-seq assay. Chromatin was incubated with primary antibodies overnight at 4 °C on a rotator followed by incubation with Protein G agarose beads for 3 hours at 4 °C on a rotator. Reversal of crosslinks and DNA purification were performed according to the ChIP-IT High-Sensitivity instructions, with the modification of incubation at 65 °C for 2-3 hours, rather than at 80 °C for 2 hours during crosslink reversal. Sequencing libraries were constructed using KAPA DNA Library Preparation Kits for Illumina® (Kapa Biosystems) and library sequencing was performed on a HiSeq 4000 System (Illumina®). Both library construction and sequencing were performed by the Institute

for Genomic Medicine (IGM) core research facility at the University of California at San Diego (UCSD).

Chromatin mapping and data quality control

Sequencing data was released from the UCSD IGM core facility after passing internal quality controls and certain benchmarks set forth by the FastQC analysis software (Andrews 2010), including total sequence reads, sequence quality and length distribution scores. Upon receipt of raw sequencing data (FASTA format), several downstream analyses were performed to ensure quality of sequencing data. First, all ChIP-seq data was mapped to the human genome utilizing the most recent consensus build (hg19/GRCh37) of the human genome available at the time of this study (Kent, Sugnet et al. 2002). Bowtie 2, v2.2.7 (Langmead and Salzberg 2012) was used to map data to the genome using the parameters defined in Table 4. Next, further quality control steps to confirm the sequence data was of acceptable quality were performed post-mapping using the Samtools v1.3.1 (Li, Handsaker et al. 2009) and HOMER v4.9 (Heinz, Benner et al. 2010) software suites (see Table 4). Various attributes of each sequence file were assessed to ensure the sequence reads met certain criteria. The number of reads not mapped to the genome build had to be within a reasonable range (1 - 2%) of the total mapped reads. *Note:* Because we mapped to a consensus reference genome, it is possible that unmapped reads represent real portions of the genome from the cells being analyzed, but that these sequences are for one reason or another not contained within the reference genome. However, for the purposes of this study, unmapped reads were discarded. A high percentage of unmapped reads could indicate an experimental problem with the immunoprecipitation itself, contaminating DNA from non-human sources or an issue with library preparation, such as the amplification of indexing primer dimers (O'Geen, Echipare et al. 2011, Head, Komori et al. 2014).

Another important quality control metric is the number of exact duplicate reads within a sequence file. Due to the nature of ChIP-seq, it is somewhat unlikely that two reads will have exactly the same sequence and length (Storvall, Ramskold et al. 2013). A high number of exact duplicates

could indicate a problem arising from the library preparation and sequencing. However, it is not always the case that a duplicate is an artifact and visualization of the data on a genome browser might help to distinguish between artifacts and true data. One last key metric is that of the multimapping read. Those reads that map to > 1 genomic region cannot effectively be used as their true position cannot be determined via the ChIP-seq method. The methods used here to align sequence reads to the genome were not based on perfect 1:1 matches, but rather allowed for certain degrees of freedom each time a read was mapped to account for potential sequencing errors and/or DNA bases that are reported as low confidence by the sequencing platform. With this in mind, we relied on the mapping quotient (MAPQ) scores assigned to each read during alignment to the genome. A certain level of confidence that a read is correctly mapped and only maps to one location is provided by the MAPQ score. If the probability that a read is incorrectly matched is equal to P and P is a value between 0 and 1 (0 to 100% probability), then the MAPQ score is generated by $-10 \times \log_{10}(P)$. A MAPQ score of 0 means the fragment definitely maps to > 1 place. If the estimate that a read maps to > 1 region is 100% then P = 1 and MAPQ = $-10 \times \log_{10}(1) = 0$. Conversely, if the probability that a fragment matches exactly one genomic region is 99.9% or 0.999, then the probability of a mismatch is P = 1 - 0.999 = 0.001 and the MAPQ = $-10 \times \log_{10}(0.001) = 30$. So, anything with a MAPQ score > 30 has an estimated chance of improper matching of less than 0.1%. For the purposes of this study, all reads with MAPQ > 0 were used. Ultimately, a sufficient amount of uniquely mapped reads from each ChIP-seq experiment are required and previous standards have been set by consortia like ENCODE (Encode Project Consortium 2012), which required >= 10 and 20 million uniquely mapped reads for TF and histone modification ChIP-seq experiments, respectively. All ChIP-seq experiments in this study meet or exceed these requirements.

After confirming sufficient reads of acceptable quality were mapped to the genome, we next measured the overall GC content of the uniquely mapped sequences to ensure it fell within expected ranges. This value can vary widely across all samples, but should be closely reproduced in biological replicates of the same cell, condition and protein immunoprecipitated. Our major

concern was to ensure that, within a single ChIP-seq experiment, the distribution of GC content was somewhat normal (Gaussian), or skewed high or low. If the experiment exhibits a bimodal distribution of GC content, with high percentages of both high and low GC content sequences, this could indicate a problem with the experiment, such as contamination of the immunoprecipitated DNA or library preparation (Head, Komori et al. 2014).

Peak calling and visualization of ChIP-seq data

Mapped ChIP-seq data served as inputs to generate tag directories using HOMER (Heinz, Benner et al. 2010). Tag directories take all mapped reads from the input and generates a "tag" spanning the appropriate chromosomal coordinates. The tags "stack" on one another to eventually generate piles of reads over certain locations which can then be called as peaks, as was done here using the findPeaks program within the HOMER software suite. Stage- and condition-matched input DNA controls were used as background when calling peaks. The Bedtools v2.17.0 (Quinlan and Hall 2010) suite of programs was used to quickly analyze whether certain peaks overlapped with other peaks or modified histone regions. For example, windowBed was used for initial in silico pilot experiments to classify enhancers based on H3K27ac states from PP1 to PP2. This was a simple binary call using the peak files generated in HOMER to determine whether a peak in PP1 was within ± 1000 bp of a peak in PP2. This was the initial method used to generate the different classifications of enhancers (i.e. active in PP1 and inactive in PP2). This served as a fast initial screen to identify interesting patterns in the ChIP-seq data. However, the binary nature of these methods were generally too restrictive to detect certain phenomena that could be biologically relevant, such as subtle changes in H3K4 methylation between two stages or conditions. For this reason, after our initial screenings we then used the getDifferentialPeaks program within HOMER, which probes for peak intensity changes between different conditions. This program allows the user to set the fold increase or decrease that must be observed to be considered a differential peak (see comments in Table 4). Differential peak analysis performed in this way allowed for the identification of things like enhancers that were in the process of being deactivated from PP1 to PP2, but not

necessarily completely devoid of H3K27ac at PP2. Table 4 lists the commands and parameters used to classify the different groups (G1, G2 and G3) of enhancers and how we identified PP1 LSD1 peaks near each of the groups.

RNA isolation and sequencing and qRT-PCR

RNA was isolated from cell samples using the RNeasy® Micro Kit (Qiagen) according to the manufacturer instructions. For each cell stage and condition analyzed between 0.1 and 1 x 10^6 cells were collected for RNA extraction. For qRT-PCR, cDNA synthesis was first performed using the iScript™ cDNA Synthesis Kit (Bio-Rad) and 500 ng of isolated RNA per reaction. qRT-PCR reactions were performed in triplicate with 10 ng of template cDNA per reaction using a CFX96™ Real-Time PCR Detection System and the iQ™ SYBR® Green Supermix (Bio-Rad). PCR of the TATA binding protein (TBP) coding sequence was used as an internal control and relative expression was quantified via double delta C_T analysis. For RNA sequencing (RNA-seq), stranded, single-end sequencing libraries were constructed from isolated RNA using the TruSeq® Stranded mRNA Library Prep Kit (Illumina®) and library sequencing was performed on a HiSeq 4000 System (Illumina®). Both library construction and sequencing were performed by the IGM core research facility at UCSD. Sequence files were mapped to the human genome (hg19/GRCh37) using the Spliced Transcripts Alignment to a Reference (STAR) aligner (Dobin, Davis et al. 2013). Tag directories were constructed from STAR outputs and normalized gene expression (fragments per kilobase per million mapped reads; FPKM) for each sequence file were determined using HOMER (Heinz, Benner et al. 2010). HOMER was used to annotate all RefSeq genes with FPKM values and to invoke the R packages edgeR (Robinson, McCarthy et al. 2010, McCarthy, Chen et al. 2012) and DESeq2 (Love, Huber et al. 2014) for various differential expression analyses. At least two biological replicates (n = 2) were analyzed for every stage and condition unless noted otherwise. For k-means clustering, normalized FPKM values for each gene were normalized to the time point with maximum expression, which was set to 1. This generated a table of genes with values ranging from 0 to 1 across the GT to PP1 to PP2 time course. Data transformed in this manner was used

to generate heatmaps as well as for k-means clustering. K-means clustering was performed in R to identify groups of genes with similar expression patterns across the time course, regardless of absolute expression values. 8 clusters were requested and clustering was performed starting from random points in the data (100 iterations). This was repeated over 10 times to ensure the same genes were reproducibly clustered together.

Primers used for RT-qPCR are as follows:

INS-F: 5'-AAGAGGCCATCAAGCAGATCA

INS-R: 5'-CAGGAGGCGCATCCACA

GCG-F: 5'-AAGCATTTACTTTGTGGCTGGATT

GCG-R: 5'-TGATCTGGATTTCTCCTCTGTGTCT

HOXA1-F*:* 5'-CGGAACTGGAGAAGGAGTTC

HOXA1-R: 5'-TTCACTTGGGTCTCGTTGAG

SST-F*:* 5'-CCCCAGACTCCGTCAGTTTC

SST-R: 5'-TCCGTCTGGTTGGGTTCAG

TBP-F: 5'-ATTAAGGGAGGGAGTGGCAC

TBP-R: 5'-GCTTTGCTTCCCTTTCCCAA

Assignment of enhancer target genes and Motif enrichment analysis

Target genes were assigned using the Genomic Regions Enrichment of Annotations Tool (GREAT) (http://bejerano.stanford.edu/great/public/html/; (McLean, Bristor et al. 2010), using the following parameters: basal plus extension, 5kb upstream, 1kb downstream and plus distal 200kb regions. HOMER (Heinz, Benner et al. 2010) was used to identify transcription factor (TF) binding motifs enriched in the G1 enhancer group over the G2 and G3 groups. G2 and G3 enhancer peak files were merged and set as the background using the appropriate option in the findMotifsGenome.pl program. G1 enhancers associated with one or more genes with FPKM ≥ 1 at the PP1 stage were used for motif analysis.

Immunofluorescence analysis.

Cell aggregates derived from hESCs were allowed to settle in microcentrifuge tubes and washed twice with PBS before fixation with 4% paraformaldehyde for 30 min at room temperature. Fixed cells were washed twice with PBS and incubated overnight at 4 °C in 30% (w/v) sucrose in PBS. Cell aggregates were then loaded into disposable embedding molds (VWR), covered in Tissue-Tek® O.C.T. Sakura® Finetek compound (VWR) and flash frozen on dry ice to prepare frozen blocks. The blocks were sectioned at 10 µm and sections were placed on Superfrost Plus® (Thermo Fisher) microscope slides and washed with PBS for 10 min. Slide-mounted cell sections were permeabilized and blocked with blocking buffer, consisting of 0.15% (v/v) Triton X-100 (Sigma) and 1% (v/v) normal donkey serum (Jackson Immuno Research Laboratories) in PBS, for 1 hour at room temperature. Slides were then incubated overnight at 4 °C with primary antibody solutions. The following day slides were washed five times with PBS and incubated for 1 hour at room temperature with secondary antibody solutions. Cells were washed five times with PBS before coverslips were applied. All antibodies were diluted in blocking buffer at the ratios indicated below. Primary antibodies used were: sheep anti-NGN3 (1:300, R&D Systems); rabbit anti-SOX9 (1:1000 dilution, Millipore); goat anti-PDX1 (1:500 dilution, Abcam); mouse anti-NKX6.1 (1:300 dilution, Developmental Studies Hybridoma Bank); rabbit anti-CHGA (1:1000, DAKO); guinea pig anti-INS(1:500, DAKO), mouse anti-GCG (1:500, Sigma), rabbit anti-SST (1:500, DAKO). Secondary antibodies against sheep, rabbit, goat, mouse and guinea pig were Alexa488-, Cy3- and Cy5-conjugated donkey antibodies and were used at dilutions of 1:1000, 1:2000, and 1:250, respectively (Jackson Immuno Research Laboratories). Representative images were obtained with a Zeiss Axio-Observer-Z1 microscope equipped with a Zeiss ApoTome and AxioCam digital camera. Figures were prepared in Adobe Creative Suite 5.

Human tissue

Human fetal pancreas donor tissue was obtained from the Birth Defects Research Laboratory of the University of Washington. Cadaveric adult pancreata used in this study were from

non-diabetic donors and were acquired through the Network for Pancreatic Organ Donors with Diabetes (nPOD) (Campbell-Thompson, Wasserfall et al. 2012). Protein expression was analyzed in nPOD donors: LSD1 and GCG in #6140 (38 year old male); LSD1 and CHGA in #6160 (22 year old male); LSD1 and SST in 6178 (25 year old female); and LSD1, INS and GCG in 6179 (21 year old female).

Mice

Pdx1-Cre, *Pdx1-CreER*^{TM} (Gu, Dubauskaite et al. 2002) and *Lsd1*^{flox} (Wang, Scully et al. 2007) mouse strains have been described previously. *Lsd1*$^{\Delta pan}$ knockouts were generated by crossing *Pdx1-Cre* and *Lsd1*^{flox} mice. Conditional *Lsd1* knockouts were generated by crossing *Pdx1-CreER*^{TM} and *Lsd1*^{flox} mice. Tamoxifen (Sigma) was dissolved in corn oil (Sigma) at 10 mg/mL, and a single dose of 3.5 mg/40 g or 4.5 mg/40 g body weight was administered by intraperitoneal injection at embryonic day (e) 10.5 or e12.5, respectively. Control mice were LSD1$^{+/+}$ littermates carrying Pdx1-Cre transgene. Midday on the day of vaginal plug appearance was considered e0.5.

FIGURES

Figure 1. Endocrine cell formation requires LSD1 activity during a short window in early pancreatic development.

(A) Immunofluorescent staining of pancreatic sections for LSD1 with the pancreatic progenitor markers PDX1 and SOX9 (55 days post-conception (dpc) fetal pancreas) or the pan-endocrine marker chromogranin A (CHGA) (94 dpc and adult pancreas). Scale bar, 50 μm.
(B) Schematic of the human embryonic stem cell (hESC) differentiation protocol to the endocrine cell stage (EN) and experimental plan for LSD1 inhibition.
(C) Immunofluorescent staining for pancreatic hormones insulin (INS), glucagon (GCG) and somatostatin (SST) or PDX1 and NKX6.1 in control EN cells compared to EN cells with early (LSD1i^{early}) and late (LSD1i^{late}) LSD1 inhibition. Scale bar, 50 μm.
(D) qRT-PCR analysis for *INS*, *GCG* and *SST* in control, LSD1i^{early} and LSD1i^{late} EN cells. Data are shown as mean ± S.E.M (n = 2 biological replicates). *$p < 0.001$.
(E) Flow cytometry analysis at EN stage for NKX6.1, PDX1 and INS comparing control, LSD1i^{early} and LSD1i^{late} cells. Isotype control for each antibody is shown in red and target protein staining in green. Percentage of cells expressing each protein is indicated.
AA, activin A; ITS, insulin-transferrin-selenium; TGFBi, TGFβ R1 kinase inhibitor; KGF, keratinocyte growth factor; RA, retinoic acid; EGF, epidermal growth factor; ES, embryonic stem cell; DE, definitive endoderm; GT, primitive gut tube; PP1, early pancreatic progenitors; PP2, late pancreatic progenitors; EN, endocrine cell stage; FSC-A, forward scatter area.
See also Figure S1.

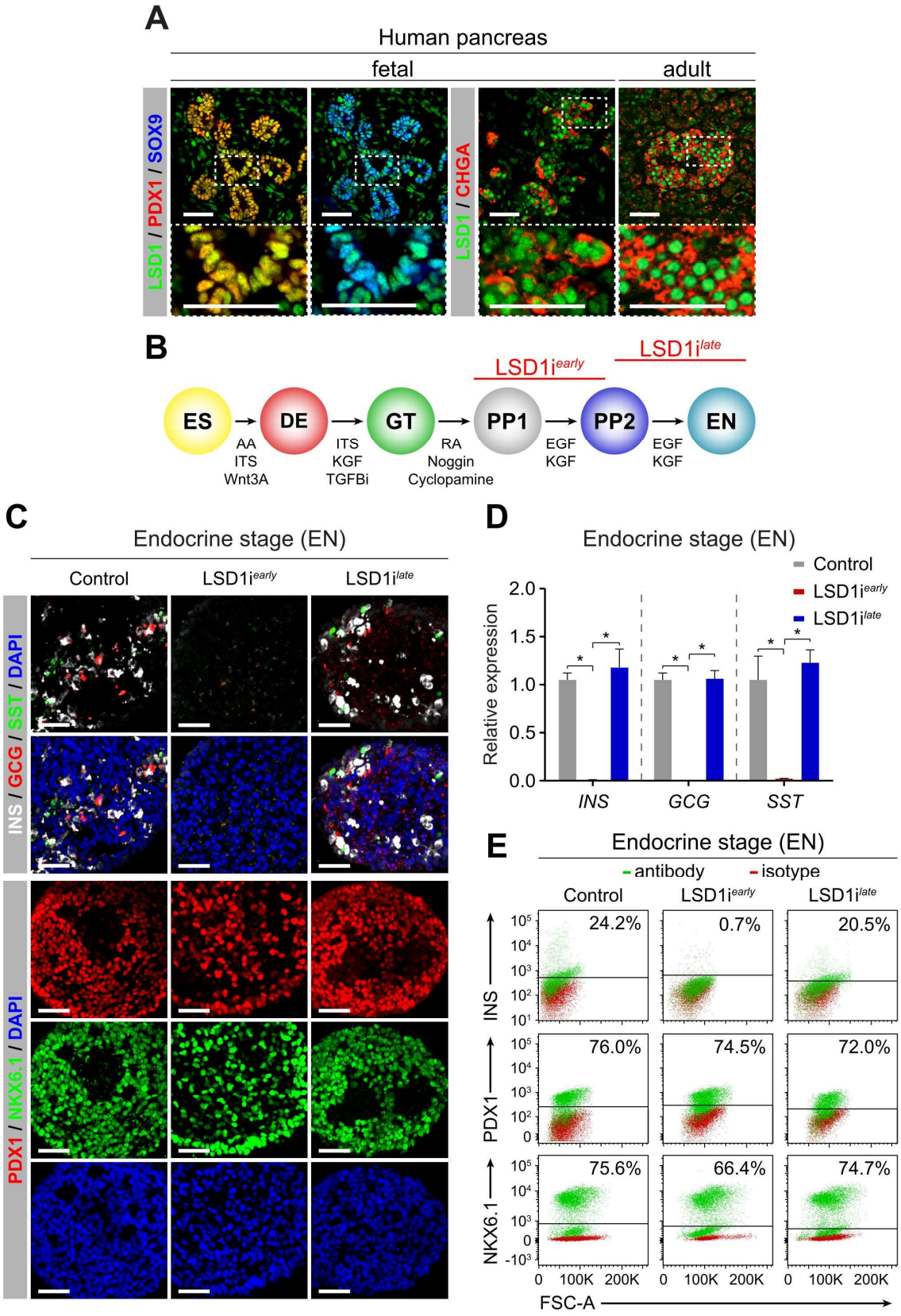
A
Human pancreas
fetal
adult
LSD1 / PDX1 / SOX9
LSD1 / CHGA
B
LSD1i^early
LSD1i^late
ES
DE
GT
PP1
PP2
EN
AA
ITS
Wnt3A
ITS
KGF
TGFBi
RA
Noggin
Cyclopamine
EGF
KGF
EGF
KGF
C
Endocrine stage (EN)
Control
LSD1i^early
LSD1i^late
INS / GCG / SST / DAPI
PDX1 / NKX6.1 / DAPI
D
Endocrine stage (EN)
Control
LSD1i^early
LSD1i^late
Relative expression
2.0
1.5
1.0
0.5
0.0
INS
GCG
SST
E
Endocrine stage (EN)
antibody
isotype
Control
LSD1i^early
LSD1i^late
INS
PDX1
NKX6.1
24.2%
0.7%
20.5%
76.0%
74.5%
72.0%
75.6%
66.4%
74.7%
FSC-A
0
100K
200K

Figure 2. LSD1 inhibition prevents decommissioning of transiently active early pancreatic enhancers.

(A) Heatmap showing density of ChIP-seq reads for LSD1 and H3K27ac centered on LSD1 peaks, spanning 10 kb. G1, G2 and G3 groups of LSD1-bound enhancers are deactivated (G1), remain active (G2), or are deactivated (G3) from PP1 to PP2.
(B) Tag density plots displaying LSD1 tag distribution at G1, G2 and G3 enhancers at PP1 and PP2 stages, centered on PP1 LSD1 peaks.
(C) Box plots of H3K4me1 and H3K4me2 ChIP-seq counts at G1, G2 and G3 enhancers at PP1 and PP2 stages. *p < 0.05; **p < 5e-12; *** < 2.2e-16.
(D) Tag density plots for G1 enhancers displaying H3K27ac, H3K4me2 and H3K4me1 tag distribution at PP1 stage and PP2 stage with and without early LSD1 inhibition (LSD1i^{early}). Plots are centered on PP1 LSD1 peaks.
(E) Model for LSD1-dependent enhancer decommissioning. Enhancer deactivation by removal of acetylation from H3K27 occurs independent of LSD1 activity. LSD1 subsequently mediates enhancer decommissioning by removal of H3K4me2 marks.
PP1, early pancreatic progenitors; PP2, late pancreatic progenitors.
See also Figure S2 and Tables S1-S6.

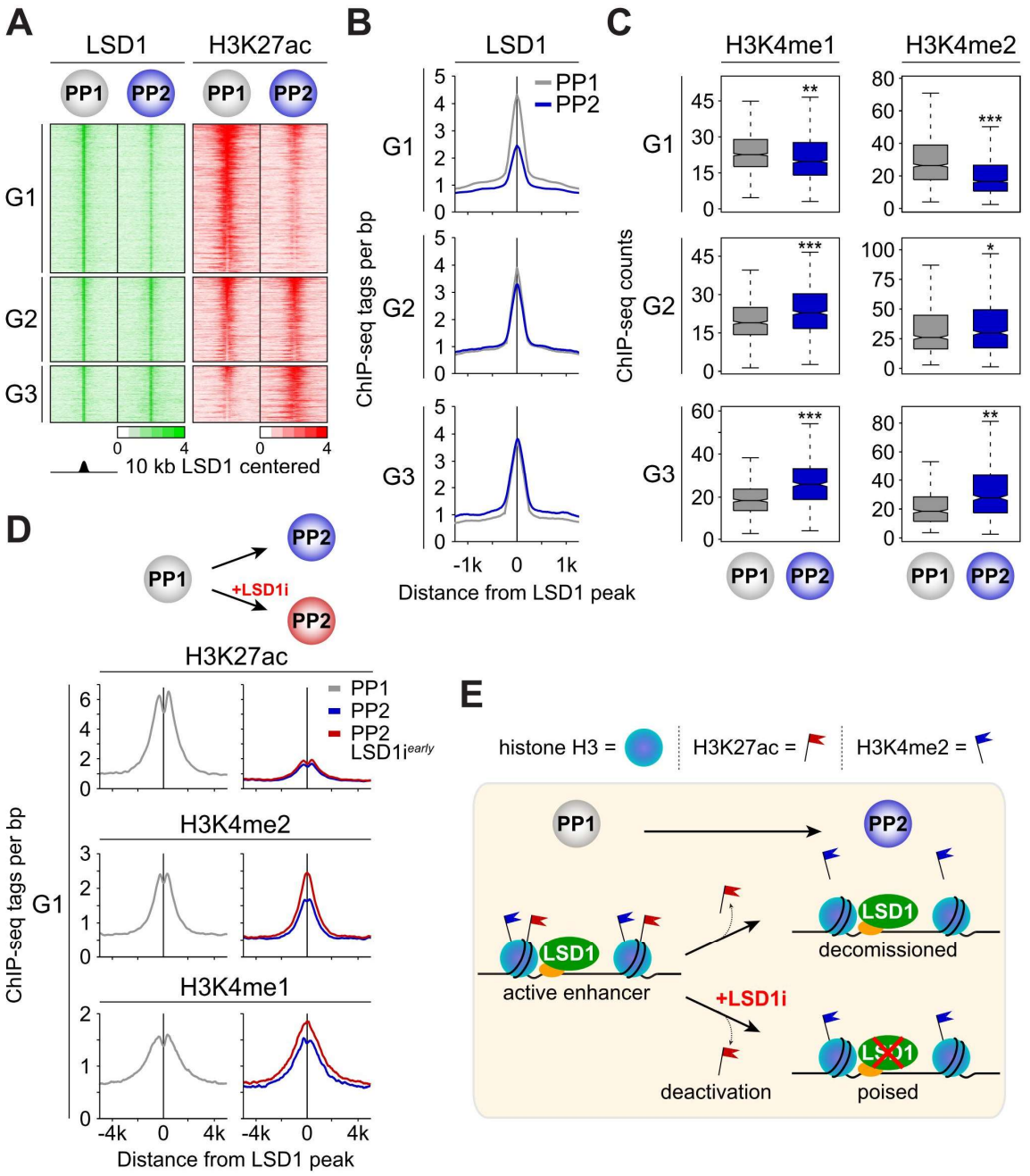
A
LSD1
H3K27ac
PP1
PP2
PP1
PP2
G1
G2
G3
0
4
0
4
10 kb LSD1 centered
B
LSD1
PP1
PP2
G1
G2
G3
ChIP-seq tags per bp
-1k
0
1k
Distance from LSD1 peak
C
H3K4me1
H3K4me2
G1
G2
G3
ChIP-seq counts
**
***
***
*
***
**
PP1
PP2
PP1
PP2
D
PP1
PP2
+LSD1i
PP2
H3K27ac
PP1
PP2
PP2
LSD1i early
H3K4me2
H3K4me1
G1
ChIP-seq tags per bp
-4k
0
4k
-4k
0
4k
Distance from LSD1 peak
E
histone H3 =
H3K27ac =
H3K4me2 =
PP1
PP2
LSD1
LSD1
active enhancer
decomissioned
+LSD1i
deactivation
poised

Figure 3. LSD1 activity is necessary for down-regulation of transiently expressed retinoic acid-dependent genes.

(A) Enriched transcription factor (TF) binding motifs with associated p-values for G1 enhancers compared to G2 and G3 enhancers.
(B) Percentage of G1 enhancers versus random genomic regions bound by RXR within ± 10kb of LSD1 peak at the PP1 stage. **p < 2.5e-8, chi-square.
(C) Schematic showing timing and duration of retinoic acid (RA) addition (top) and coincident changes in H3K27ac levels at RXR-bound G1 enhancers (bottom) during hESC differentiation toward endocrine (EN) cells with and without LSD1 inhibition from PP1 to PP2 (LSD1i^{early}). ***p < 2.2e-16, Wilcoxon.
(D) K-means clustering of genes associated with RXR-bound G1 enhancers (Table 2) based on mRNA expression (FPKM) (n=3). Genes were assigned to enhancers using the Genomic Regions Enrichment of Annotations Tool (GREAT) within a 200kb window. mRNA levels shown as relative to maximum per gene across time course. Yellow box highlights gene cluster exhibiting RA-dependent (PP1-specific) expression pattern.
(E) Heatmap of gene expression for PP1-specific genes associated with RXR-bound G1 enhancers across GT, PP1, and PP2 (n=74) with and without LSD1 inhibition (LSD1i^{early}). Gene set defined by FPKM at PP1 ≥ 1 and PP1 mRNA levels ≥ 2-fold compared to GT and PP2. mRNA levels (FPKM) shown as relative to maximum per gene across time course.
(F) Box plots of mRNA levels for genes shown in E. *p < 0.005, Wilcoxon.
(G) LSD1, RXR, H3K4me2, and H3K27ac ChIP-seq profiles at enhancers near HOXA1 and HOXC4.
GT, primitive gut tube; PP1, early pancreatic progenitors; PP2, late pancreatic progenitors.
See also Figure S3 and Tables 1-3.

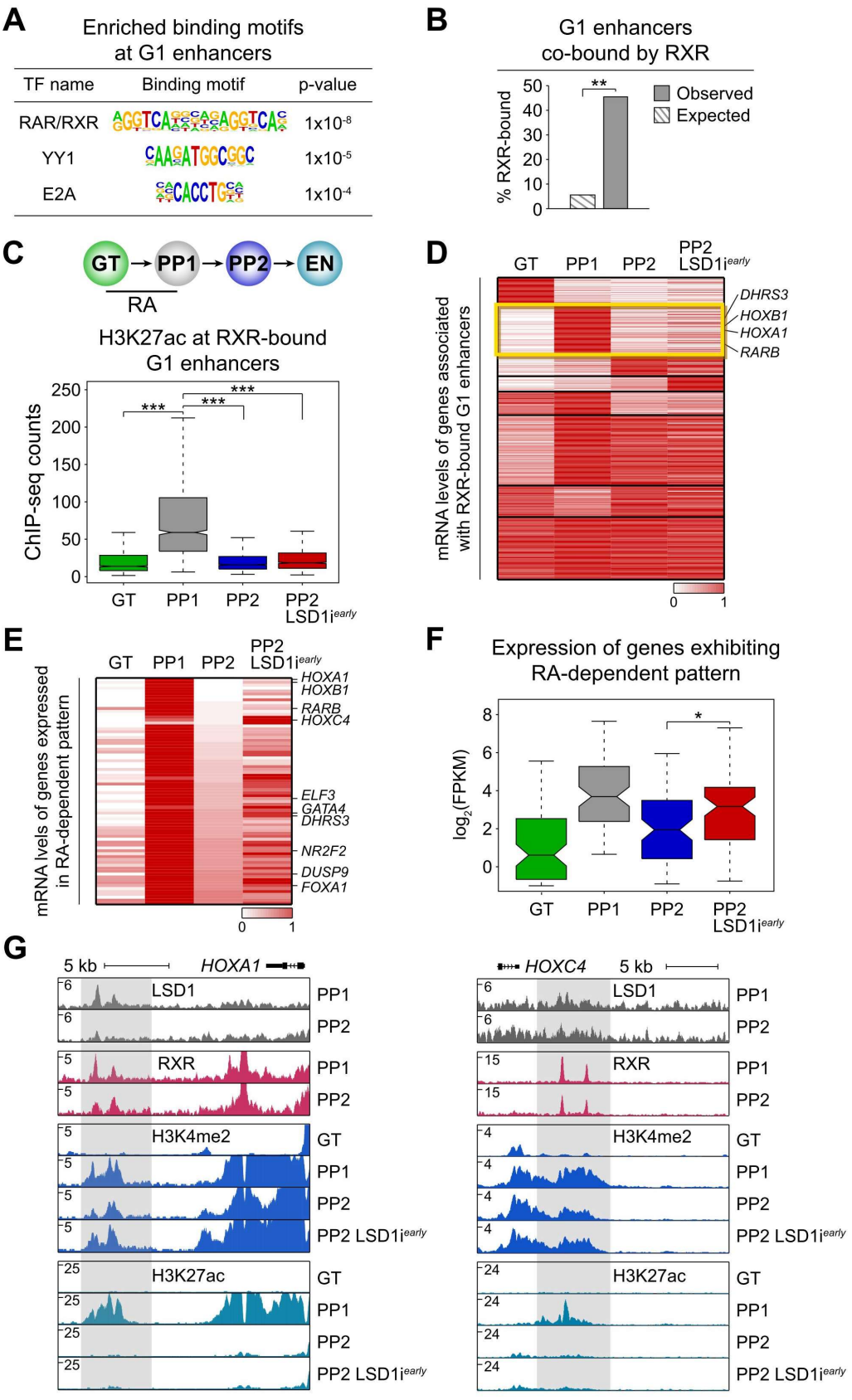
A
Enriched binding motifs at G1 enhancers
TF name
Binding motif
p-value
RAR/RXR
1x10-8
YY1
1x10-5
E2A
1x10-4
B
G1 enhancers co-bound by RXR
% RXR-bound
Observed
Expected
C
GT
PP1
PP2
EN
RA
H3K27ac at RXR-bound G1 enhancers
ChIP-seq counts
PP2 LSD1iearly
D
mRNA levels of genes associated with RXR-bound G1 enhancers
DHRS3
HOXB1
HOXA1
RARB
E
mRNA levels of genes expressed in RA-dependent pattern
HOXA1
HOXB1
RARB
HOXC4
ELF3
GATA4
DHRS3
NR2F2
DUSP9
FOXA1
F
Expression of genes exhibiting RA-dependent pattern
log2(FPKM)
G
5 kb
HOXA1
HOXC4
LSD1
RXR
H3K4me2
H3K27ac
PP1
PP2
PP2 LSD1iearly

Figure 4. Prolonged retinoic acid exposure of early pancreatic progenitor cells phenocopies LSD1 inhibition.

(A) Experimental plan to extend retinoic acid (RA) exposure through the PP1 to PP2 transition (RAextended) during hESC differentiation to the endocrine cell stage (EN).
(B) Heatmap of gene expression for the 74 PP1-specific genes associated with RXR-bound G1 enhancers (Table 3) at PP2 with and without extended RA treatment ($RA^{extended}$).
(C) Relative normalized expression of select genes from group in (B) at PP2 with and without extended RA treatment ($RA^{extended}$). Data shown as mean ± S.E.M. relative to control values (blue bars), which were set to 1. *$p < 0.05$; **$p < 0.0005$, DESeq2 output.
(D) Immunofluorescent staining for insulin (INS), glucagon (GCG) and somatostatin (SST) in control EN cells compared to EN cells with extended RA treatment ($RA^{extended}$). Scale bar, 50 μm.
(E) Flow cytometry analysis at EN stage for NKX6.1, PDX1 and INS comparing control and RAextended cultures. Isotype control for each antibody is shown in red and target protein staining in green. Percentage of cells expressing each protein is indicated.
GT, primitive gut tube; PP1, early pancreatic progenitors; PP2, late pancreatic progenitors.
See also Figure S4.

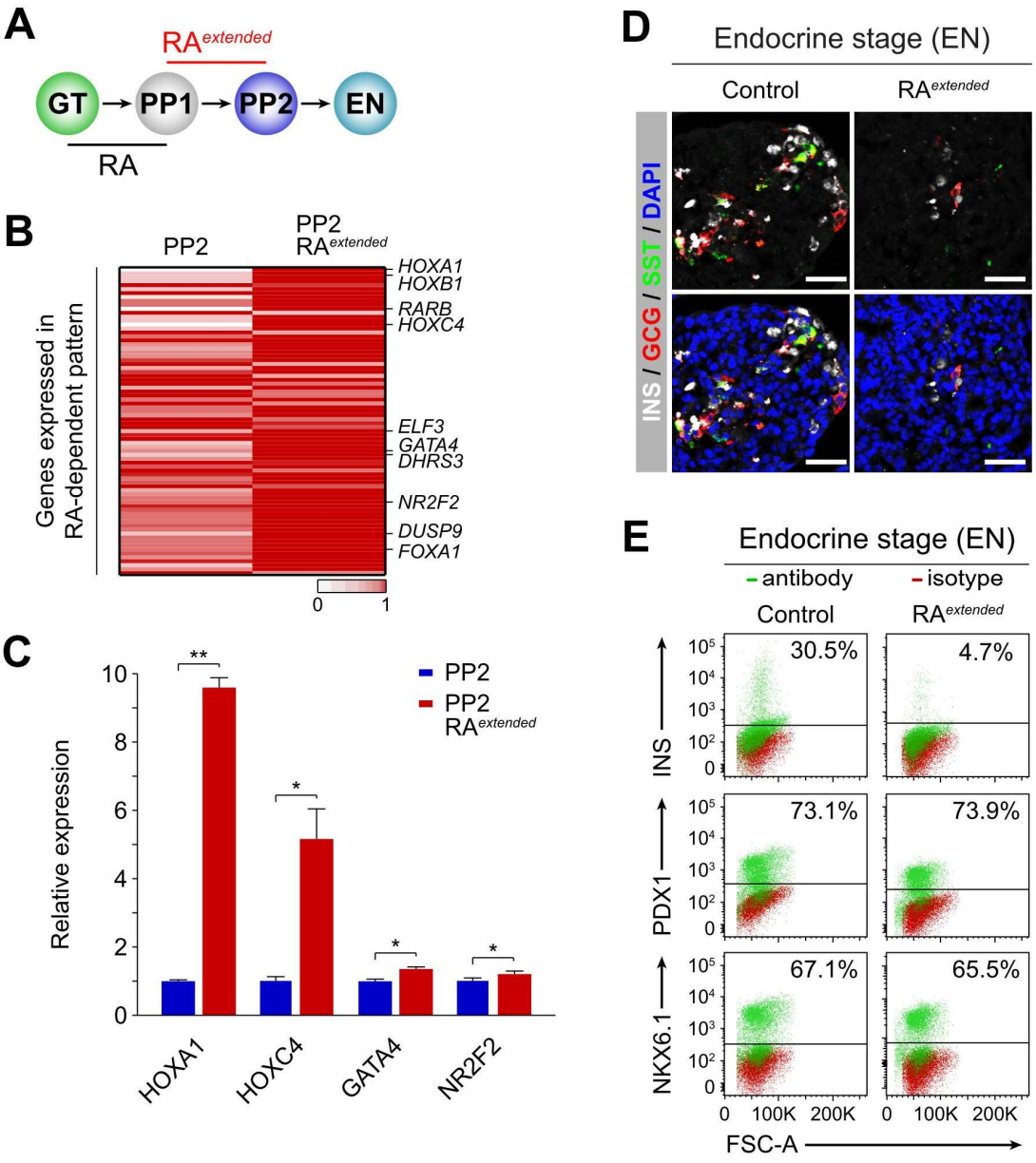
A
RA extended
GT
PP1
PP2
EN
RA
B
PP2
PP2 RA extended
Genes expressed in RA-dependent pattern
HOXA1
HOXB1
RARB
HOXC4
ELF3
GATA4
DHRS3
NR2F2
DUSP9
FOXA1
0
1
C
Relative expression
PP2
PP2 RA extended
HOXA1
HOXC4
GATA4
NR2F2
D
Endocrine stage (EN)
Control
RA extended
INS / GCG / SST / DAPI
E
Endocrine stage (EN)
antibody
isotype
Control
RA extended
INS
PDX1
NKX6.1
30.5%
4.7%
73.1%
73.9%
67.1%
65.5%
FSC-A

Figure 5. LSD1 prevents aberrant reactivation of transient early retinoic acid-dependent genes.

(A) Experimental plan to re-introduce retinoic acid (RA) during the PP2 to endocrine (EN) transition (RA^{late}) of hESC differentiation.
(B) Immunofluorescent staining for insulin (INS), glucagon (GCG) and somatostatin (SST) in control EN cells compared to EN cells with late RA treatment (RA^{late}). Scale bar, 50 μm.
(C) Flow cytometry analysis at EN stage for NKX6.1, PDX1 and INS comparing control and RA^{late} cells. Isotype control for each antibody is shown in red and target protein staining in green. Percentage of cells expressing each protein is indicated.
(D) Heatmap of gene expression for the 74 PP1-specific genes associated with RXR-bound G1 enhancers (Table 3) at EN stage with and without late RA treatment (RA^{late}).
(E) Relative normalized expression of select genes from group in (D) at EN stage with and without late RA treatment (RA^{late}). Data shown as mean ± S.E.M. relative to control values (blue bars), which were set to 1. n.s., not significant; DESeq2 output.
(F) Experimental plan to re-introduce RA during the PP2 to EN transition (RA^{late}) after early inhibition of LSD1 ($LSD1i^{early}$).
(G) Immunofluorescent staining for INS, GCG and SST in control EN cells compared to LSD1iearly EN cells with and without late RA treatment (RA^{late}). Scale bar, 50 μm.
(H) Heatmap of gene expression for the 74 PP1-specific genes associated with RXR-bound G1 enhancers (Table 3) at EN stage with LSD1iearly alone and LSD1iearly plus late RA treatment (RA^{late}).
(I) Relative normalized expression of select genes from group in (H) at EN stage with $LSD1i^{early}$ alone and $LSD1i^{early}$ plus late RA treatment (RA^{late}). Data shown as mean ± S.E.M. relative to $LSD1i^{early}$ values (blue bars), which were set to 1. *$p < 0.05$; **$p < 0.005$, ***$p < 1e\text{-}17$. DESeq2 output.
GT, primitive gut tube; PP1, early pancreatic progenitors; PP2, late pancreatic progenitors.
See also Figure S5.

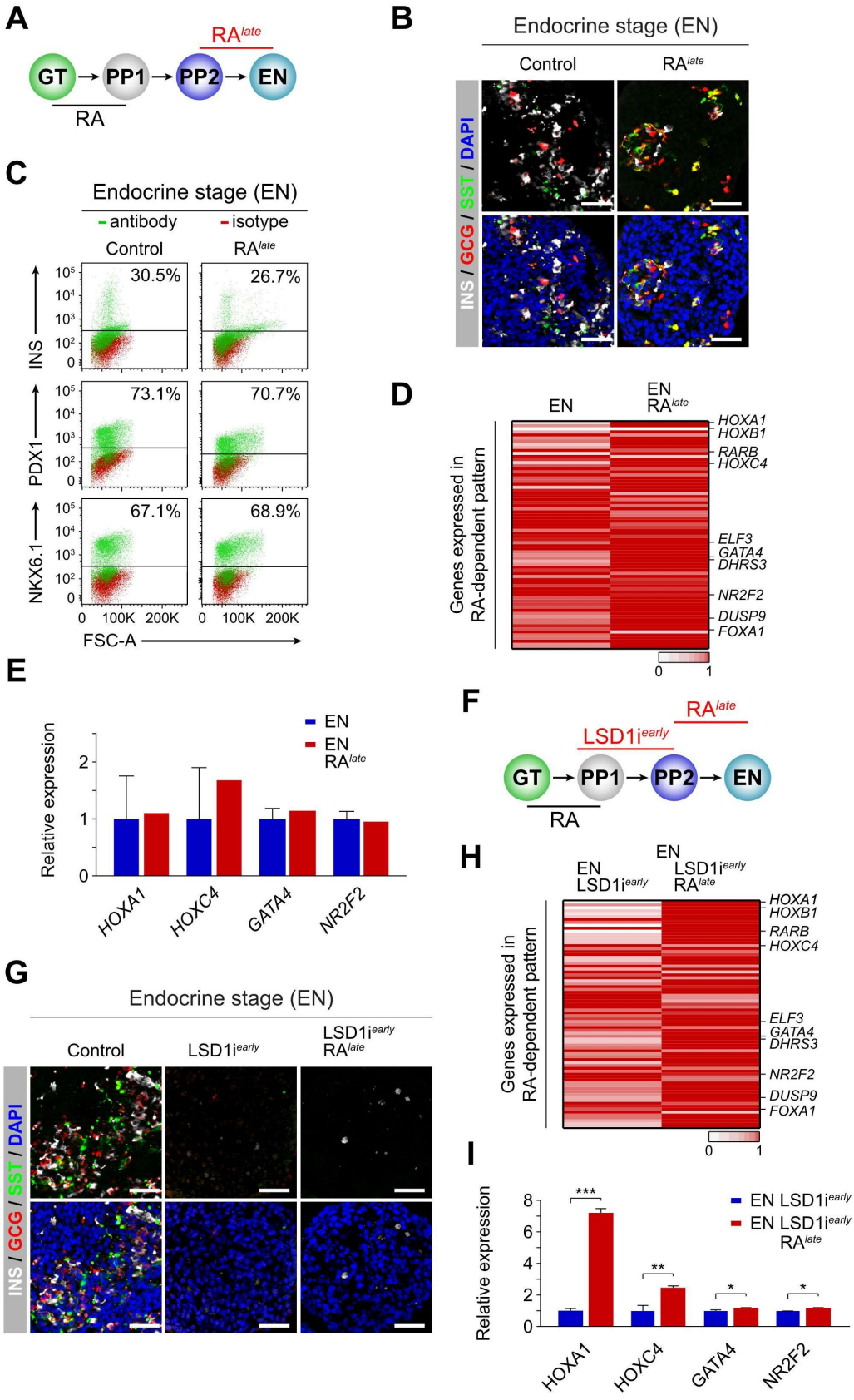
A
RA^late
GT
PP1
PP2
EN
RA
B
Endocrine stage (EN)
Control
RA^late
INS / GCG / SST / DAPI
C
Endocrine stage (EN)
antibody
isotype
Control
RA^late
30.5%
26.7%
73.1%
70.7%
67.1%
68.9%
INS
PDX1
NKX6.1
FSC-A
D
EN
EN RA^late
Genes expressed in RA-dependent pattern
HOXA1
HOXB1
RARB
HOXC4
ELF3
GATA4
DHRS3
NR2F2
DUSP9
FOXA1
E
Relative expression
EN
EN RA^late
HOXA1
HOXC4
GATA4
NR2F2
F
RA^late
LSD1i^early
GT
PP1
PP2
EN
RA
G
Endocrine stage (EN)
Control
LSD1i^early
LSD1i^early RA^late
INS / GCG / SST / DAPI
H
EN
EN LSD1i^early
EN LSD1i^early RA^late
Genes expressed in RA-dependent pattern
HOXA1
HOXB1
RARB
HOXC4
ELF3
GATA4
DHRS3
NR2F2
DUSP9
FOXA1
I
Relative expression
EN LSD1i^early
EN LSD1i^early RA^late
HOXA1
HOXC4
GATA4
NR2F2

Figure 6. Selective requirement for *Lsd1* in endocrine cell formation during a short window in early pancreatic development of mice.

(A) Strategy for conditional *Lsd1* deletion in embryonic pancreatic progenitors of mice (*Lsd1*$^{\Delta pan}$). Yellow boxes: exons; green triangles: *loxP* sites.
(B) Immunofluorescent staining for Pdx1 at embryonic day (e) 12.5 and Lsd1, insulin (Ins) and glucagon (Gcg) at postnatal day (P) 0 in control and *Lsd1*$^{\Delta pan}$ mice. Boxed areas are shown in higher magnification. Scale bar, 50 μm.
(C) Quantification of pancreatic epithelial area at e12.5 and e15.5. Data shown as means ± SEM (n = 3 biological replicates). n.s., not significant, Student t-test.
(D) Immunofluorescent staining for Ins with somatostatin (Sst), pancreatic polypeptide (Ppy) and ghrelin (Ghrl) at P0 in control and *Lsd1*$^{\Delta pan}$ mice. Scale bar, 25 μm.
(E) Strategy for tamoxifen-inducible *Lsd1* deletion in embryonic pancreatic progenitors of mice at e10.5 (*Lsd1*$^{\Delta early}$) and e12.5 (*Lsd1*$^{\Delta late}$). Yellow boxes: exons; green triangles: *loxP* sites.
(F) Immunofluorescent staining for Lsd1, Ins and Gcg at e18.5 in control, *Lsd1*$^{\Delta early}$ and *Lsd1*$^{\Delta late}$ mice. Boxed areas are shown in higher magnification. Scale bar, 50 μm.
(G) Heatmap of gene expression in dissected pancreata from control and *Lsd1*$^{\Delta pan}$ mice at e13.5. Shown are PP1-specific genes associated with RXR-bound G1 enhancers (Table 3).
(H) Relative normalized expression of select genes from group in (G) in *Lsd1*$^{\Delta pan}$ mice at e13.5. Data shown as mean ± S.E.M. relative to control values (blue bars), which were set to 1. *p < 0.05; **p < 0.01; **p < 5e-5; n.s., not significant, DESeq2 output.
See also Figure S6.

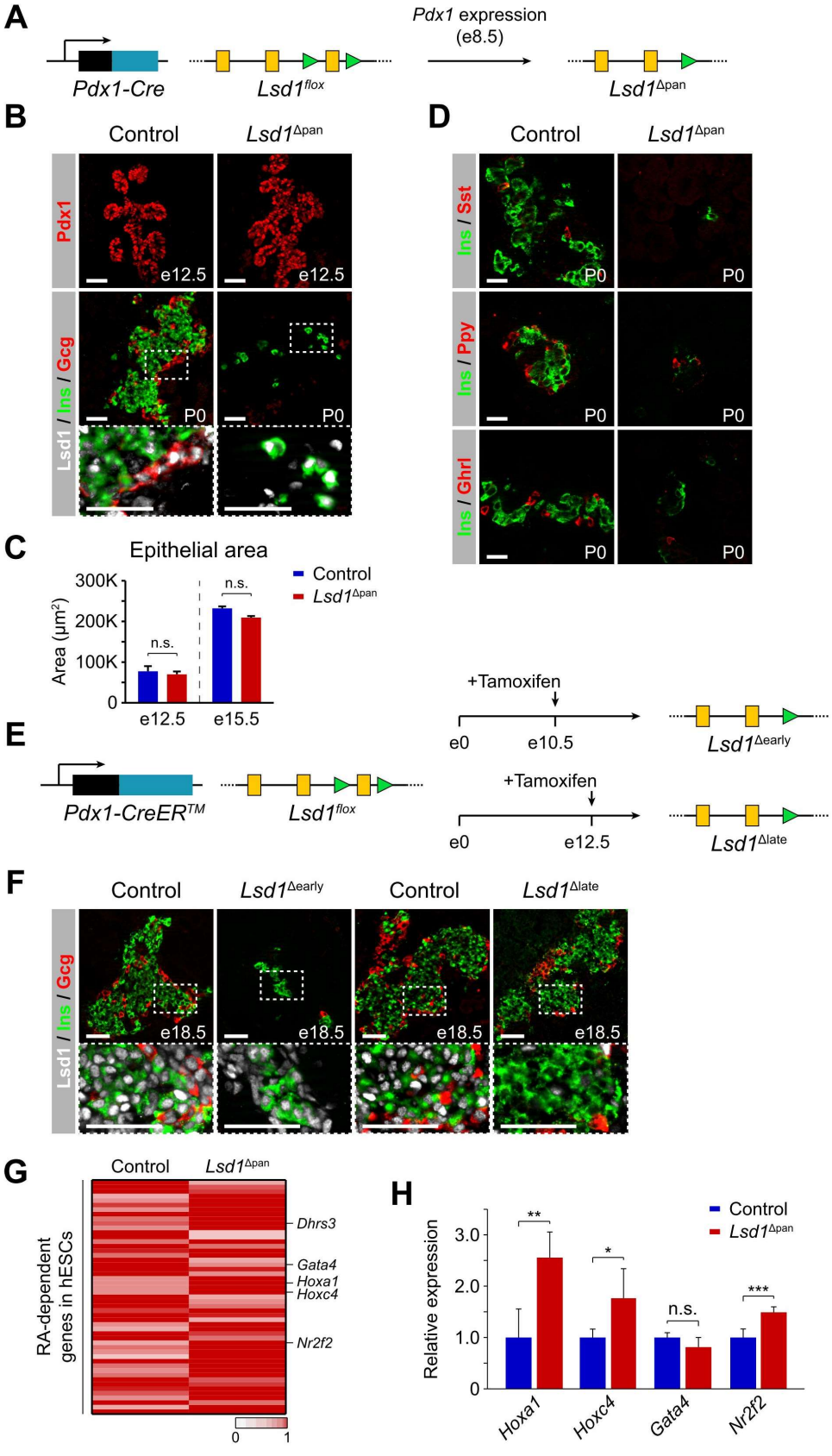
A
Pdx1 expression
(e8.5)
Pdx1-Cre
Lsd1flox
Lsd1Δpan
B
Control
Lsd1Δpan
Pdx1
e12.5
Lsd1 / Ins / Gcg
P0
D
Ins / Sst
Ins / Ppy
Ins / Ghrl
C
Epithelial area
Control
Lsd1Δpan
Area (μm2)
300K
200K
100K
0
n.s.
e12.5
e15.5
E
Pdx1-CreERTM
+Tamoxifen
e0
e10.5
Lsd1Δearly
e12.5
Lsd1Δlate
F
Control
Lsd1Δearly
Control
Lsd1Δlate
e18.5
G
RA-dependent genes in hESCs
Dhrs3
Gata4
Hoxa1
Hoxc4
Nr2f2
0
1
H
Relative expression
3.0
2.0
1.0
0
**
*
n.s.
***
Hoxa1
Hoxc4
Gata4
Nr2f2

Figure S1. Related to Figure 1. Characterization of LSD1 expression and effects of LSD1 inhibition on pancreatic progenitor cells.

(A) Immunofluorescent staining for LSD1 with insulin (INS), glucagon (GCG) and somatostatin (SST) in adult human pancreas. Scale bar, 10 μm.
(B) *LSD1* mRNA expression at each stage of differentiation determined by RNA-seq, measured in fragments per kilobase per million fragments mapped (FPKM). Values shown as $\log_2$(FPKM).
(C) Immunofluorescent staining for LSD1 at each stage of hESC differentiation. Scale bar, 25 μm.
(D) Immunofluorescent staining for NKX6.1 and PDX1 in control and LSD1i^{early} PP2 cells. Scale bar, 50 μm.
(E) Flow cytometry analysis for NKX6.1 and PDX1 comparing control and LSD1i^{early} PP2 cells.
ES, embryonic stem cell; DE, definitive endoderm; GT, primitive gut tube; PP1, early pancreatic progenitors; PP2, late pancreatic progenitors; EN, endocrine cell stage; FSC-A, forward scatter area.

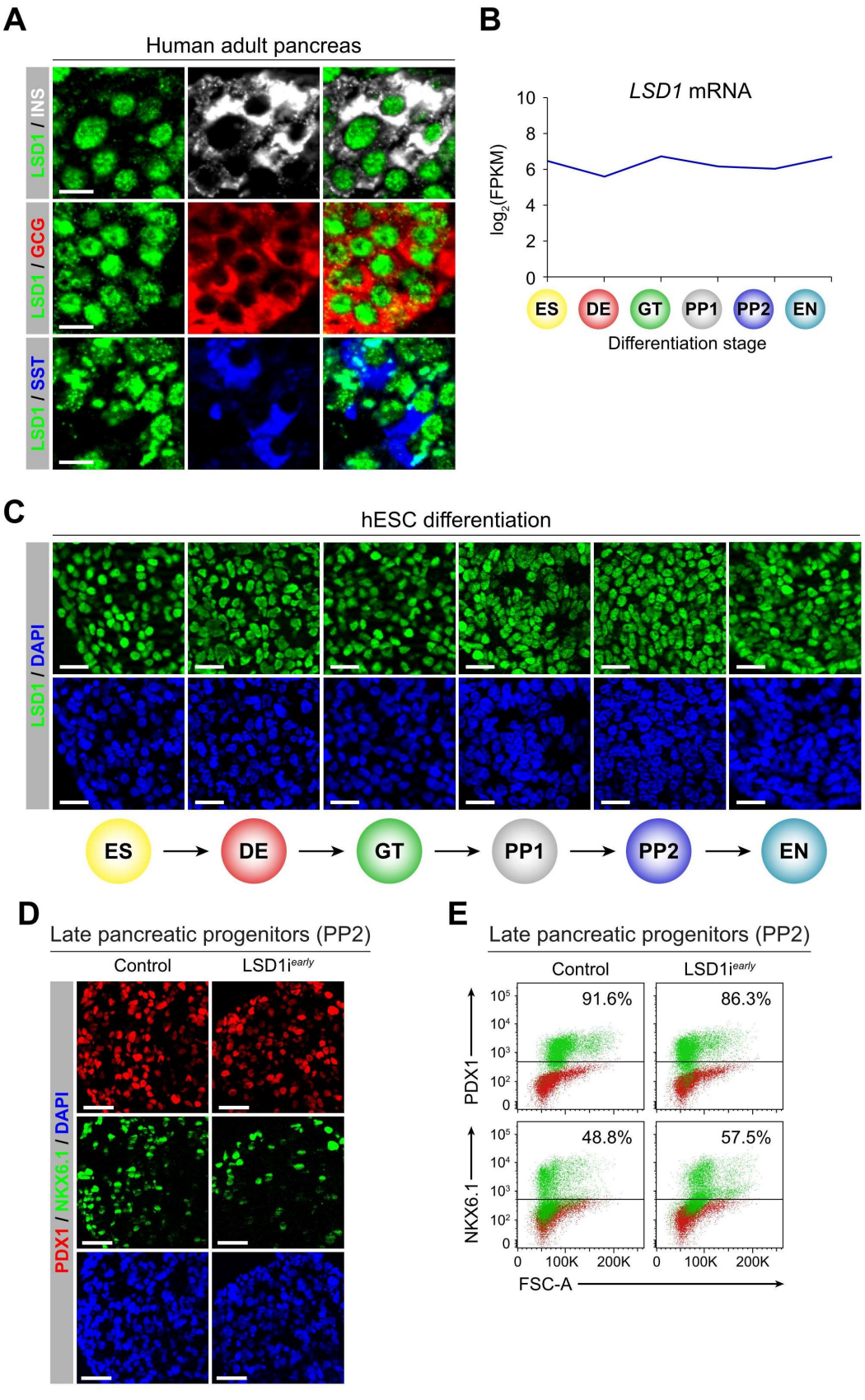
A
Human adult pancreas
LSD1 / INS
LSD1 / GCG
LSD1 / SST
B
LSD1 mRNA
log2(FPKM)
10
8
6
4
2
0
ES
DE
GT
PP1
PP2
EN
Differentiation stage
C
hESC differentiation
LSD1 / DAPI
ES
DE
GT
PP1
PP2
EN
D
Late pancreatic progenitors (PP2)
Control
LSD1i early
PDX1 / NKX6.1 / DAPI
E
Late pancreatic progenitors (PP2)
Control
LSD1i early
91.6%
86.3%
48.8%
57.5%
PDX1
NKX6.1
0
100K
200K
FSC-A

Figure S2. Related to Figure 2. Characterization of LSD1-bound genomics regions.

(A) LSD1 peak localization across the genome relative to transcriptional start sites (TSSs). 15,084 total LSD1 peaks identified in PP1. 3,285 peaks are proximal (within 3kb of a TSS) and 11,799 distal (> 3kb from a TSS).
(B) Tag density plots for G2 and G3 enhancers displaying H3K27ac, H3K4me2 and H3K4me1 tag distribution at P1 stage and PP2 stage with and without early LSD1 inhibition (LSD1i^{early}). Plots are centered on PP1 LSD1 peaks.
UTR, untranslated region; TTS, transcription termination site; ncRNA, non-coding RNA; PP1, early pancreatic progenitors; PP2, late pancreatic progenitors.

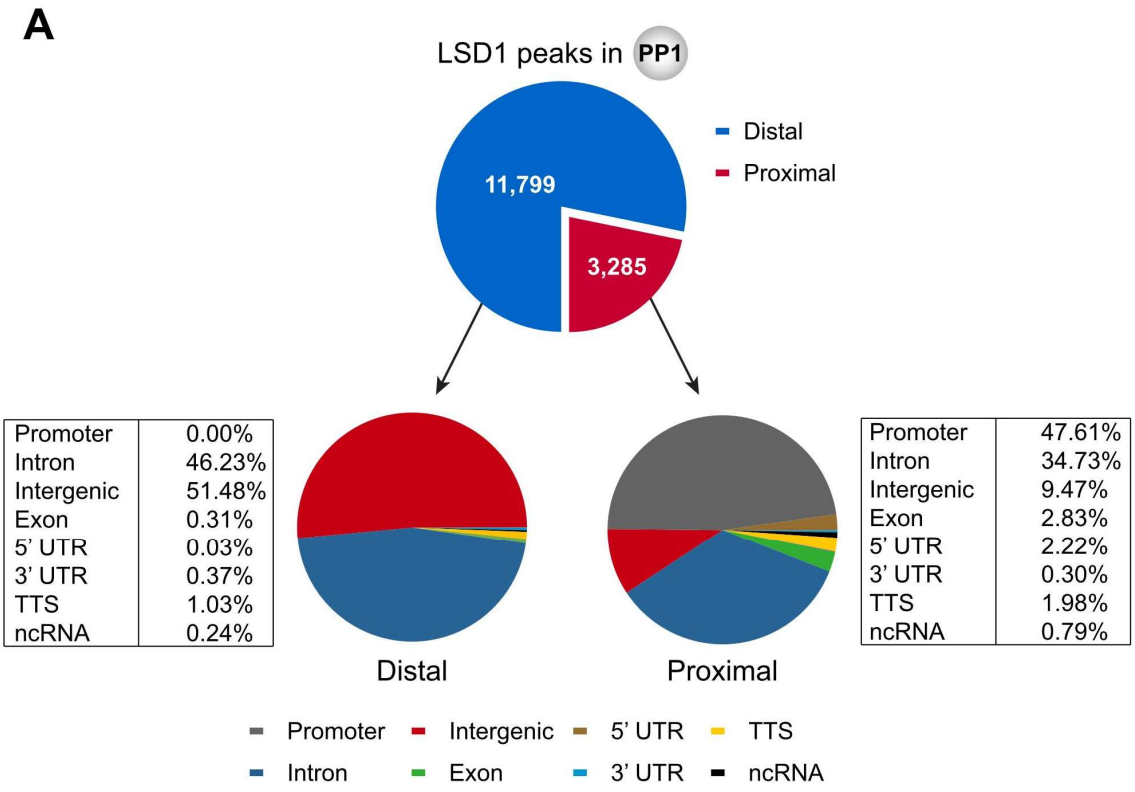
A
LSD1 peaks in PP1
Distal
Proximal
11,799
3,285
Promoter 0.00%
Intron 46.23%
Intergenic 51.48%
Exon 0.31%
5' UTR 0.03%
3' UTR 0.37%
TTS 1.03%
ncRNA 0.24%
Promoter 47.61%
Intron 34.73%
Intergenic 9.47%
Exon 2.83%
5' UTR 2.22%
3' UTR 0.30%
TTS 1.98%
ncRNA 0.79%
Distal
Proximal
Promoter
Intron
Intergenic
Exon
5' UTR
3' UTR
TTS
ncRNA

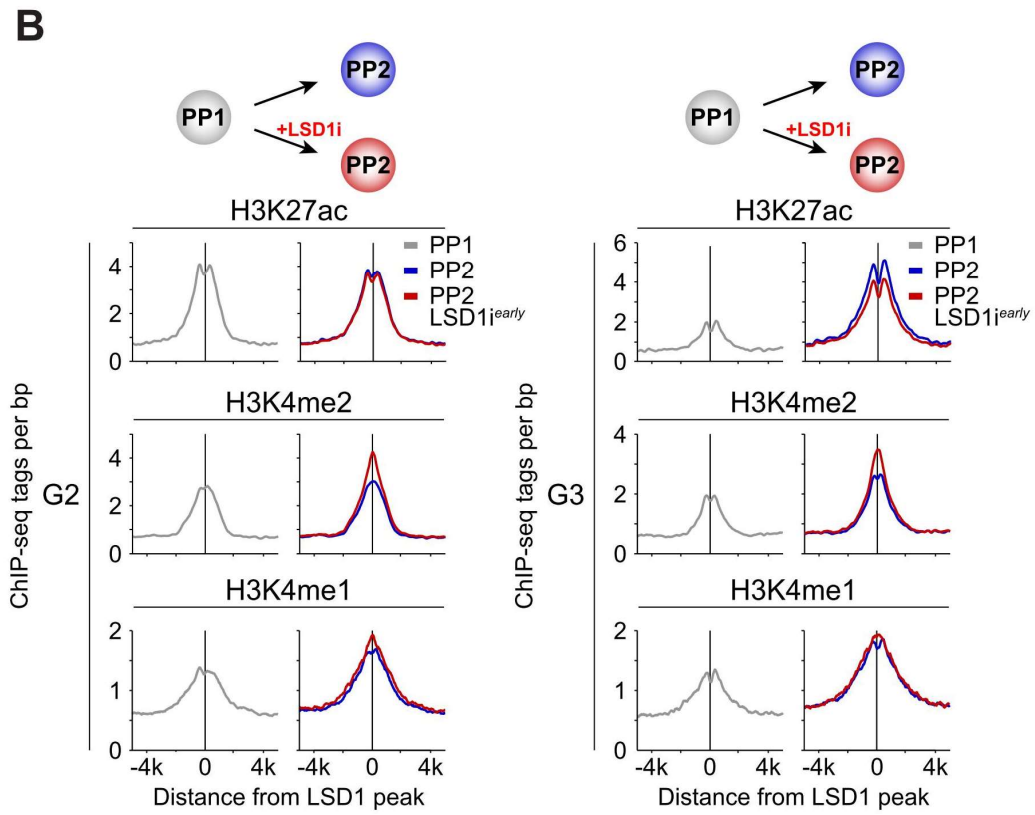
B
PP1
PP2
+LSD1i
PP2
H3K27ac
H3K4me2
H3K4me1
PP1
PP2
PP2 LSD1i early
ChIP-seq tags per bp
G2
G3
-4k
0
4k
Distance from LSD1 peak

Figure S3. Related to Figure 3. G1 enhancers exhibit greater enrichment for RXR binding than G2 and G3 enhancers.

(A) Percentage of G1, G2 and G3 enhancers versus random genomic regions bound by RXR within ± 10kb of LSD1 peak at the PP1 stage. Significantly higher enrichment in G1 enhancers than in G2 and G3 enhancers. **p < 5e-4, chi-square.
(B) Changes in H3K4me1 and H3K4me2 levels at RXR-bound G1 enhancers during human embryonic stem cell differentiation with and without LSD1 inhibition (LSD1i^{early}). *p < 0.005; ***p < 2.2e-16; n.s., not significant, Wilcoxon.
(C) Relative normalized gene expression at the PP2 stage with and without early LSD1 inhibition (LSD1i^{early}). Genes were selected from group of 74 genes exhibiting RA-dependent expression (Fig. 3E; Table 3). Data shown as mean ± S.E.M. relative to control values (blue bars), which were set to 1. *p < 0.005; **p < 5e-4, DESeq2 output.
(D) LSD1, RXR, H3K4me2, and H3K27ac ChIP-seq profiles at enhancers near *GATA4* and *DHRS3*.
GT, primitive gut tube; PP1, early pancreatic progenitors; PP2, late pancreatic progenitors.

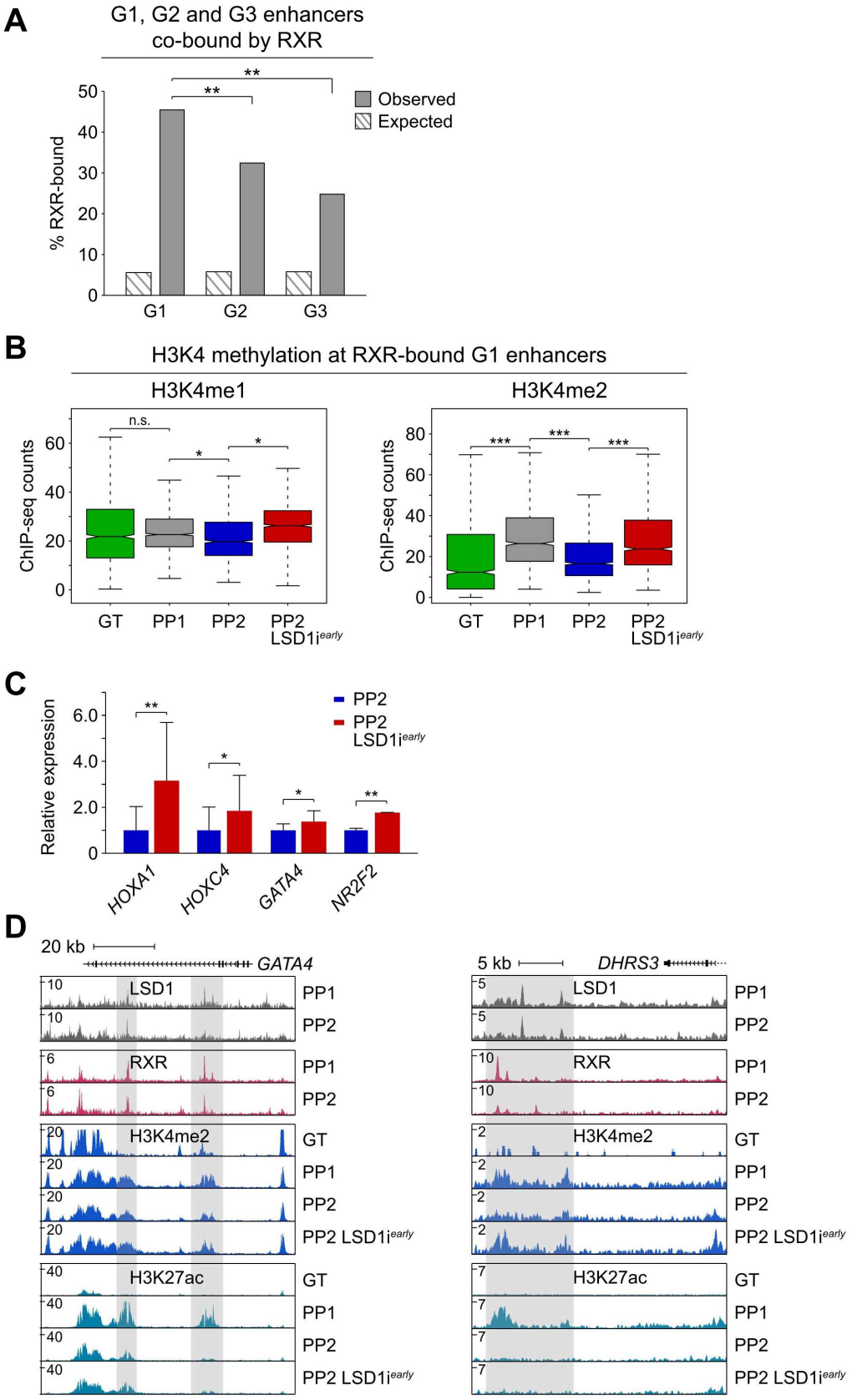
A
G1, G2 and G3 enhancers co-bound by RXR
% RXR-bound
Observed
Expected
G1
G2
G3
B
H3K4 methylation at RXR-bound G1 enhancers
H3K4me1
H3K4me2
ChIP-seq counts
n.s.
GT
PP1
PP2
PP2 LSD1i early
C
Relative expression
PP2
PP2 LSD1i early
HOXA1
HOXC4
GATA4
NR2F2
D
20 kb
GATA4
5 kb
DHRS3
LSD1
RXR
H3K4me2
H3K27ac
GT
PP1
PP2
PP2 LSD1i early

Figure S4. Related to Figure 4. Effects of prolonged retinoic acid treatment on pancreatic progenitor and endocrine cell phenotypes.

(A) Box plot of mRNA levels for genes exhibiting retinoic acid (RA)-dependent pattern (Table 3) comparing control and RA^{extended} PP2 cells. *p < 0.01, Wilcoxon.
(B) qRT-PCR analysis for *insulin* (*INS)*, *glucagon* (*GCG)* and *somatostatin* (*SST)* in control and RA^{extended} EN cells. Data are shown as average ± S.E.M (n = 2 biological replicates). **p < 0.001, Student t-test.
(C) Immunofluorescent staining for PDX1 and NKX6.1 in control endocrine stage cells (EN) compared to EN cells with extended RA treatment (RA^{extended}). Scale bar, 50 μm.
GT, primitive gut tube; PP1, early pancreatic progenitors; PP2, late pancreatic progenitors.

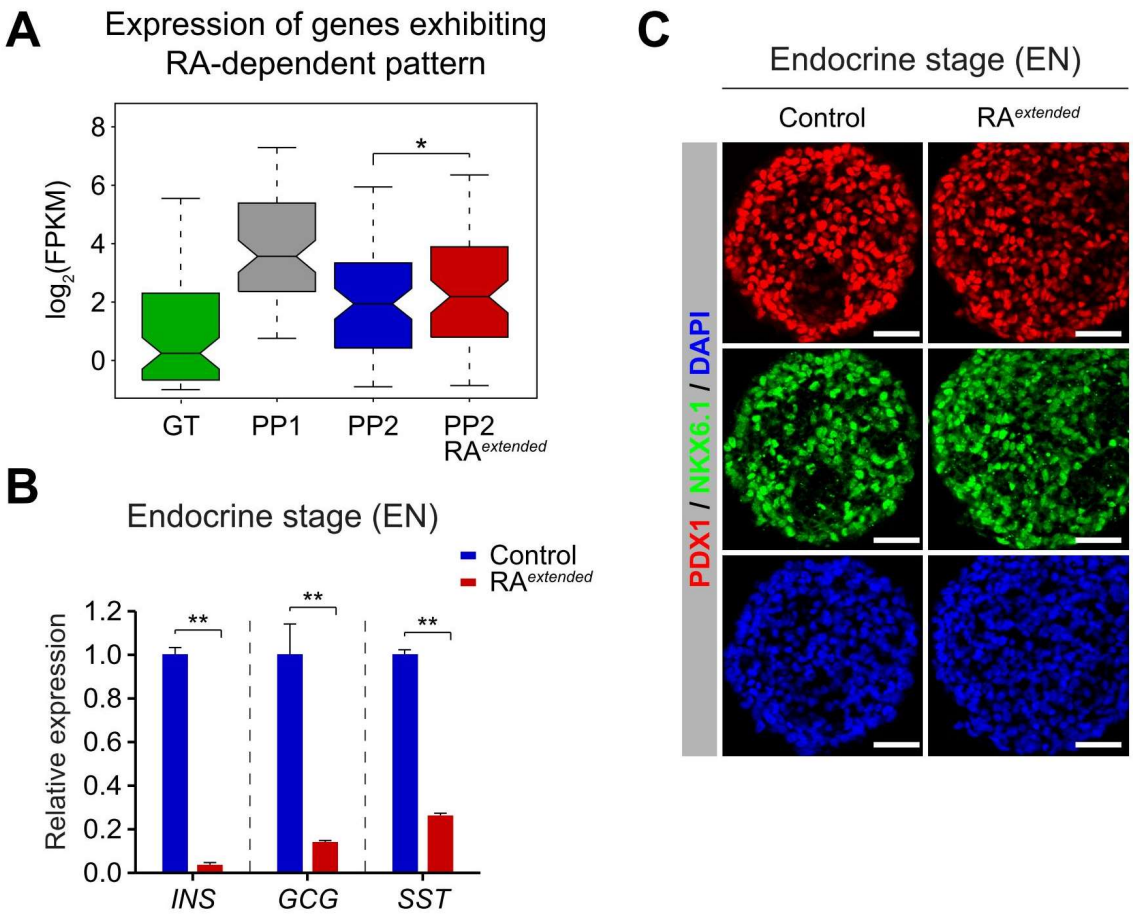
A
Expression of genes exhibiting RA-dependent pattern
log2(FPKM)
8
6
4
2
0
*
GT
PP1
PP2
PP2 RA extended
B
Endocrine stage (EN)
Control
RA extended
Relative expression
1.2
1.0
0.8
0.6
0.4
0.2
0.0
**
**
**
INS
GCG
SST
C
Endocrine stage (EN)
Control
RA extended
PDX1 / NKX6.1 / DAPI

Figure S5. Related to Figure 5. Effects of re-introducing retinoic acid during endocrine cell differentiation with and without prior LSD1 inhibition.

(A) Immunofluorescent staining for PDX1 and NKX6.1 in control endocrine stage cells (EN) compared to EN cells with late retinoic acid (RA) treatment (RA^{late}). Scale bar, 50 μm.
(B) qRT-PCR analysis for *INS*, *GCG* and *SST* in control and RA^{late} EN cells. Data are shown as average ± S.E.M (n = 2 biological replicates).
(C) Box plot of mRNA levels for genes exhibiting RA-dependent pattern (Table 3) comparing control and RA^{late} EN cells. n.s., not significant.
(D) Flow cytometry analysis at EN stage for NKX6.1, PDX1 and INS comparing control EN cells to $LSD1i^{early}$ EN cells with and without late RA treatment (RA^{late}). Isotype control for each antibody is shown in red and target protein staining in green. Percentage of cells expressing each protein is indicated.
(E) Box plot of mRNA levels for genes exhibiting RA-dependent pattern (Table 3) comparing EN cells treated with $LSD1i^{early}$ alone and $LSD1i^{early}$ plus RA^{late}. *$p < 0.005$, Wilcoxon.
(F) Tag density plots displaying RXR tag distribution at RXR-bound G1 enhancers at the PP1 stage and PP2 stage with and without LSD1 inhibition ($LSD1i^{early}$). Plots are centered on PP1 LSD1 peaks.
GT, primitive gut tube; PP1, early pancreatic progenitors; PP2, late pancreatic progenitors; EN, endocrine stage; FSC-A, forward scatter area.

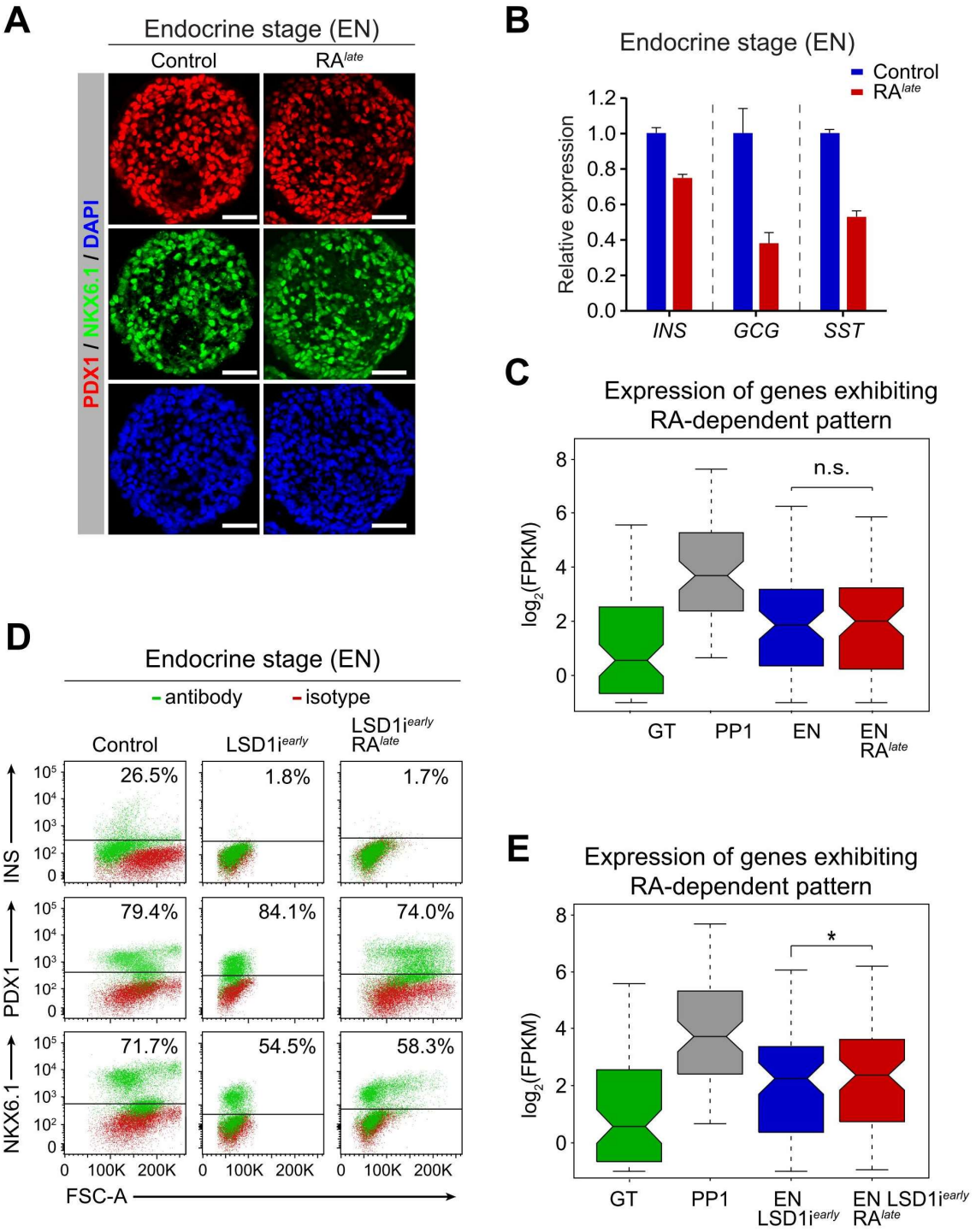
A
Endocrine stage (EN)
Control
RA late
PDX1 / NKX6.1 / DAPI
B
Endocrine stage (EN)
Control
RA late
Relative expression
1.2
1.0
0.8
0.6
0.4
0.2
0.0
INS
GCG
SST
C
Expression of genes exhibiting RA-dependent pattern
log2(FPKM)
n.s.
GT
PP1
EN
EN RA late
D
Endocrine stage (EN)
antibody
isotype
Control
LSD1i early
LSD1i early RA late
INS
PDX1
NKX6.1
26.5%
1.8%
1.7%
79.4%
84.1%
74.0%
71.7%
54.5%
58.3%
0
100K
200K
FSC-A
E
Expression of genes exhibiting RA-dependent pattern
log2(FPKM)
*
GT
PP1
EN LSD1i early
EN LSD1i early RA late

Figure S6. Related to Figure 6. Phenotypic characterization of *Lsd1*$^{\Delta pan}$ mice.

(A) Immunofluorescent staining of embryonic (e) and neonatal (P0) mouse pancreas for Lsd1 with the pancreatic progenitor markers Pdx1 and Sox9, the acinar marker carboxypeptidase 1 (Cpa1) or insulin (Ins) and glucagon (Gcg). Boxed areas are shown in higher magnification. Scale bar, 50 μm.
(B) Immunofluorescent staining for Lsd1 with Ins, Gcg and Sst in mice at P0. Scale bar, 10 μm.
(C) Immunofluorescent staining of pancreas (Pan) from control and *Lsd1*$^{\Delta pan}$ embryos for Lsd1, Ptf1a, Nkx6.1, phospho histone H3 (pHH3), Pdx1, E-cadherin (Cdh1), osteopontin (Opn), amylase (Amy), and TUNEL. The nuclear counterstain, 4′,6-diamidino-2-phenylindole (DAPI) is shown together with TUNEL staining. Scale bar, 50 μm.
(D) Quantification of pHH3^{+} cells at e12.5 and apoptotic cells (TUNEL^{+}) at e15.5 relative to pancreatic epithelial area. Data are shown means ± SEM (n = 3 biological replicates). n.s, not significant, Student t-test.
(E) Quantification of hormone^{+} cells staining positive for Lsd1 in control, *Lsd1*$^{\Delta pan}$, *Lsd1*$^{\Delta early}$, and *Lsd1*$^{\Delta late}$ mice at P0. A total of 189-1057 hormone^{+} cells (insulin^{+} or glucagon^{+}) were analyzed per genotype and set as 100% (n = 3 per genotype).
(F) Box plots of mRNA levels in mouse pancreas for PP1-specific genes associated with RXR-bound G1 enhancers (Table 3). Relative gene expression determined by microarray analysis of sorted Sox9^{+} pancreatic progenitor cells at e10.5 and e15.5 (left). Gene expression determined by RNA-seq of dissected pancreata from control and *Lsd1*$^{\Delta pan}$ mice at e13.5 (right) (n = 3 biological replicates).

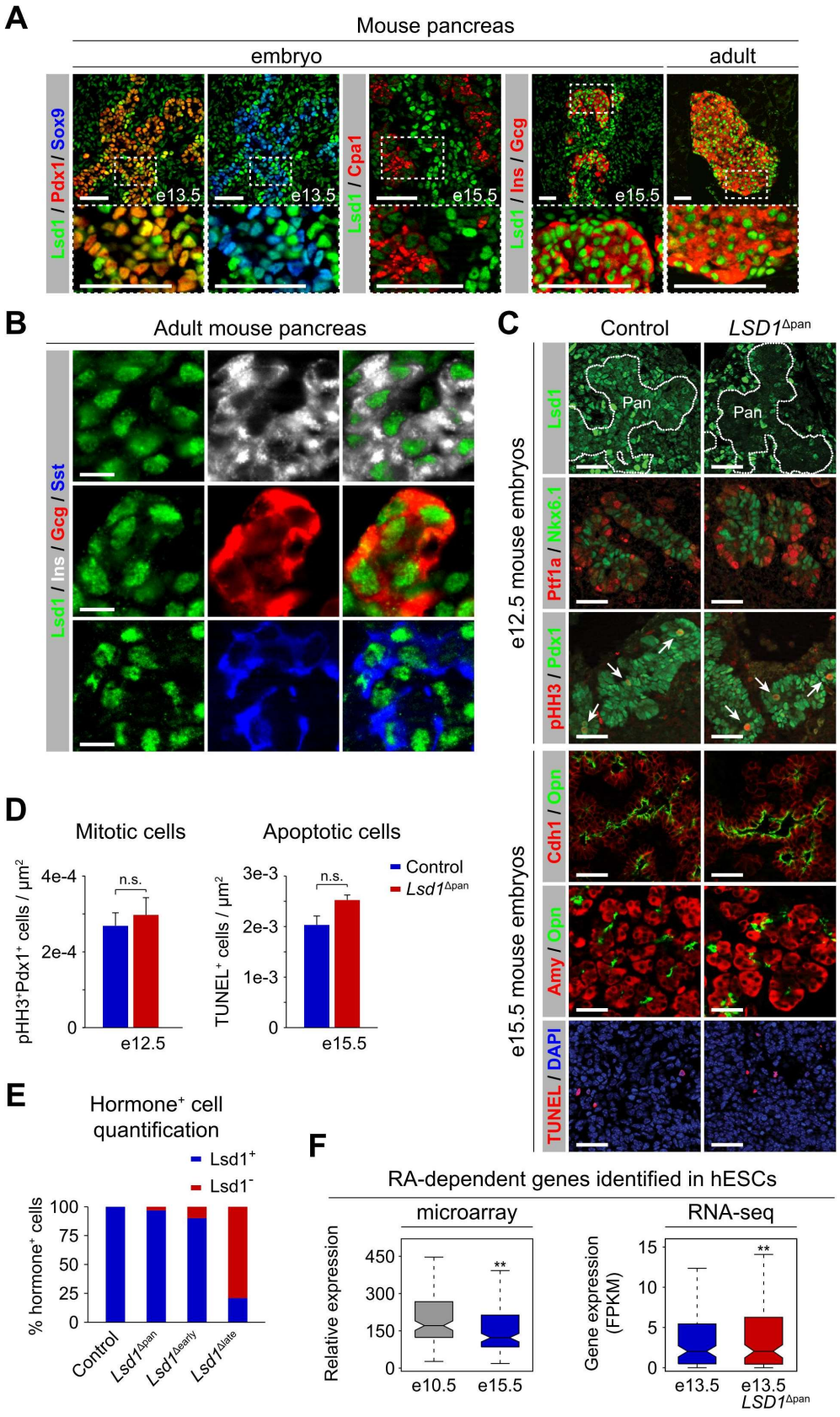
A
Mouse pancreas
embryo
adult
Lsd1 / Pdx1 / Sox9
Lsd1 / Cpa1
Lsd1 / Ins / Gcg
e13.5
e13.5
e15.5
e15.5
B
Adult mouse pancreas
Lsd1 / Ins / Gcg / Sst
C
Control
LSD1Δpan
e12.5 mouse embryos
e15.5 mouse embryos
Lsd1
Pan
Pan
Ptf1a / Nkx6.1
pHH3 / Pdx1
Cdh1 / Opn
Amy / Opn
TUNEL / DAPI
D
Mitotic cells
Apoptotic cells
pHH3+Pdx1+ cells / µm2
TUNEL+ cells / µm2
4e-4
2e-4
0
3e-3
2e-3
1e-3
0
n.s.
n.s.
e12.5
e15.5
Control
Lsd1Δpan
E
Hormone+ cell quantification
Lsd1+
Lsd1-
% hormone+ cells
100
75
50
25
0
Control
Lsd1Δpan
Lsd1Δearly
Lsd1Δlate
F
RA-dependent genes identified in hESCs
microarray
RNA-seq
Relative expression
450
300
150
0
e10.5
e15.5
**
Gene expression (FPKM)
15
10
5
0
e13.5
e13.5
LSD1Δpan
**

TABLES

Table 1. Chromosomal coordinates of 612 RXR-bound G1 enhancers identified in the early pancreatic progenitor (PP1) stage of pancreatic differentiation of hESCs.

chr	start	end	PeakID	chr	start	end	PeakID	chr	start	end	PeakID	chr	start	end	PeakID	chr	start	end	PeakID	chr	start	end	PeakID
chr8	74242644	74242851	chr8-248	chr15	85277586	85277793	chr15-48	chr5	136549123	136549330	chr5-347	chr19	18031406	18031613	chr19-836	chr19	7786650	7786857	chr19-357	chr6	119358586	119358793	chr6-150
chr11	69816867	69817074	chr11-22	chr1	42359834	42360041	chr1-49	chr10	95163876	95164083	chr10-226	chr7	75427823	75428030	chr7-326	chr5	115869359	115869566	chr5-225	chr15	40550517	40550724	chr15-235
chr10	10596384	10596591	chr10-198	chr12	68752815	68753022	chr12-615	chr11	72999703	72999910	chr11-95	chr16	85965562	85965769	chr16-869	chr16	11707837	11708044	chr16-28	chr11	66368266	66368473	chr11-1267
chr5	120062381	120062588	chr5-649	chrX	131119663	131119870	chrX-12	chr16	26208624	26208831	chr16-271	chr11	21020120	21020327	chr11-1707	chr20	37780918	37781125	chr20-68	chr20	44548178	44548385	chr20-136
chr18	29166590	29166797	chr18-65	chr18	71883973	71884180	chr18-121	chr10	120230457	120230664	chr10-32	chr4	114671960	114672167	chr4-215	chr7	66658530	66658737	chr7-751	chr15	75958037	75958244	chr15-108
chr9	123623612	123623819	chr9-233	chr10	76800347	76800554	chr10-479	chr2	5634826	5635033	chr2-110	chr7	139345069	139345276	chr7-30	chr15	68696866	68697073	chr15-16	chr3	51372613	51372820	chr3-110
chr1	204264623	204264830	chr1-610	chr22	38743880	38744087	chr22-276	chrX	143358654	143358861	chrX-120	chr12	121664660	121664867	chr12-1991	chr12	647976	648183	chr12-444	chr18	23232515	23232722	chr18-52
chr3	61516963	61517170	chr3-818	chr9	123148322	123148529	chr9-332	chr19	14654717	14654924	chr19-158	chr7	66824118	66824325	chr7-15	chr7	129598508	129598715	chr7-183	chr5	172731395	172731602	chr5-173
chr7	66825098	66825305	chr7-136	chr4	106101962	106102169	chr4-861	chr15	53739485	53739692	chr15-182	chr3	38029233	38029440	chr3-407	chr3	64519848	64520055	chr3-27	chr3	166547882	166548089	chr3-2336
chr1	12664462	12664669	chr1-129	chr3	156833365	156833572	chr3-115	chr2	28086919	28087126	chr2-289	chr9	26665008	26665215	chr9-1020	chr2	208081160	208081367	chr2-189	chr17	42621597	42621804	chr17-27
chr11	74258041	74258248	chr11-1283	chr4	100458379	100458586	chr4-35	chr3	57959875	57960082	chr3-616	chr16	25918917	25919124	chr16-26	chr10	101210781	101210988	chr10-100	chr1	98521593	98521800	chr1-402
chr17	66375380	66375587	chr17-935	chr15	96597103	96597310	chr15-173	chr3	59650073	59650280	chr3-364	chr15	79471593	79471800	chr15-683	chr6	35371897	35372104	chr6-488	chr14	96690608	96690815	chr14-291
chr9	74930636	74930843	chr9-896	chr13	28625121	28625328	chr13-415	chr16	66932938	66933145	chr16-379	chr7	27119427	27119634	chr7-58	chrX	36037414	36037621	chrX-56	chr19	47274452	47274659	chr19-640
chr14	65693769	65693976	chr14-89	chr6	91521405	91521612	chr6-90	chr10	117996830	117997037	chr10-129	chr1	112247523	112247730	chr1-797	chr10	80349424	80349631	chr10-204	chr3	69555457	69555664	chr3-4
chr20	22654976	22655183	chr20-302	chr17	3515725	3515932	chr17-307	chr1	22199658	22199865	chr1-1034	chr5	142275298	142275505	chr5-57	chr17	48195219	48195426	chr17-158	chr6	21403628	21403835	chr6-261
chr1	159132134	159132341	chr1-1888	chr2	121941727	121941934	chr2-149	chr9	114045754	114045961	chr9-137	chr1	183912226	183912433	chr1-813	chr18	11500910	11501117	chr18-57	chr11	129736152	129736359	chr11-200
chr20	36490357	36490564	chr20-199	chr7	30116459	30116666	chr7-522	chr3	128152293	128152500	chr3-122	chr10	87077307	87077514	chr10-190	chr22	32225289	32225496	chr22-332	chr16	85746206	85746413	chr16-25
chr1	179671650	179671857	chr1-7	chr9	80127887	80128094	chr9-452	chr2	205882513	205882720	chr2-246	chr16	46910711	46910918	chr16-111	chr12	114314086	114314293	chr12-744	chr1	44698190	44698397	chr1-470
chr8	110592422	110592629	chr8-151	chr5	127220919	127221126	chr5-227	chr4	82319200	82319407	chr4-249	chr12	60971810	60972017	chr12-16	chr16	87965868	87966075	chr16-584	chr6	100622553	100622760	chr6-284
chr1	156441225	156441432	chr1-276	chr22	29616840	29617047	chr22-46	chr7	156459796	156460003	chr7-64	chr17	78135229	78135436	chr17-188	chr14	64877062	64877269	chr14-78	chrY	6768252	6768459	chrY-15
chr4	8561502	8561709	chr4-64	chr3	140418721	140418928	chr3-751	chr6	43956591	43956798	chr6-179	chr7	126125923	126126130	chr7-47	chr1	177715592	177715799	chr1-253	chr14	68943000	68943207	chr14-127
chr6	54743996	54744203	chr6-499	chr12	76801606	76801813	chr12-621	chr9	114717467	114717674	chr9-1302	chr14	77803705	77803912	chr14-549	chr2	5634320	5634527	chr2-154	chr16	56335004	56335211	chr16-196
chr11	75053774	75053981	chr11-400	chr1	162317153	162317360	chr1-117	chr5	175101205	175101412	chr5-75	chr5	115860702	115860909	chr5-63	chr3	197274801	197275008	chr3-1012	chr3	61630985	61631192	chr3-928
chr6	33597000	33597207	chr6-222	chr15	93325562	93325769	chr15-335	chr20	44547450	44547657	chr20-165	chr8	125733095	125733302	chr8-21	chr1	228556046	228556253	chr1-154	chr20	45757994	45758201	chr20-64
chr12	53509733	53509940	chr12-810	chr20	30913609	30913816	chr20-140	chr1	59569238	59569445	chr1-361	chr16	78274927	78275134	chr16-147	chr19	17608987	17609194	chr19-1337	chr16	52299194	52299401	chr16-816
chr11	60774838	60775045	chr11-354	chr12	113855606	113855813	chr12-39	chr19	18843705	18843912	chr19-945	chr16	85557855	85558062	chr16-388	chr2	128680564	128680771	chr2-16	chr6	3371701	3371908	chr6-1606
chr1	12493742	12493949	chr1-79	chr2	128685550	128685757	chr2-127	chr3	37806156	37806363	chr3-49	chr14	76439025	76439232	chr14-223	chr10	52303907	52304114	chr10-472	chr8	37449084	37449291	chr8-134
chr17	3875628	3875835	chr17-242	chr11	66809554	66809761	chr11-234	chr14	67895202	67895409	chr14-119	chr4	153960721	153960928	chr4-643	chr11	30412989	30413196	chr11-1032	chr1	14214598	14214805	chr1-2307
chr6	89682773	89682980	chr6-20	chr8	8798262	8798469	chr8-158	chr20	7127946	7128153	chr20-10	chr3	177332831	177333038	chr3-764	chr12	42675306	42675513	chr12-235	chr6	99514749	99514956	chr6-52
chr15	92169770	92169977	chr15-13	chr15	74100264	74100471	chr15-28	chr13	70965914	70966121	chr13-50	chr3	194234046	194234253	chr3-184	chr18	23970361	23970568	chr18-200	chr10	83728479	83728686	chr10-1390
chr11	34845099	34845306	chr11-1038	chr11	100602865	100603072	chr11-333	chr1	184709534	184709741	chr1-187	chr16	79042369	79042576	chr16-40	chr6	80310755	80310962	chr6-164	chr4	55803736	55803943	chr4-84
chr1	240286021	240286228	chr1-495	chr1	177714761	177714968	chr1-996	chr2	35676347	35676554	chr2-255	chr13	32523255	32523462	chr13-9	chr18	55680911	55681118	chr18-49	chr17	76112980	76113187	chr17-441
chr5	75676736	75676943	chr5-488	chr2	149255480	149255687	chr2-343	chr1	156660101	156660308	chr1-59	chr9	132475307	132475514	chr9-182	chr1	48509153	48509360	chr1-427	chr6	105770964	105771171	chr6-1064
chr3	128153520	128153727	chr3-218	chr8	37412902	37413109	chr8-56	chr12	114019202	114019409	chr12-649	chr6	33494245	33494452	chr6-102	chr1	184874891	184875098	chr1-60	chr8	125468208	125468415	chr8-177
chr2	167471384	167471591	chr2-25	chr10	22090668	22090875	chr10-324	chr3	144709846	144710053	chr3-754	chr7	31010053	31010260	chr7-16	chr4	139832121	139832328	chr4-88	chr4	174186111	174186318	chr4-1708
chr7	123258449	123258656	chr7-422	chr3	183049466	183049673	chr3-1963	chr1	59665692	59665899	chr1-227	chr14	70409844	70410051	chr14-69	chr2	203009250	203009457	chr2-314	chr1	36952699	36952906	chr1-266
chr15	61377494	61377701	chr15-45	chr6	90008072	90008279	chr6-665	chr21	19087357	19087564	chr21-73	chr8	132594600	132594807	chr8-9	chr5	16272033	16272240	chr5-298	chr2	178580601	178580808	chr2-211
chr5	92713840	92714047	chr5-252	chrX	152911348	152911555	chrX-54	chr14	101576022	101576229	chr14-1	chr12	106034571	106034778	chr12-544	chr7	46553227	46553434	chr7-135	chr1	95587697	95587904	chr1-107
chr4	139834195	139834402	chr4-107	chr15	77897425	77897632	chr15-21	chr17	14952966	14953173	chr17-866	chr11	115128647	115128854	chr11-81	chr4	26040906	26041113	chr4-957	chr8	58788302	58788509	chr8-694
chr3	52162363	52162570	chr3-917	chr11	12286449	12286656	chr11-97	chr1	236056488	236056695	chr1-220	chr17	8175850	8176057	chr17-853	chr18	19559771	19559978	chr18-35	chr2	129066491	129066698	chr2-109
chr17	66790332	66790539	chr17-485	chr6	157205239	157205446	chr6-2270	chr15	66944502	66944709	chr15-85	chr7	12425053	12425260	chr7-349	chr10	73798404	73798611	chr10-10	chr16	56334470	56334677	chr16-68
chr1	236111310	236111517	chr1-1016	chr20	43706203	43706410	chr20-1025	chr1	16439362	16439569	chr1-80	chr17	42638100	42638307	chr17-157	chr3	193775447	193775654	chr3-144	chr12	41462174	41462381	chr12-279
chr1	177041433	177041640	chr1-905	chr8	30688119	30688326	chr8-104	chr3	30817948	30818155	chr3-127	chr15	69754824	69755031	chr15-219	chr3	170875106	170875313	chr3-1374	chr2	210366435	210366642	chr2-1137
chr8	93617766	93617973	chr8-1425	chr1	109801899	109802106	chr1-1088	chr14	71654135	71654342	chr14-218	chr8	121060102	121060309	chr8-527	chr4	8315983	8316190	chr4-943	chr13	31759098	31759305	chr13-357
chr22	28692709	28692916	chr22-27	chr3	30300433	30300640	chr3-109	chr5	16271133	16271340	chr5-474	chr17	42685866	42686073	chr17-200	chr2	129067429	129067636	chr2-84	chr10	96876551	96876758	chr10-750
chr10	13326162	13326369	chr10-783	chr19	4623563	4623770	chr19-731	chr21	22627992	22628199	chr21-48	chr8	18420749	18420956	chr8-484	chr6	4274511	4274718	chr6-142	chr1	87289580	87289787	chr1-332
chr11	131395912	131396119	chr11-63	chr2	8666006	8666213	chr2-359	chr8	38312150	38312357	chr8-126	chr5	110645359	110645566	chr5-552	chr16	88563831	88564038	chr16-61	chr6	100794060	100794267	chr6-21
chrX	152912193	152912400	chrX-14	chr16	52290355	52290562	chr16-495	chr19	5422299	5422506	chr19-300	chr14	101585935	101586142	chr14-145	chr16	48166682	48166889	chr16-330	chr8	11601690	11601897	chr8-101
chr16	1480821	1481028	chr16-527	chr18	9673018	9673225	chr18-416	chr21	36035041	36035248	chr21-298	chr12	53515618	53515825	chr12-237	chr4	136198759	136198966	chr4-295	chrX	145167043	145167250	chrX-40
chr12	105055866	105056073	chr12-158	chr3	34884093	34884300	chr3-100	chr3	123104431	123104638	chr3-740	chr16	11203574	11203781	chr16-434	chr20	29534689	29534896	chr20-408	chr18	3665750	3665957	chr18-181
chr12	319499	319706	chr12-151	chr4	75067871	75068078	chr4-7	chr12	3538019	3538226	chr12-1715	chr5	38367464	38367671	chr5-21	chr12	76353290	76353497	chr12-56	chr17	39697062	39697269	chr17-7
chr15	23656653	23656860	chr15-846	chrY	14486648	14486855	chrY-19	chr1	154159620	154159827	chr1-370	chr20	47010964	47011171	chr20-504	chr1	145669291	145669498	chr1-802	chr17	52265324	52265531	chr17-170
chr5	103231547	103231754	chr5-115	chr8	89244408	89244615	chr8-195	chr2	60521603	60521810	chr2-145	chr1	185563668	185563875	chr1-277	chr11	34805750	34805957	chr11-183	chr12	76329588	76329795	chr12-315
chr3	129363679	129363886	chr3-963	chr9	7237623	7237830	chr9-96	chr3	37811359	37811566	chr3-354	chr3	52962844	52963051	chr3-918	chr13	99159778	99159985	chr13-81	chr11	10371852	10372059	chr11-225
chr15	89998884	89999091	chr15-125	chr7	89817624	89817831	chr7-1077	chr3	125785560	125785767	chr3-139	chr12	124560463	124560670	chr12-192	chr15	53588889	53589096	chr15-114	chr17	29805130	29805337	chr17-773
chr12	68469257	68469464	chr12-403	chr6	39413244	39413451	chr6-1418	chr1	48551769	48551976	chr1-1064	chr11	6301053	6301260	chr11-494	chr6	139960253	139960460	chr6-86	chr21	43486538	43486745	chr21-4
chr2	6099246	6099453	chr2-357	chr12	113856489	113856696	chr12-11	chr7	135621570	135621777	chr7-140	chr4	41079791	41079998	chr4-816	chr6	35431444	35431651	chr6-1004	chr2	18981696	18981903	chr2-41
chr16	73467947	73468154	chr16-59	chr7	28185480	28185687	chr7-25	chr8	144072387	144072594	chr8-474	chr5	160350988	160351195	chr5-104	chr12	115112709	115112916	chr12-58	chr2	10557871	10558078	chr2-1179
chr7	13057070	13057277	chr7-235	chr2	136883880	136884087	chr2-341	chr6	157508347	157508554	chr6-326	chr5	16272729	16272936	chr5-687	chr1	12611694	12611901	chr1-385	chr12	118936397	118936604	chr12-226
chr15	68240651	68240858	chr15-256	chr20	31045598	31045805	chr20-67	chr16	11729789	11729996	chr16-237	chr7	105577974	105578181	chr7-35	chr11	119746011	119746218	chr11-30	chr1	33521153	33521360	chr1-2820
chr6	4488697	4488904	chr6-1136	chrX	112094516	112094723	chrX-116	chr20	45956588	45956795	chr20-255	chr8	141948889	141949096	chr8-631	chr14	96691605	96691812	chr14-569	chr1	44105424	44105631	chr1-966
chr11	34229112	34229319	chr11-70	chr2	112704603	112704810	chr2-2114	chr5	159413215	159413422	chr5-1722	chr17	46104696	46104903	chr17-233	chr3	193569256	193569463	chr3-53	chr10	36164890	36165097	chr10-467
chr1	167786322	167786529	chr1-3080	chr2	32653739	32653946	chr2-753	chr9	38381254	38381461	chr9-313	chr4	62996012	62996219	chr4-146	chr12	115049454	115049661	chr12-130	chr6	42449255	42449462	chr6-866
chr2	38065886	38066093	chr2-292	chr1	26217312	26217519	chr1-209	chr8	112783444	112783651	chr8-1471	chr16	1950765	1950972	chr16-132	chr15	68691874	68692081	chr15-57	chr22	33176628	33176835	chr22-481
chr1	202036217	202036424	chr1-109	chr17	44073257	44073464	chr17-471	chr4	148512355	148512562	chr4-1083	chr12	104440034	104440241	chr12-5	chr3	7370258	7370465	chr3-125	chr10	114777868	114778075	chr10-103
chr1	23163902	23164109	chr1-17	chr1	36952063	36952270	chr1-2	chr2	127858331	127858538	chr2-528	chr12	3071869	3072076	chr12-301	chr12	606683	606890	chr12-335	chr2	50065060	50065267	chr2-331
chr14	38072966	38073173	chr14-305	chr5	143837679	143837886	chr5-31	chr15	68238885	68239092	chr15-119	chr6	100658401	100658608	chr6-197	chrX	133670700	133670907	chrX-99	chr2	66018066	66018273	chr2-1037
chr1	22182707	22182914	chr1-70	chr19	8523387	8523594	chr19-1035	chr17	47029875	47030082	chr17-255	chr9	96053445	96053652	chr9-319	chr4	79220884	79221091	chr4-1006	chr2	23734354	23734561	chr2-167
chr8	129615618	129615825	chr8-86	chr3	197082538	197082745	chr3-596	chr4	185384112	185384319	chr4-310	chr21	40326793	40327000	chr21-3	chr3	184289857	184290064	chr3-143	chr5	16684432	16684639	chr5-1491
chr2	60353630	60353837	chr2-575	chr1	9473012	9473219	chr1-690	chr15	101300050	101300257	chr15-157	chr7	54532817	54533024	chr7-1252	chr4	114471344	114471551	chr4-466	chr12	54528964	54529171	chr12-73
chr10	80539421	80539628	chr10-39	chr13	26335499	26335706	chr13-98	chr3	184354314	184354521	chr3-278	chr20	49485008	49485215	chr20-137	chr2	167465970	167466177	chr2-241	chr17	13128818	13129025	chr17-455
chr17	68851653	68851860	chr17-939	chr1	233496545	233496752	chr1-453	chr3	168985989	168986196	chr3-445	chr1	65624386	65624593	chr1-713	chr8	120095164	120095371	chr8-138	chr14	21317568	21317775	chr14-18
chr22	31441994	31442201	chr22-540	chr8	124955199	124955406	chr8-154	chr3	119513344	119513551	chr3-739	chr6	117709881	117710088	chr6-166	chr18	71884567	71884774	chr18-153	chr20	55587832	55588039	chr20-66
chr1	163442064	163442271	chr1-809	chr18	74685689	74685896	chr18-245	chr3	128394390	128394597	chr3-378	chr4	152450627	152450834	chr4-750	chr20	48210024	48210231	chr20-75	chr2	19008761	19008968	chr2-177
chr3	184321123	184321330	chr3-28	chr13	24204658	24204865	chr13-66	chr11	94479840	94480047	chr11-405	chr5	134667314	134667521	chr5-877	chr3	197274092	197274299	chr3-1410	chr9	132257993	132258200	chr9-24
chr3	38584663	38584870	chr3-543	chr3	25489483	25489690	chr3-38	chr14	39519792	39519999	chr14-106	chr10	72129306	72129513	chr10-57	chr9	120754329	120754536	chr9-1108	chr3	110302253	110302460	chr3-496
chr12	106144132	106144339	chr12-36	chr8	53542111	53542318	chr8-93	chr4	141636091	141636298	chr4-123	chr19	18490708	18490915	chr19-106	chr12	42709798	42710005	chr12-925	chr13	27597593	27597800	chr13-45
chr4	54325815	54326022	chr4-75	chr21	43477025	43477232	chr21-68	chr15	101528557	101528764	chr15-710	chr20	36926830	36927037	chr20-373	chr11	19273235	19273442	chr11-1023	chr1	164559242	164559449	chr1-151
chr20	48199917	48200124	chr20-19	chr8	125732032	125732239	chr8-23	chr12	106254461	106254668	chr12-61	chr1	23077613	23077820	chr1-634	chr6	117708672	117708879	chr6-200	chr18	56563070	56563277	chr18-343
chr5	121985164	121985371	chr5-341	chr14	91869189	91869396	chr14-285	chr1	218844301	218844508	chr1-451	chr16	65807757	65807964	chr16-562	chr2	218657697	218657904	chr2-43	chr5	92468560	92468767	chr5-62
chr7	78078239	78078446	chr7-77	chr1	5575849	5576056	chr1-143	chr10	30826984	30827191	chr10-46	chr8	9651255	9651462	chr8-545	chr7	29461566	29461773	chr7-394	chr9	129435267	129435474	chr9-132
chr1	18488295	18488502	chr1-5	chr8	125274445	125274652	chr8-69	chr22	29614786	29614993	chr22-92	chr8	61910590	61910797	chr8-437	chr2	38093655	38093862	chr2-27	chr15	89656031	89656238	chr15-124
chr14	91033931	91034138	chr14-196	chr3	96680964	96681171	chr3-1534	chr2	38078363	38078570	chr2-1016	chr2	196739411	196739618	chr2-439	chr15	96752713	96752920	chr15-1034	chr2	217911960	217912167	chr2-64
chr7	36853978	36854185	chr7-315	chr1	12714696	12714903	chr1-418	chr1	146565038	146565245	chr1-1247	chr2	43390566	43390773	chr2-37	chr5	146012273	146012480	chr5-102	chr8	131322213	131322420	chr8-254
chr5	134640403	134640610	chr5-10	chr6	37482298	37482505	chr6-224	chr18	23972270	23972477	chr18-38	chr11	78512554	78512761	chr11-805	chr1	224920800	224921007	chr1-82	chr10	35002497	35002704	chr10-328
chr17	44071654	44071861	chr17-203	chr19	38695087	38695294	chr19-208	chr9	120131663	120131870	chr9-112	chr4	189359849	189360056	chr4-2	chr1	240760072	240760279	chr1-414	chr5	75668210	75668417	chr5-724
chr21	40293534	40293741	chr21-17	chr4	160997068	160997275	chr4-41	chr10	99798015	99798222	chr10-491	chr3	77843343	77843550	chr3-241	chr12	128588738	128588945	chr12-1216	chr22	44807168	44807375	chr22-173
chr2	197971734	197971941	chr2-1313	chr17	48194346	48194553	chr17-16	chr1	22228941	22229148	chr1-112	chr3	169177695	169177902	chr3-142	chr10	120286604	120286811	chr10-1036	chr6	151639188	151639395	chr6-325
chr16	11244240	11244447	chr16-321	chr22	40387444	40387651	chr22-39	chr13	72289089	72289296	chr13-103	chr4	68579396	68579603	chr4-330	chr1	212662881	212663088	chr1-549	chr1	218539801	218540008	chr1-13
chr5	159687983	159688190	chr5-189	chr9	129436027	129436234	chr9-110	chr6	43302914	43303121	chr6-563	chr2	135443738	135443945	chr2-594	chr3	59664145	59664352	chr3-294	chr10	112617048	112617255	chr10-15
chr15	91252187	91252394	chr15-30	chr2	98343181	98343388	chr2-586	chr4	82300745	82300952	chr4-30	chr20	29533657	29533864	chr20-558	chr2	5329867	5330074	chr2-991	chr2	23734927	23735134	chr2-52
chr1	233609746	233609953	chr1-1298	chr12	115601715	115601922	chr12-141	chr13	24694019	24694226	chr13-96	chr17	46598915	46599122	chr17-36	chr10	10519065	10519272	chr10-589	chr6	13864100	13864307	chr6-171
chr6	14544563	14544770	chr6-144	chr11	131400857	131401064	chr11-247	chr12	119811113	119811320	chr12-331	chrX	36234095	36234302	chrX-5	chr9	92284191	92284398	chr9-168	chr3	68884356	68884563	chr3-828
chr14	39132632	39132839	chr14-149	chr16	26376303	26376510	chr16-124	chr9	129438893	129439100	chr9-162	chr9	85212252	85212459	chr9-55	chr8	94886311	94886518	chr8-377	chr5	142276250	142276457	chr5-4
chr14	63724021	63724228	chr14-77	chr11	19274042	19274249	chr11-503	chr10	125795225	125795432	chr10-138	chr6	6968820	6969027	chr6-258	chr13	24187442	24187649	chr13-37	chr14	22137482	22137689	chr14-74
chr17	42680408	42680615	chr17-199	chr20	45966224	45966431	chr20-1224	chr5	142281092	142281299	chr5-202	chr7	129615523	129615730	chr7-578	chr17	36754741	36754948	chr17-196	chr16	12706692	12706899	chr16-671
chr8	30351177	30351384	chr8-114	chr5	89649085	89649292	chr5-335	chr1	153548772	153548979	chr1-3664	chr20	615808	616015	chr20-354	chr11	75052413	75052620	chr11-399	chr14	96384887	96385094	chr14-199
chr1	171179550	171179757	chr1-902	chr10	77359708	77359915	chr10-9	chr20	29532869	29533076	chr20-30	chr6	106344113	106344320	chr6-39	chr4	102449705	102449912	chr4-26	chr9	78044894	78045101	chr9-356
chr20	55578813	55579020	chr20-27	chr17	36755338	36755545	chr17-123	chr2	173099756	173099963	chr2-76	chr1	30128531	30128738	chr1-16	chr9	71659508	71659715	chr9-391	chr7	31815080	31815287	chr7-126
chr3	184286861	184287068	chr3-449	chr19	49321942	49322149	chr19-69	chr17	35276851	35277058	chr17-105	chr2	180921318	180921525	chr2-1301	chr17	78641294	78641501	chr17-722	chr1	36352615	36352822	chr1-36
chr4	6932854	6933061	chr4-199	chr15	66943682	66943889	chr15-72	chr18	29568144	29568351	chr18-377	chr19	14656001	14656208	chr19-362	chr3	195478522	195478729	chr3-459	chr5	160107811	160108018	chr5-352
chr19	10989697	10989904	chr19-206	chr11	12270408	12270615	chr11-102	chr18	29167582	29167789	chr18-108	chr6	43879824	43880031	chr6-5	chrX	88092533	88092740	chrX-2	chr15	96724569	96724776	chr15-227

Table 2. 634 genes associated with RXR-bound G1 enhancers. Associated PeakID(s) and their distances from the nearest TSS are provided. Genes were assigned using GREAT version 3.0.0 (McLean, Bristor et al. 2010). Species assembly: hg19. Association rule: Basal+extension: 5000 bp upstream, 1000 bp downstream, 200000 bp max extension, curated regulatory domains included.

Gene	Associated RXR-bound G1 PeakID (bp distance from gene TSS)	Gene	Associated RXR-bound G1 PeakID (bp distance from gene TSS)	Gene	Associated RXR-bound G1 PeakID (bp distance from gene TSS)	Gene	Associated RXR-bound G1 PeakID (bp distance from gene TSS)	Gene	Associated RXR-bound G1 PeakID (bp distance from gene TSS)	Gene	Associated RXR-bound G1 PeakID (bp distance from gene TSS)
AADACL3	chr1-418 (-61346)	CHD2	chr15-335 (-117392)	FOXA2	chr20-302 (-89979)	MBP	chr18-245 (+158932)	PTGIS	chr20-75 (-25445), chr20-19 (-15338)	TAF4B	chr18-200 (+164565), chr18-38 (+166474)
AADACL4	chr1-418 (+10234)	CHDC2	chrX-56 (-27535), chrX-5 (+169146)	FRMD4B	chr3-4 (-120337)	MCF2L2	chr3-1963 (+96493)	PTK2	chr8-631 (+62264)	TBC1D14	chr4-199 (+21386)
ABCA8	chr17-485 (+161056)	CHST15	chr10-138 (+56641)	FRY	chr13-9 (-82078)	MCHR2	chr6-284 (-180558)	PTPRF	chr1-966 (+108981)	TBC1D21	chr15-28 (-65600)
ABCC12	chr16-330 (+13895)	CHST3	chr10-10 (+74385)	FUT8	chr14-89 (-183437)	MCM9	chr6-150 (-102363)	PTPRG	chr3-818 (-30518), chr3-928 (+83504)	TBC1D9	chr4-123 (+41079)
ABHD2	chr15-124 (+24754)	CLCNKB	chr1-80 (+69194)	FXN	chr9-391 (+9437)	MCUR1	chr6-171 (-49404)	PTPRS	chr19-300 (-81589)	TBL1Y	chrY-15 (-10371)
ABTB2	chr11-70 (+150339)	CLEC2L	chr7-30 (+136571)	FZD2	chr17-27 (-13224), chr17-157 (+3279), chr17-199 (+45587), chr17-200 (+51045)	MDGA1	chr6-224 (+183364)	PVRL1	chr11-30 (-146321)	TBX3	chr12-58 (+8582), chr12-130 (+71837)
ACOX3	chr4-943 (+126351)	CLEC4G	chr19-357 (+10303)	FZD7	chr2-314 (+110044)	MDM1	chr12-615 (-26807)	R3HCC1L	chr10-491 (-96309)	TCF15	chr20-354 (-24870)
ADAMTS9	chr3-27 (+153724)	CLIC6	chr21-298 (-6543)	GABRR1	chr6-665 (-81024)	MECOM	chr3-445 (-122000)	RAB11FIP4	chr17-773 (+86592)	TCF7L2	chr10-103 (+67963)
ADC	chr1-2820 (-29457)	CNIH3	chr1-82 (+116909)	GABRR2	chr6-665 (+16842)	MEF2D	chr1-276 (+29291)	RAB31	chr18-416 (-35040)	TDG	chr12-5 (+80556)
ADCY10	chr1-3080 (+96914)	COL14A1	chr8-527 (-77141)	GADD45G	chr9-168 (+64367)	MEIOB	chr16-132 (-28690)	RAB7A	chr3-378 (-50471)	TDRD5	chr1-7 (+110729)
ADCY5	chr3-740 (+64070)	COLEC10	chr8-138 (+15788)	GADL1	chr3-127 (+118205)	MERTK	chr2-2114 (+48651)	RANGRF	chr17-853 (-15661)	TEAD4	chr12-301 (+3393)
ADCYAP1R1	chr7-16 (-92653)	COLGALT2	chr1-813 (+94533)	GALNT7	chr4-1708 (+96311)	MICAL2	chr11-102 (+138374), chr11-97 (+154415)	RAP1A	chr1-797 (+85222)	TECR	chr19-158 (+14449), chr19-362 (+15733)
ADH7	chr4-35 (-102192)	COMP	chr19-945 (+58314)	GATA4	chr8-101 (+40081)	MICALCL	chr11-102 (-37935), chr11-97 (-21894)	RARB	chr3-38 (+19785)	TET2	chr4-861 (+34616)
ADM	chr11-225 (+45325)	COPZ2	chr17-233 (+10339)	GATA6	chr18-35 (-189529)	MKRN3	chr15-846 (-153697)	RASGEF1B	chr4-249 (+73765), chr4-30 (+92220)	TEX15	chr8-104 (+18385)
ADNP	chr20-137 (+62638)	CPLX2	chr5-75 (-122004)	GDA	chr9-896 (+166447)	MMP16	chr8-195 (+95205)	RASGRF1	chr15-683 (-88582)	TFCP2L1	chr2-149 (+100952)
ADRA1B	chr5-1722 (+69529)	CPPED1	chr16-671 (+191078)	GDF15	chr19-106 (-2168)	MNF1	chr6-222 (+82400)	RB1CC1	chr8-93 (+84777)	TGFB2	chr1-13 (+20328)
AGO1	chr1-36 (+3909)	CPXCR1	chrX-2 (+90411)	GFRA1	chr10-129 (+36045)	MORC2	chr22-540 (-77911)	RBM14	chr11-1267 (-15683)	TGFB3	chr14-223 (+8405)
AGO3	chr1-36 (-43960)	CPXM2	chr10-138 (-143999)	GHRHR	chr7-16 (+6519)	MPPED2	chr11-1032 (+188950)	RBM19	chr12-744 (+88921)	TGFBR2	chr3-127 (+169959)
AIM2	chr1-1888 (-85547)	CRABP2	chr1-59 (+15188)	GINS2	chr16-25 (-23705)	MPZL1	chr1-3080 (+95239)	RBPMS	chr8-114 (+109254)	TGM2	chr20-373 (-133160)
AK2	chr1-2820 (-18664)	CRIP3	chr6-563 (-26483)	GIP	chr17-255 (+15979)	MRPL33	chr2-289 (+92439)	RCAN1	chr21-298 (-47704)	TIMM21	chr18-121 (+68331), chr18-153 (+68925)
AK4	chr1-713 (+10977)	CRTAC1	chr10-491 (-7534)	GLT8D2	chr12-5 (+3777)	MTHFD1	chr14-78 (+22407)	RDH10	chr8-248 (+35901)	TIMP3	chr22-481 (-20955)
AKAP12	chr6-325 (+78158)	CRTC1	chr19-945 (+49321)	GNA14	chr9-452 (+135232)	MTHFD2L	chr4-7 (+44146)	RHBDD3	chr22-46 (+47023), chr22-92 (+49077)	TJP2	chr9-391 (-160466)
AKAP5	chr14-78 (-56659)	CRTC3	chr15-30 (+178991)	GNAL	chr18-57 (-187941)	MTPN	chr7-140 (+40390)	RHCG	chr15-125 (+40856)	TMC6	chr17-441 (+11694)
ALDH1A3	chr15-157 (-119427)	CSAD	chr12-237 (+58658), chr12-810 (+64543)	GNAO1	chr16-68 (+108686), chr16-196 (+109220)	MTSS1	chr8-21 (+7471), chr8-23 (+8534)	RHOD	chr11-234 (-14631)	TMED3	chr15-683 (-131707)
ALDH1B1	chr9-313 (-11303)	CSF3R	chr1-266 (-3924), chr1-2 (-3288)	GNRHR	chr4-330 (+40578)	MUC20	chr3-459 (+30873)	RHOJ	chr14-77 (+52999)	TMED8	chr14-549 (+39643)
AMELY	chrY-15 (-26288)	CSNK1E	chr22-276 (-30571)	GOLGA8S	chr15-846 (+56764)	MUC4	chr3-459 (+60522)	RLBP1	chr15-124 (+108847)	TMEM106B	chr7-349 (+174231)
AMFR	chr16-196 (+124342), chr16-68 (+124876)	CSPG4	chr15-108 (+47048)	GOLT1A	chr1-610 (-81507)	MYOF	chr10-226 (+7791)	RMDN2	chr2-292 (-111616), chr2-1016 (-99139), chr2-27 (-83847)	TMEM110	chr3-918 (-31336)
AMOT	chrX-116 (-28266)	CTDSPL	chr3-49 (-97405), chr3-354 (-92202)	GOT1	chr10-100 (-20535)	NAT10	chr11-70 (+102067)	RNASE1	chr14-18 (-46235)	TMEM132C	chr12-1216 (-163106)
AMOTL1	chr11-405 (-21593)	CTNNBL1	chr20-199 (+168053)	GPATCH8	chr17-27 (-40932)	NAT2	chr8-484 (+172098)	RNASE3	chr14-18 (-41886)	TMEM163	chr2-594 (+32728)
AMPD3	chr11-225 (-100272)	CWC22	chr2-1301 (-49642)	GPR151	chr5-102 (-116624)	NBPF12	chr1-1247 (+191086)	RNF115	chr1-1247 (+191086)	TMEM184C	chr4-1083 (-26075)
ANO1	chr11-22 (-107437)	CXCR4	chr2-341 (-10171)	GPR37L1	chr1-109 (-55665)	NDUFB7	chr19-362 (+26769), chr19-158 (+28053)	RNF125	chr18-377 (-30087)	TMEM229B	chr14-119 (+86715)
AOAH	chr7-315 (-89929)	CYB5A	chr18-153 (+74580), chr18-121 (+75174)	GPR68	chr14-285 (-149024)	NDUFB9	chr8-23 (+180792), chr8-21 (+181855)	RNF139	chr8-177 (-18867)	TMEM44	chr3-184 (+120000)
APBB2	chr4-816 (+136654)	CYP11B2	chr8-474 (-73232)	GPR78	chr4-64 (-20687)	NEDD4L	chr18-49 (-30595)	RNF182	chr6-171 (-60894)	TMEM45B	chr11-200 (+50542)
APIP	chr11-1038 (+92843), chr11-183 (+132192)	CYP2C8	chr10-750 (-47401)	GPT2	chr16-111 (-7475)	NENF	chr1-549 (+56756)	RNF32	chr7-64 (+26422)	TMEM63B	chr6-179 (-137956)
ARHGAP23	chr17-196 (+170183), chr17-123 (+170780)	DACH1	chr13-103 (+152137)	GRAP2	chr22-39 (+90462)	NES	chr1-59 (-13016)	RNGTT	chr6-20 (-9562)	TMEM65	chr8-69 (+110384)
ARHGAP26	chr5-57 (+125453), chr5-4 (+126405), chr5-202 (+131247)	DBF4B	chr17-157 (+147847), chr17-199 (-105539), chr17-200 (-100081)	GREM2	chr1-414 (+15273)	NFRKB	chr11-200 (+26648)	ROPN1B	chr3-139 (+97677)	TMEM67	chr8-377 (+119330)
ARHGAP42	chr11-333 (+44562)	DDX20	chr1-797 (-50300)	GSE1	chr16-388 (-88863)	NID1	chr1-1016 (+117048), chr1-220 (+171870)	ROS1	chr6-1016 (+37033), chr6-200 (+38242)	TMEM87B	chr2-2114 (-108093)
ARHGEF17	chr11-95 (-19527)	DEPDC5	chr22-332 (+74555)	H2AFY	chr5-877 (+67894), chr5-10 (+94805)	NINJ2	chr12-444 (+124865), chr12-335 (+166158)	RPL10A	chr6-1004 (-4637)	TNFRSF19	chr13-37 (+34047), chr13-66 (+51263)
ARID1B	chr6-2270 (+106280)	DEPTOR	chr8-527 (+174249)	HES1	chr3-144 (-78383)	NKX2-3	chr10-100 (-81805)	RPLP1	chr15-219 (+9805)	TNP1	chr2-84 (-187277)
ARL14EP	chr11-1032 (+68495)	DHRS3	chr1-129 (+13171), chr1-385 (+65939), chr1-79 (+183891)	HIPK2	chr7-30 (+132344)	NKX2-5	chr5-173 (-69139)	RPN1	chr3-378 (-24802)	TNRC6B	chr22-39 (-186381)
ARRB1	chr11-400 (+8871), chr11-399 (+10232)	DHX35	chr20-68 (+190044)	HIVEP3	chr1-49 (+24231)	NPFFR1	chr10-57 (-85970)	RPTOR	chr17-722 (+122330)	TNRC6C	chr17-441 (+111947)
ASAP1	chr8-254 (+91900)	DLG1	chr3-596 (-57195)	HMCN1	chr1-277 (-139911)	NR1I2	chr3-739 (+11891)	RREB1	chr6-258 (-139117)	TNS1	chr2-43 (+151050)
ASB15	chr7-422 (+51489)	DLX2	chr2-76 (-132232)	HMG20A	chr15-21 (+184513)	NR2F2	chr15-227 (-149273), chr15-1034 (-121129)	RWDD3	chr1-107 (-111910)	TPBGL	chr11-399 (+100567), chr11-400 (+101928)
ASB7	chr15-157 (+157415)	DMAP1	chr1-470 (+19131)	HMGB2	chr4-1708 (+70061)	NRG3	chr10-1390 (+93513)	S100A16	chr1-3664 (+32937)	TPM3	chr1-370 (+4963)
ASTN1	chr1-905 (+92289)	DNAH14	chr1-82 (-196465)	HNRNPM	chr19-1035 (+13649)	NTMT1	chr9-24 (-13066)	S100A2	chr1-3664 (-10535)	TRABD2B	chr1-1064 (-89306), chr1-427 (-46690)
ASTN2	chr9-112 (+45581)	DNAH7	chr2-439 (+194021)	HOXA1	chr7-58 (+16062)	NUF2	chr1-809 (+150424)	SAP130	chr2-127 (+99215), chr2-16 (+104201)	TRAPPC8	chr18-377 (-45185)
ASXL1	chr20-140 (-32442), chr20-67 (+99547)	DNAJB8	chr3-218 (+32187), chr3-122 (+33414)	HOXB1	chr17-36 (+9340)	NUP210L	chr1-370 (-32132)	SCN5A	chr3-543 (+106396)	TRERF1	chr6-866 (-29576)
ATF3	chr1-549 (-119027)	DNAJC6	chr1-713 (-150738)	HOXC4	chr12-73 (+81407)	OBSCN	chr1-154 (+160319)	SCN7A	chr2-25 (-128010), chr2-241 (-122596)	TRIM11	chr1-154 (+38391)
ATP10B	chr5-104 (-71873), chr5-352 (+171304)	DPF1	chr19-208 (+19699)	HPCAL1	chr2-1179 (+114149)	ODC1	chr2-1179 (+30655)	SDSL	chr12-39 (-4332), chr12-11 (-3449)	TRIM2	chr4-643 (-164793)
ATP13A3	chr3-184 (-15057)	DPYD	chr1-402 (-135118)	HPRT1	chrX-99 (+76621)	OR2K2	chr9-137 (+44855)	SEC11A	chr15-48 (-17743)	TRIM42	chr3-751 (+21944)
ATP2A3	chr17-242 (-8147)	DUPD1	chr10-479 (+17821)	HRH2	chr5-75 (+16276)	OR4E2	chr14-74 (+4289)	SEC22A	chr3-740 (+177366)	TRMT10A	chr4-35 (+26342)
B3GALTL	chr13-357 (-14871)	DUSP7	chr3-917 (-71901)	HS2ST1	chr1-332 (-90673)	OSBPL8	chr12-621 (+151879)	SEC23A	chr14-106 (+52836)	TRMT12	chr8-177 (+5264)
B3GNT5	chr3-1963 (+78538)	DUSP9	chrX-54 (-1198), chrX-14 (-353)	HS3ST6	chr16-132 (+17362)	P2RX4	chr12-1991 (+16896)	SEMA6A	chr5-225 (+41167), chr5-63 (+49824)	TRMT44	chr4-64 (+119056)
B4GALNT3	chr12-335 (+37257), chr12-444 (+78550)	E2F8	chr11-503 (-10979), chr11-1023 (-10172)	HS6ST1	chr2-84 (+8618), chr2-109 (+9556)	P2RY6	chr11-95 (+16560)	SEMA6B	chr19-731 (-63847)	TSPAN9	chr12-301 (-114570)
B4GALT5	chr20-75 (+120287), chr20-19 (+130394)	EBAG9	chr8-151 (+40120)	HSD17B14	chr19-69 (+17889)	PAK6	chr15-235 (+19000)	SFMBT1	chr3-918 (+117136)	TTC1	chr5-1722 (-22801)
BAK1	chr6-102 (+53670)	ECI2	chr6-142 (-138784)	HSPB8	chr12-331 (+194770)	PAQR7	chr1-209 (-19672)	SGMS1	chr10-472 (+79732)	TTC27	chr2-753 (-199286)
BBS10	chr12-621 (-59488)	EDEM3	chr1-60 (-150948), chr1-187 (+14409)	HSPG2	chr1-112 (+34745), chr1-1034 (+64028), chr1-70 (+80979)	PARD3	chr10-328 (+101648)	SH2D1B	chr1-117 (+64659)	TTC30A	chr2-211 (-97011)
BCAS4	chr20-137 (+73681)	EDNRA	chr4-1083 (+110375)	HSPH1	chr13-357 (-23138)	PBX1	chr1-151 (+30474)	SH3BGRL2	chr6-164 (-30141)	TTR	chr18-65 (-4995), chr18-108 (-4003)
BCAT2	chr19-69 (-7769)	EGFLAM	chr5-21 (+109057)	HTRA3	chr4-943 (+44595)	PCIF1	chr20-165 (-15713), chr20-136 (-14985)	SH3GLB1	chr1-332 (+119106)	TUBB2B	chr6-1606 (-143836)
BDH1	chr3-1012 (+7953), chr3-1410 (+8662)	EHF	chr11-183 (+151843), chr11-1038 (+191192)	ID2	chr2-359 (-152865)	PDCD4	chr10-15 (-144133)	SHH	chr7-64 (-854933)	TYW1	chr7-751 (+196832)
BDKRB1	chr14-291 (-31449), chr14-569 (-30452)	EIF4A3	chr17-188 (-14351)	IFNG	chr12-403 (+84166)	PDK2	chr17-16 (+21811), chr17-158 (+22684)	SIM1	chr6-21 (+118641)	UBA6	chr4-330 (-12603)
BDKRB2	chr14-291 (+19577), chr14-569 (+20574)	EIF4EBP2	chr10-57 (-34725)	IGSF21	chr1-5 (+54159)	PDP1	chr8-377 (-42760)	SKAP1	chr17-36 (-91467)	UBE2H	chr7-578 (-22838), chr7-183 (-5823)
BIN1	chr2-528 (+6496)	ELF3	chr1-109 (+59248)	IMP3	chr15-108 (-17094)	PDP2	chr16-379 (+18778)	SKOR1	chr15-119 (+126947), chr15-256 (+128713)	UBR2	chr6-866 (-28441)
BIRC6	chr2-753 (+71747)	EMC8	chr16-25 (+86836)	IQGAP2	chr5-724 (-30760), chr5-488 (-22234)	PDZRN4	chr12-279 (-119972)	SLC12A2	chr5-227 (-198435)	UCMA	chr10-783 (-49935)
BLM	chr15-30 (-8267)	EMID1	chr22-92 (+13050), chr22-46 (+15104)	IQSEC3	chr12-151 (+143672)	PFAS	chr17-853 (+23350)	SLC16A6	chr17-935 (-88227)	UCP1	chr4-123 (-146236)
BPI	chr20-373 (-5591)	ENSG00000134602	chrX-12 (-37526)	IRF2	chr4-310 (+11518)	PGAP1	chr2-1313 (-180383)	SLC1A5	chr19-640 (+17295)	UGCG	chr9-1302 (+58525)
BRE	chr2-289 (-26573)	ENSG00000143674	chr1-453 (+33135), chr1-1298 (+146336)	IRF8	chr16-869 (+33257)	PGLS	chr19-1337 (-13347)	SLC22A23	chr6-1606 (+84988)	UMODL1	chr21-68 (-14297), chr21-4 (-4784)
BTG3	chr21-73 (-102299)	ENSG00000262304	chr17-307 (-3124)	ITGA11	chr15-16 (+27522), chr15-57 (+32514)	PHF19	chr9-233 (+15890)	SLC25A33	chr1-690 (-126425)	URAD	chr13-415 (-62451)
C10orf11	chr10-9 (-182707)	ENSG00000271092	chr1-107 (+4322)	ITGA6	chr2-76 (-192657)	PHLDA1	chr12-56 (+74318), chr12-315 (+98020)	SLC27A1	chr19-1337 (+27838)	USP12	chr13-45 (+148336)
C10orf129	chr10-750 (-77302)	EPC2	chr2-343 (-146969)	ITPR3	chr6-222 (+8962)	PHYH	chr10-783 (+15835)	SLC2A2	chr3-1374 (-130671)	VEGFA	chr6-5 (+141484)
C14orf132	chr14-199 (-120670)	EPGN	chr4-7 (-106215)	JAZF1	chr7-25 (+34778)	PIAS1	chr15-119 (-107528), chr15-256 (-105762)	SLC41A3	chr3-139 (+17483)	VGLL2	chr6-200 (+122039), chr6-166 (+123248)
C16orf87	chr16-111 (-45492)	EPHA2	chr1-80 (+43116)	KCNJ4	chr22-276 (+107221)	PIWIL4	chr11-405 (+179470)	SLC5A5	chr19-836 (+48728)	VILL	chr3-407 (-213)
C16orf91	chr16-527 (-1580)	EPHA6	chr3-1534 (+147638)	KCNK1	chr1-1298 (-139900)	PLAC1	chrX-99 (+121709)	SLC5A9	chr1-427 (-179102), chr1-1064 (-136486)	VPS8	chr3-278 (-175513)
C19orf10	chr19-731 (+46715)	EPHB2	chr1-634 (+40254), chr1-17 (+126543)	KCNK16	chr6-1418 (-123032)	PLCB2	chr15-235 (+49502)	SLC6A12	chr12-151 (+4086)	VSTM2A	chr7-1252 (-77097)
C1QTNF9	chr13-96 (-187181)	EPHB3	chr3-449 (+7393), chr3-143 (+10389), chr3-28 (+41655), chr3-278 (+74846)	KCNS1	chr20-1025 (+23446)	PLEK2	chr14-119 (-16389)	SLC7A5	chr16-584 (-62878)	VSTM2L	chr20-199 (-41045)
C1orf61	chr1-276 (-42145)	ERI1	chr8-158 (-61291)	KCTD1	chr18-38 (+157025), chr18-200 (+158934)	PLEKHA6	chr1-610 (+64317)	SMAD6	chr15-72 (-50780), chr15-85 (-49960)	VWDE	chr7-349 (+18374)
C8orf49	chr8-101 (-17102)	ERI3	chr1-470 (+122586)	KDM1A	chr1-17 (-181980)	PLEKHA8	chr7-522 (+48534)	SMIM18	chr8-114 (-144836)	WIPI1	chr17-935 (+78078)
CA5A	chr16-584 (+4150)	ETS2	chr21-17 (+116407), chr21-3 (+149666)	KDM4A	chr1-966 (-10301)	PLTP	chr20-136 (-7596), chr20-165 (-6868)	SMIM20	chr4-957 (+125184)	WNK2	chr9-319 (+106337)
CADM3	chr1-1888 (-9161)	EXOG	chr3-543 (+47004)	KDR	chr4-84 (+187916)	PLXND1	chr3-963 (-38122)	SMOC1	chr14-69 (+63815)	WWOX	chr16-147 (+141721)
CALM1	chr14-196 (+170708)	FABP6	chr5-189 (+73713)	KIAA1644	chr22-173 (-98541)	PNRC1	chr6-20 (-107620)	SMTN	chr22-540 (-35207)	YAF2	chr12-925 (-77864), chr12-235 (-43372)
CAMK2D	chr4-215 (+10160)	FAM110B	chr8-694 (-118707)	KIF3B	chr20-140 (+48246)	POC1A	chr3-917 (+25961)	SMUG1	chr12-73 (+53710)	YIPF2	chr19-206 (+49528)
CAMK4	chr5-552 (+85679)	FAM120A	chr9-319 (-160455)	KLF7	chr2-189 (-50595)	POLD3	chr11-1283 (-45430)	SNF8	chr17-255 (-7500)	YWHAH	chr22-332 (-115054)
CAMKK2	chr12-1991 (+71347)	FAM129A	chr1-60 (+68687)	KRT19	chr17-7 (-12606)	POLG	chr15-125 (-120910)	SNN	chr16-28 (-54329), chr16-237 (-32377)	ZAP70	chr2-586 (+13262)
CARD14	chr17-188 (-8478)	FAM134B	chr5-1491 (-67369)	KRT9	chr17-7 (+31144)	POLR2D	chr2-127 (-69923), chr2-16 (-64937)	SNX2	chr5-341 (-125423)	ZBTB2	chr6-325 (+73391)
CARM1	chr19-206 (+7612)	FAM150A	chr8-93 (-64148)	LCA5	chr6-164 (-63712)	POMT2	chr14-549 (-16582)	SOAT2	chr12-810 (+12535), chr12-237 (+18420)	ZBTB21	chr21-68 (-46663)
CCDC124	chr19-836 (-14395)	FAM163A	chr1-7 (-40544)	LCTL	chr15-85 (-86771), chr15-72 (-85951)	POPDC3	chr6-1064 (-143333)	SOCS1	chr16-321 (+105692), chr16-434 (+146358)	ZBTB43	chr9-132 (-131923), chr9-110 (-131163), chr9-162 (-128297)
CCDC167	chr6-224 (-14704)	FAM174B	chr15-335 (-126478)	LDLRAD2	chr1-70 (+60436), chr1-1034 (+61004), chr1-112 (+90287)	PPARD	chr6-488 (+61610)	SOX11	chr2-154 (-198375), chr2-110 (-197869)	ZBTB9	chr6-102 (+71993)
CCDC87	chr11-1267 (-7816)	FAM180A	chr7-140 (-188080)	LETM2	chr8-126 (+68235)	PPP1R17	chr7-126 (+88855)	SOX4	chr6-261 (-190240)	ZC3H18	chr16-61 (-72854)
CCDC88C	chr14-285 (+14828)	FAM184A	chr6-150 (+41218)	LHX1	chr17-105 (-17129)	PPP1R9B	chr17-158 (+32554), chr17-16 (+33427)	SPATA13	chr13-96 (+140179)	ZC3HC1	chr7-578 (+75664), chr7-183 (+92679)
CCKBR	chr11-494 (+20191)	FAM19A4	chr3-828 (+97301)	LHX5	chr12-649 (-109429)	PPP2CB	chr8-104 (-17835)	SPOCK2	chr10-10 (+50023)	ZCRB1	chr12-925 (+10005), chr12-235 (+44497)
CCL24	chr7-326 (+24747)	FAM20A	chr17-485 (-192906)	LINGO1	chr15-21 (+27303)	PPP3CA	chr4-26 (-181172)	SPSB1	chr1-690 (+120177)	ZFAND5	chr9-896 (+49423)
CCL26	chr7-326 (-8713)	FANCE	chr6-488 (-48137)	LIPT2	chr11-1283 (-53367)	PPP4R1	chr18-416 (-58566)	SRCIN1	chr17-123 (+6741), chr17-196 (+7338)	ZFP36L2	chr2-37 (+63078)
CCNJL	chr5-189 (+51520)	FBXL4	chr6-52 (-119051)	LITAF	chr16-237 (-48474), chr16-28 (-26522)	PRAM1	chr19-1035 (+44505)	SRXN1	chr20-354 (+18102)	ZFPM1	chr16-61 (+44210)
CCNL1	chr3-115 (+44533)	FCER2	chr19-357 (-19722)	LMOD2	chr7-422 (-37308)	PRDM1	chr6-39 (-189978)	STC2	chr5-173 (+25007)	ZMYND8	chr20-1224 (+19086), chr20-255 (+28722)
CCRN4L	chr4-88 (-104718), chr4-107 (-102644)	FEM1B	chr15-57 (+121837), chr15-16 (+126829)	LMX1B	chr9-132 (+58649), chr9-110 (+59409), chr9-162 (+62275)	PRDM2	chr1-2307 (+183352)	STEAP1	chr7-1077 (+34039)	ZNF236	chr18-245 (+149677)
CD160	chr1-802 (+37466)	FER1L6	chr8-154 (+91076)	LNX1	chr4-75 (+131864)	PREP	chr6-1064 (+79891)	STEAP2	chr7-1077 (-23272)	ZNF318	chr6-563 (+34163)
CD276	chr15-28 (-123814)	FGF3	chr11-22 (-183179)	LRRK1	chr15-710 (+69241)	PRKAB2	chr1-1247 (+78981)	STH	chr17-203 (-4858), chr17-471 (-3255)	ZNF503	chr10-9 (-198148)
CD5	chr11-354 (-94925)	FGFR1	chr8-126 (+13109)	LY6E	chr8-474 (-27454)	PRKCDBP	chr11-494 (+40720)	STK24	chr13-81 (+14370)	ZNF532	chr18-343 (+33342)
CD6	chr11-354 (+35790)	FGGY	chr1-361 (-193311), chr1-227 (-96857)	LYST	chr1-1016 (-81194), chr1-220 (-26372)	PRKG2	chr4-249 (-183116), chr4-30 (-164661)	STK4	chr20-1025 (+111192)	ZNF592	chr15-48 (-48195)
CDC42EP3	chr2-27 (-194425), chr2-1016 (-179133), chr2-292 (-166656)	FIP1L1	chr4-75 (+82107)	LYZL2	chr10-46 (+91603)	PRLHR	chr10-1036 (+68452), chr10-32 (+124599)	STMN1	chr1-209 (+15541)	ZNF622	chr5-687 (+193068), chr5-298 (+193764), chr5-474 (+194664)
CDH16	chr16-379 (+19845)	FLNB	chr3-616 (-34148)	MAL2	chr8-138 (-125342)	PRMT8	chr12-1715 (-62279)	STRN4	chr19-640 (-24418)	ZNF664	chr12-192 (+102897)
CDHR3	chr7-35 (-25607)	FLT3	chr13-415 (+49504)	MANF	chr3-110 (+49761)	PRR15	chr7-394 (-141757)	SUDS3	chr12-226 (+122316)	ZNF703	chr8-56 (-140263), chr8-134 (-104081)
CDK5RAP2	chr9-332 (+194010)	FMN2	chr1-495 (+30945)	MAP2	chr2-1137 (-77606)	PRRX2	chr9-182 (+47491)	SUMO1	chr2-314 (+93977)	ZNRF4	chr19-300 (-33023)
CDK5RAP3	chr17-233 (+56393)	FMO1	chr1-902 (-47442)	MAP3K8	chr10-46 (+104222)	PSMD5	chr9-233 (-18454)	SYBU	chr8-151 (+111494)	ZZEF1	chr17-242 (+170582)
CELSR2	chr1-1088 (+9362)	FMO2	chr1-902 (+25266)	MARCH11	chr5-687 (-92949), chr5-298 (-92253), chr5-474 (-91353)	PSRC1	chr1-1088 (+23787)	SYT12	chr11-234 (+35409)		
CETN3	chr5-335 (+56414)	FOXA1	chr14-305 (-8831)	MAX	chr14-89 (-124685)	PTGES	chr9-182 (+39915)	TADA2B	chr4-199 (-112160)		

Table 3. Subset of 74 genes from the 634 genes associated with RXR-bound G1 enhancers. That exhibited RA-dependent gene expression patterns across the gut tube (GT), early (PP1) and late (PP2) pancreatic progenitor stages of pancreatic differentiation of hESCs.

Gene Names				
ABCA8	DHRS3	GLT8D2	MKRN3	RNF182
ADM	DNAH7	GPR37L1	MUC20	ROS1
AGO1	DUSP9	HMCN1	MYOF	SHH
ANO1	EHF	HOXA1	NEDD4L	SLC6A12
ASTN1	ELF3	HOXB1	NR2F2	SMOC1
ATP10B	EPHB3	HOXC4	PAQR7	STC2
B4GALNT3	ETS2	HSD17B14	PBX1	TMC6
C8orf49	FAM129A	IQGAP2	PLTP	TMEM110
CADM3	FANCE	ITGA11	POPDC3	TMEM44
CDC42EP3	FOXA1	ITGA6	PPARD	TRABD2B
CDHR3	GADD45G	ITPR3	PRKAB2	TTC30A
CHST15	GADL1	KCNJ4	PRKCDBP	VEGFA
CLIC6	GATA4	LNX1	PRR15	VILL
COLGALT	GFRA1	LYST	PTGIS	ZNF703
CSF3R	GIP	MECOM	RARB	

Table 4. Example commands and software packages used for ChIP- and RNA-seq data analysis workflow.

Command	Comments	Software package
bowtie2 -t --very-sensitive -x <hg19> input.fastq > output.sam	Map ChIP-seq data to the human genome. The option "--very-sensitive" sets multiple parameters. Specifically, it is equivalent to setting all the following options: -D 20 -R 3 -N 0 -L 20 -i S,1,0.50	Bowtie 2 v2.2.7
samtools view -bhu output.sam > output.bam	Convert SAM file format to BAM in order to sort.	Samtools v1.3.1
samtools sort output.bam > sorted_output.bam	Sort BAM file in order to remove duplicates.	Samtools v1.3.1
samtools rmdup -s sorted_output.bam rmdup_output.bam	Remove exact duplicate read sequences.	Samtools v1.3.1
makeTagDirectory rmdup_output_tagDir/ rmdup_output.bam -genome hg19 -checkGC	Generate tag directories for downstream analyses and analyze GC content of sequencing results.	HOMER v4.9
makeUCSCfile rmdup_output_tagDir/ -o auto -bigWig ~/chrom.sizes -fsize 1e20 > rmdup_output.trackInfo.txt	Generate a file for data visualization on a genome browser.	HOMER v4.9
getDifferentialPeaks PP1_H3K27ac_regions PP1_H3K27ac_tag_directory/ PP1_H3K27ac_tag_directory/ -F 2	Uses tag directories to analyze for differential peak intensity between samples. The -F 2 option designates >= 2-fold difference in peak intensity is a considered differential peak.	HOMER v4.9
windowBed -a distal_PP1_LSD1_peaks -b deactivating_enhancers_PP1_to_PP2 -w 1000 -u	Identify peaks in file “-a” that are near peaks/regions from file “-b”. The -w 1000 option looks for overlap ± 1000 bp of the peak.	Bedtools v2.17.0

ACKNOWLEDGEMENTS

Chapter 1 includes material that is currently being prepared for submission for publication, Vinckier, Nicholas; Patel, Nisha; Wang, Allen; Wang, Jinzhao; Carrano, Andrea; Benner, Christopher and Sander, Maike. “LSD1-mediated Decommissioning of Developmental Enhancers is Required for Proper Pancreatic Endocrine Formation”. The dissertation author was the primary investigator and author of this material. This work was supported by funds granted to MS from the National Institutes of Health, Pediatrics Diabetes Research Consortium and the California Institute for Regenerative Medicine.

CHAPTER 2 - DISSECTING THE ROLE OF NEUROGENIN-3 IN HUMAN ENDOCRINE DEVELOPMENT

ABSTRACT

Diabetes mellitus is a widespread pancreatic disease that is characterized by the loss or dysfunction of insulin-producing beta-cells. One method of treating diabetes is the transplantation of beta cells from cadaver donors to diabetic patients. However, the lack of donor material and the need for lifelong immunosuppression has precluded widespread use of this therapy. Generation of functional beta-cells from human embryonic stem cells (hESCs) would not only provide an attractive and renewable cell-replacement therapy, but would also greatly increase our ability to understand human pancreas endocrine development and the pathogenesis of related diseases. Current in vitro pancreatic differentiation protocols exist that can generate properly specified hESC-derived pancreatic progenitors which are capable of becoming functional beta-cells in vivo after engraftment into mice. Recent advances in the field have progressed the state of the art such that functional, glucose-responsive, insulin-secreting cells can now be generated entirely in vitro. However, these hESC-derived beta cells often secrete low levels of insulin in a manner that is reminiscent of immature fetal beta cells (Russ, Sintov et al. 2011, Pagliuca, Millman et al. 2014, Rezania, Bruin et al. 2014). Moreover, the time required to reach this stage, beginning from the hESC state, can be a month or longer (Russ, Sintov et al. 2011, Pagliuca, Millman et al. 2014, Rezania, Bruin et al. 2014). Thus, as they exist now, these cells are not yet suitable as beta-cell replacements. While this shows it is possible to make beta-cells from hESCs, there remains a great desire to more rapidly produce fully functional and mature beta-cells entirely in vitro. Understanding the events that dictate cell fate decisions during pancreas development is critical to improving current protocols to rapidly generate functional beta cells in vitro. To achieve this goal, a greater understanding of the transcriptional events that specify proper human endocrine formation is required.

INTRODUCTION

The pancreas is a vital organ composed of three main compartments: acinar, ductal and endocrine. The endocrine cells are localized together forming the islets of Langerhans. Within these islets are five endocrine cell subtypes: alpha, beta, delta, epsilon and PP cells, which produce the hormones glucagon, insulin, somatostatin, ghrelin and pancreatic polypeptide, respectively (Shih, Wang et al. 2013). The insulin-producing beta cells are responsible for maintaining blood glucose homeostasis and their dysfunction results in diabetes. The need for better treatments and understanding of this incredibly prevalent disease has instigated a massive effort to generate beta cells *in vitro* (Schulz 2015). The many advances that have been made in the development of *in vitro* pancreatic differentiation protocols have been inspired by lessons learned from the mouse. During early murine development, the pancreas emerges from the early embryonic structure called the posterior foregut (Seymour and Sander 2011, Shih, Wang et al. 2013). At this stage the nascent pancreatic buds consist entirely of multipotent progenitor cells (MPCs) marked by the transcription factors PDX1, SOX9, PTF1A and NKX6.1 (Seymour and Sander 2011, Arda, Benitez et al. 2013, Shih, Wang et al. 2013). These MPC's subsequently undergo a series of morphogenetic changes and cell fate decisions which result in generation of the diverse cell types and complex structure of the mature pancreas. The first fate decision undergone by MPCs determines whether the cells will be restricted to the tip domain (acinar cells) or trunk domain (ductal and endocrine cells). The transcription factors PTF1A and NKX6.1 act as master regulators of this decision, where PTF1A specifies tip identity, while NKX6.1 specifies trunk identity. Although they are co-expressed in early MPCs, mutual repression between PTF1A and NKX6.1 ensures complete segregation of the two domains giving rise to $PTF1A^{+}$ acinar cells and $NKX6.1^{+}$ bipotent trunk progenitors (Schaffer, Freude et al. 2010, Shih, Wang et al. 2013). These trunk progenitors can become either ductal or endocrine cells. The basic helix-loop-helix transcription factor neurogenin-3 (NGN3) is the major driver of the endocrine cell fate. In mice, deletion of *Ngn3* results in a total absence of endocrine cells, whereas ectopic expression in early MPCs induces premature differentiation to endocrine cells (Gradwohl, Dierich et al. 2000, Johansson, Dursun et al. 2007). Ngn3 is expressed for a short

time window in a subset of the bipotent trunk progenitors, during which it initiates cell-cycle exit and promotes terminal differentiation toward the endocrine fate (Schwitzgebel, Scheel et al. 2000, Gu, Dubauskaite et al. 2002, Gasa, Mrejen et al. 2004, Rukstalis and Habener 2009). Immunohistology of human embryonic tissue shows NGN3 follows a similar expression pattern to that observed in mice. Therefore, it is widely believed that NGN3 plays the same role in humans as it does in mice. However, studies of *NGN3* mutations, identified in non-diabetic humans, have raised some controversy over whether NGN3 is strictly required for human endocrine development.

In addition to the requirement of Ngn3 for endocrine development in mice, the timing of its expression is critical for proper development of endocrine subtypes. Genetic experiments in mice have shown that premature expression of Ngn3 in the developing embryo results in the production of polyhormonal endocrine cells (Apelqvist, Li et al. 1999, Schwitzgebel, Scheel et al. 2000, Johansson, Dursun et al. 2007). In addition, through slight alterations of the timing of Ngn3 expression during development in a *Ngn3*-null background, it was shown that different endocrine subtypes were produced depending on when Ngn3 was expressed (Johansson, Dursun et al. 2007). For example, when Ngn3 was reconstituted at a time prior to the onset of endogenous Ngn3 expression the majority of cells formed were glucagon$^+$ (Johansson, Dursun et al. 2007). While many of these cells appeared to be normal alpha cells, a large proportion (~30%) co-expressed hormones other than glucagon. Conversely, when Ngn3 was reconstituted at a time coincident with endogenous Ngn3 expression, the majority of cells formed were insulin$^+$. In this case, the insulin$^+$ cells obtained were fully functional beta cells, virtually indistinguishable from wild-type beta cells. Moreover, there was a complete absence of any polyhormonal cells in the resulting endocrine population. These studies indicate that the timing of Ngn3 expression is crucial not only for proper endocrine differentiation, but also in determining the subtype of endocrine cells produced.

Our lab employed a step-wise hESC differentiation protocol that mimics early endodermal and pancreatic development as shown by the correct induction of specific pancreatic markers, such as PDX1. This protocol reliably and efficiently generates pancreatic progenitors and endocrine cells in vitro. The resulting pancreatic progenitors are functional, as they are capable of further

differentiating into functional beta cells in vivo, following implantation into mice for 3-4 months (D'Amour, Bang et al. 2006, Kroon, Martinson et al. 2008, Schulz, Young et al. 2012). At the time of this study, however, the in vitro-derived endocrine cells were non-functional, characterized by the expression of multiple hormones, lack of true beta cell markers (NKX6.1, PDX1, MAFA), and the inability to secrete insulin in response to glucose stimulation. These endocrine cells are strikingly similar to the polyhormonal cells that result from early expression of Ngn3 in the aforementioned mice studies (Johansson, Dursun et al. 2007). Perhaps unsurprisingly, NGN3 is expressed too early during in vitro differentiation, preceding the appearance of the trunk progenitor markers SOX9, PDX1 and NKX6.1d. Based on mouse studies as well as our own observations, we hypothesized that this premature expression of NGN3, during the in vitro differentiation, induces endocrine formation in cells that have not been properly restricted to one subtype, causing them to express multiple hormones. Furthermore, we speculated that suppression of NGN3 expression until after the emergence of pancreatic progenitors could provide the cells sufficient time to become restricted to a single potential subtype. In this study, we examined the results of forced misexpression of NGN3 during pancreatic differentiation of human embryonic stem cells. Using lentiviral overexpression and shRNA knockdown strategies, we studied the role of NGN3 expression in pancreatic progenitors and demonstrated that NGN3 knockdown prevents endocrine formation while its overexpression induces differentiation to the endocrine stage. Our results provide direct evidence that, as in mice, NGN3 expression is necessary and sufficient for endocrine specification in human cells.

RESULTS

Knockdown of NGN3 in hESCs results in a decrease of endocrine cells.

To study human pancreatic endocrine development, our lab uses a step-wise differentiation protocol in which hESCs are aggregated in non-adherent conditions and differentiated to pancreatic progenitors and polyhormonal endocrine cells. These non-functional endocrine cells typically emerge by D13, which marks the end of the differentiation (Figure 7A). To determine whether

NGN3 is necessary for endocrine specification in our hESC differentiation system, we performed specific knockdown of *NGN3* in hESCs using lentiviral short hairpin RNAs (shRNAs). To do this, we used four lentiviral constructs, each containing a constitutively expressed shRNA sequence targeting a different region of the endogenous human *NGN3* transcript. Lentiviruses were constructed using our 2nd generation lentiviral assembly protocol and hESCs were transduced with a mixture of the four viruses. A scrambled shRNA construct was used to generate cell lines to be used as a negative control. A puromycin resistance gene within the construct allowed for selection of cells that had efficiently integrated the viral payload. Following expansion under puromycin selection, cells were passaged into non-adherent culture conditions and prepared for pancreatic differentiation. During normal differentiation, endogenous *NGN3* expression peaks at day 8 (D8) (Figure 7B). Quantitative PCR (qPCR) of both *NGN3* knockdown (*NGN3* KD) and control cells at D8 showed only about a 50% reduction in expression (Figure 8A). Although *NGN3* was only reduced by half, expression of *NEUROD1*, a direct target of NGN3, was reduced by about 75%. Immunofluorescence and qPCR analysis of D13 *NGN3* KD cells showed a drastic reduction of insulin and glucagon protein and mRNA levels, respectively (Figure 8B). This finding suggests that NGN3 is necessary for human endocrine development. Moreover, nearly all *NGN3* KD cells expressed pancreatic progenitor markers, suggesting NGN3 is dispensable for progenitor formation *in vitro* (Figure 8C). These observations are in agreement with results from studies of *Ngn3*$^{-/-}$ mice (Gradwohl, Dierich et al. 2000), which showed a complete lack of endocrine cells without Ngn3. However, because RNA knockdown did not fully abolish *NGN3* expression, and endocrine cells were still made, it became clear that a full knockout of *NGN3* in hESCs would be necessary to conclusively determine its necessity for human endocrine formation.

Overexpression of NGN3 in differentiating cells results in an increase of hormone expression.

To determine whether NGN3 is sufficient to induce endocrine formation, we constructed a lentiviral transfer vector comprised of the human cDNA sequence for *NGN3* preceded by the constitutive phosphoglycerate kinase (PGK) promoter. An identical construct expressing GFP was

used as a control. hESCs were differentiated in aggregate form to D7, dissociated and transduced with either the NGN3 overexpression (*NGN3* OE) or GFP lentivirus. Cells were allowed to re-aggregate and differentiation was continued normally to D13. 24 hours after transduction, samples were analyzed for expression of NGN3 by qPCR and immunofluorescence. While a robust increase in both endogenous and transgenic mRNA was observed, no significant change in NGN3 protein levels was detected (Figure 9A and data not shown). 3 days after transduction (D10) NGN3 protein expression appeared was slightly increased over controls, while qPCR analysis revealed *NGN3* transcript levels remained much higher than controls (Figure 9A and data not shown). By D13, *NGN3* mRNA levels were still very high compared to controls, but only a few NGN3$^+$ cells were observed by immunofluorescence (Figure 9A and 9B). Analysis of *NGN3* OE cells at D10 and D13 showed little to no increase in insulin and glucagon protein expression, while qPCR showed slightly elevated levels of hormone transcripts at D13 (Figure 9B). These results suggest that forced expression of NGN3 does not induce endocrine formation. This was most likely due to the lack of protein overexpression, despite clearly elevated levels of *NGN3* mRNA.

Due to the discrepancy between mRNA and protein expression, we suspected complex regulation of NGN3 was at play. Literature searches revealed abundant biochemical and *in vivo* evidence showing that NGN3, and the related NGN2, are heavily regulated at both the post-transcriptional and post-translational levels (Vosper, Fiore-Heriche et al. 2007, Vosper, McDowell et al. 2009, McDowell, Kucerova et al. 2010, Ali, Hindley et al. 2011, Hindley, Ali et al. 2012). Reasoning that the negative regulation of NGN3 might be brought on by its own expression, we sought to overexpress NGN3 at a later time to escape this regulation. we therefore overexpressed NGN3 at D10, when endogenous *NGN3* transcript has largely disappeared (Figure 7B). 3 days after transduction (D13) a significant increase in NGN3 protein expression was seen in *NGN3* OE cells but not in controls (Figure 9C). Insulin and glucagon mRNA levels were drastically increased in D13 *NGN3* OE cells compared to controls. In addition, immunofluorescence staining showed slightly more glucagon$^+$ cells in *NGN3* OE conditions compared to controls (Figure 9C). These results suggest NGN3 may be sufficient to induce endocrine specification in human cells.

During normal differentiation, a large proportion of cells express pancreatic progenitor markers by D10. However, many hormone$^+$ endocrine cells, as well as those destined to become endocrine cells, also exist at this stage. This is likely due to the endogenous wave of NGN3 expression observed around D8. As this endogenous expression preceded the transgenic overexpression at D10, it is possible that *NGN3* OE simply caused an increase in hormone expression in the endocrine/pre-endocrine cells rather than inducing pancreatic progenitors to become endocrine cells. In order to conclusively determine if NGN3 is sufficient to drive pancreatic progenitors to the endocrine fate, we induced NGN3 overexpression in sorted pancreatic progenitors prior to the premature wave of NGN3.

Overexpression of NGN3 in sorted hESC-derived progenitors induces the endocrine fate.

As previously stated, the in vitro protocol we use generates both pancreatic progenitors and polyhormonal endocrine cells. The heterogeneity of the differentiated cells has precluded our efforts to determine whether NGN3 can induce endocrine formation from hESC-derived pancreatic progenitors. In order to answer this question, we require a method to isolate the progenitors from the endocrine cells. Prior research by ViaCyte Inc. identified CD142 and CD200, as cell surface markers expressed on pancreatic progenitors or polyhormonal endocrine cells, respectively (Kelly, Chan et al. 2011). Fluorescence-activated cell sorting (FACS) using these markers allows for efficient separation of the two cell types (Kelly, Chan et al. 2011). Low cell viability following FACS precluded ViaCyte Inc.'s efforts to perform transplant experiments with purified progenitors. However, by employing a gentler method of magnetic-activated cell sorting (MACS), they showed that CD142$^+$ progenitors are capable of becoming functional beta-cells following transplantation, while CD200$^+$ endocrine cells are not (Kelly, Chan et al. 2011). We recently optimized a similar MACS method for use in our hESC differentiation system allowing for longer cell survival in culture.

Using the optimized MACS protocol, we were able to isolate a highly pure population of CD142$^+$ pancreatic progenitors at D13. To determine if NGN3 expression is sufficient to drive these progenitors to the endocrine fate, we transduced them with *NGN3* OE lentivirus, re-aggregated the

cells and continued culturing them for 9 days (D22). Immunofluorescence analysis showed robust NGN3 protein expression that was sustained to D22 (Figure 10A). Additionally, more hormone$^+$ cells, marked by the pan-endocrine protein chromogranin A (CHGA), were seen in *NGN3* OE cells compared to controls (Figure 10A). This result suggests NGN3 expression is sufficient to drive endocrine differentiation from pancreatic progenitors. To assess whether forced NGN3 expression in D13 progenitors made more monohormonal cells than cells expressing NGN3 earlier, we analyzed expression of the individual hormones insulin and glucagon in the endocrine cells produced (Figure 10B). The clear segregation of insulin and glucagon expression in those endocrine cells suggests the later progenitors, upon NGN3 expression, are capable of becoming monohormonal cells *in vitro* (Figure 10B). However, further characterization of these cells is necessary to ensure other pancreatic hormones are not co-expressed. Many of the *NGN3* OE cells that were insulin$^+$ also expressed the beta-cell marker NKX6.1 (Figure 10C), a characteristic lacking in the polyhormonal cells generated during normal differentiation. In contrast, the single insulin$^+$ cell identified in control cells did not co-express NKX6.1 (Figure 10C). Previous work from our lab has highlighted the extreme importance of NKX6.1 expression for both the differentiation to, and maintenance of, functional beta-cells in vivo (Sander, Sussel et al. 2000, Taylor, Liu et al. 2013). Up to this point, we had not observed robust NKX6.1 expression in any hormone$^+$ cells generated in vitro. While these results are encouraging, more work is required to fully assess the whether these hormone$^+$ cells generated via NGN3 overexpression in hESC-derived pancreatic progenitors can function as beta cells and secrete insulin in response to glucose stimulation.

DISCUSSION

The results presented here suggest that NGN3 is both necessary and sufficient to drive pancreatic endocrine formation in human cells, as it is in mice. In recent years, conclusive evidence in support of these conclusions has been published (McGrath, Watson et al. 2015). To continue to dissect the role of NGN3 in pancreatic endocrine specification and build upon this research, experiments in which NGN3 expression is rescued at different times during differentiation of *NGN3*-

null hESCs could determine whether timing and duration of NGN3 expression dictates the pancreatic endocrine subtypes that are formed. Aside from filling a knowledge gap in how NGN3 controls pancreatic endocrine formation, these experiments could ultimately pave the way for researchers to begin to generate whole human islets, complete with all endocrine subtypes, entirely in vitro. Although the topic of a cell replacement therapy for diabetes often solely focuses on the beta cell, there is evidence that other endocrine subtypes such as the glucagon-producing alpha cells may be vital for maintaining proper beta cell function (Rodriguez-Diaz, Dando et al. 2011). Therefore, generating whole pancreatic islets from hESCs may, someday become the gold standard of cell replacement therapies for diabetes.

A comprehensive understanding of the importance of proper spatial and temporal expression of transcription factors, like NGN3, during differentiation is crucial to advancing the state of the art of in vitro generation of hESC-based cell and organ replacement therapies (Trounson and DeWitt 2016). As the knowledge of the scientific community grows, one can envision a future in which generation of various different cell types from hESCs can be achieved entirely through precise manipulation of external signals, without the need for viral transductions or transfections of exogenous DNA or RNA. These methods could eventually be applied to patient-derived induced pluripotent cells to generate patient-specific replacement cells that are safe and effective and do not require immunosuppression, providing a virtually limitless source of “self-donor” material for patients who suffer from any number of ailments.

METHODS

Human embryonic stem cell (hESC) culture and expansion.

CyT49 human embryonic stem cells (NIH registration number: 0041) were maintained as previously described (Xie, Everett et al. 2013, Wang, Yue et al. 2015). Briefly, expansion of hESCs was achieved by passing cells every 3 days and culturing in sterile T-75 culture flasks (Corning®). Accutase™ (Innovative Cell Technologies) was used for cell dissociation and flasks were coated with a 10% (vol/vol) solution of human AB serum (Valley Biomedical). Flasks were seeded with 4 x

10^6 hESCs for 3 days of culture before passaging. Fresh maintenance media was supplied for hESCs each day and consisted of DMEM/F12 (Life Technologies) supplemented with 10% (vol/vol) KnockOut™ Serum Replacement XenoFree (Life Technologies), 0.1 mM MEM non-essential amino acids (Mediatech), 1X GlutaMAX™ (Life Technologies), 1% (vol/vol) penicillin/streptomycin (Life Technologies), 0.1 mM 2-mercaptoethanol (Life Technologies), 10 ng/mL Activin A (R&D Systems), and 10 ng/mL Heregulin-β1 (PeproTech).

Pancreatic differentiation of hESCs.

Pancreatic differentiation was performed as previously described (Schulz, Young et al. 2012, Xie, Everett et al. 2013, Wang, Yue et al. 2015). Briefly, we used a suspension-based culture format to differentiate cells in aggregate form. Undifferentiated aggregates of hESCs were formed by re-suspending dissociated cells in hESC maintenance media at a concentration of 1 x 10^6 cells/mL and plating 5.5 mL per well of the cell suspension in 6-well ultra-low attachment plates (Costar). The cells were cultured overnight on an orbital rotator (Innova2000, New Brunswick Scientific) at 95 rpm. After 24 hours the undifferentiated aggregates were washed once with RPMI media and supplied with 5.5 mL of Day 0 differentiation media. Thereafter, cells were supplied with the fresh media for the appropriate day of differentiation (see below). Cells were continually rotated at 95 rpm, or 105 rpm on days 4 through 8 and no media change was performed on Day10. Both RPMI (Mediatech) and DMEM High Glucose (HyClone) media were supplemented with 1X GlutaMAX™ and 1% penicillin/streptomycin. Human activin A, mouse Wnt3a, human KGF, human Noggin, and human EGF were purchased from R&D systems. Other added components included FBS (HyClone), B-27® supplement (Life Technologies), Insulin-Transferrin-Selenium (ITS; Life Technologies), TGFβ R1 kinase inhibitor IV (EMD Bioscience), KAAD-Cyclopamine (KC; Toronto Research Chemicals), and the retinoic receptor agonist TTNPB (RA; Sigma Aldrich). Day-specific media differentiation media formulations were as follows: Days 0 and 1: RPMI + 0.2% (v/v) FBS, 100 ng/mL Activin, 50 ng/mL mouse Wnt3a, 1:5000 ITS. Days 1 and 2: RPMI + 0.2% (v/v) FBS, 100ng/mL Activin, 1:5000 ITS. Days 2 and 3: RPMI + 0.2% (v/v) FBS, 2.5 mM TGFβ R1 kinase

inhibitor IV, 25 ng/mL KGF, 1:1000 ITS. Days 3 – 5: RPMI + 0.2% (v/v) FBS, 25 ng/mL KGF, 1:1000 ITS. Days 5 – 8: DMEM + 0.5X B-27® Supplement, 3 nM TTNPB, 0.25 mM Cyclopamine, 50 ng/mL Noggin. Days 8 – 12: DMEM/B27, 50 ng/mL KGF, 50 ng/mL EGF.

Design and construction of overexpression and knockdown lentiviruses.

Overexpression lentivirus was constructed using the pRRLSIN.cPPT.PGK-GFP.WPRE payload vector backbone. The GFP cassette was replaced by human *NGN3* cDNA through standard restriction digest and ligation cloning. *NGN3* cDNA was generated from hESC genomic DNA using the following primers: *NGN3*-F 5'- ATGACGCCTCAACCCTCG-3' and *NGN3*-R 5'-TCACAGAAAATCTGAGAAAGCC-3'. Knockdown lentivirus was constructed using payload vectors containing shRNA sequences targeting *NGN3* that have been previously described (McGrath, Watson et al. 2015). Lentiviruses were assembled via co-transfection of HEK293T cells with either overexpression or knockdown vectors, along with pCMV R8.74 and pMD.G helper plasmids. Viral supernatant was collected and concentrated by ultracentrifugation at 19,400 rpm for 2 hours using an Optima L-80 XP Ultracentrifuge (Beckman Coulter). To generate *NGN3* knockdown cell lines, undifferentiated hESCs were transduced with lentiviruses containing shRNAs targeting *NGN3* and maintained as described above, with the addition of 2 µg/mL puromycin to select for cells expressing the shRNA. Cells were maintained under antibiotic selection throughout expansion prior to seeding for differentiation. In order to overexpress *NGN3* during differentiation aggregated cells were first dissociated into single cells using Accutase™ and supplied with fresh differentiation media for the appropriate day, with 50 µL of viral concentrate added to the media. Plates were then placed back on the orbital rotator at 95 rpm at 37 °C overnight, to induce re-aggregation. Either GFP overexpression or scrambled shRNA viruses served as controls.

Magnetic sorting of pancreatic progenitors

Magnetic-activated cell sorting (MACS) to isolate pancreatic progenitors from polyhormonal cells was performed using the MACS® Cell Separation kit (Miltenyi Biotec). At Day

10 of differentiation, hESC-derived cell aggregates were dissociated using the reagents included with the MACS® Cell Suspension kit. This and all subsequent steps were carried out according to the manufacturer instructions. Primary antibodies targeting the cell-surface proteins used to distinguish progenitors from endocrine cells were CD200-APC and CD142-PE (1:10, BD Biosciences). Separated cells were collected in wells of new 6-well Ultra-low attachment plates and supplied with fresh Day 10 media. For *NGN3* overexpression experiments, sorted CD142$^+$ cells were transduced with *NGN3* overexpression virus prior to placing plates were back on the orbital rotator at 95 rpm at 37 °C overnight, to induce re-aggregation, and differentiation was continued normally.

Immunofluorescence analysis.

Cell aggregates derived from hESCs were allowed to settle in microcentrifuge tubes and washed twice with PBS before fixation with 4% paraformaldehyde for 30 min at room temperature. Fixed cells were washed twice with PBS and incubated overnight at 4 °C in 30% (w/v) sucrose in PBS. Cell aggregates were then loaded into disposable embedding molds (VWR), covered in Tissue-Tek® O.C.T. Sakura® Finetek compound (VWR) and flash frozen on dry ice to prepare frozen blocks. The blocks were sectioned at 10 µm and sections were placed on Superfrost Plus® (Thermo Fisher) microscope slides and washed with PBS for 10 min. Slide-mounted cell sections were permeabilized and blocked with blocking buffer, consisting of 0.15% (v/v) Triton X-100 (Sigma) and 1% (v/v) normal donkey serum (Jackson Immuno Research Laboratories) in PBS, for 1 hour at room temperature. Slides were then incubated overnight at 4 °C with primary antibody solutions. The following day slides were washed five times with PBS and incubated for 1 hour at room temperature with secondary antibody solutions. Cells were washed five times with PBS before coverslips were applied. All antibodies were diluted in blocking buffer at the ratios indicated below. Primary antibodies used were: sheep anti-NGN3 (1:300, R&D Systems); rabbit anti-SOX9 (1:1000 dilution, Millipore); goat anti-PDX1 (1:500 dilution, Abcam); mouse anti-NKX6.1 (1:300 dilution, Developmental Studies Hybridoma Bank); rabbit anti-CHGA (1:1000, DAKO); guinea pig anti-INS

(1:500, DAKO), mouse anti-GCG (1:500, Sigma), rabbit anti-SST (1:500, DAKO). Secondary antibodies against sheep, rabbit, goat, mouse and guinea pig were Alexa488-, Cy3- and Cy5-conjugated donkey antibodies and were used at dilutions of 1:1000, 1:2000, and 1:250, respectively (Jackson Immuno Research Laboratories). Representative images were obtained with a Zeiss Axio-Observer-Z1 microscope equipped with a Zeiss ApoTome and AxioCam digital camera. Figures were prepared in Adobe Creative Suite 5.

Reverse Transcription and Quantitative PCR (RT-qPCR) analysis.

Total RNA was isolated from hESC-derived cell aggregates using the RNeasy® Micro Kit (Qiagen). Synthesis of cDNA was performed using the iScript™ cDNA Synthesis Kit (Bio-Rad) and 500 ng of isolated RNA per reaction. PCR reactions were performed in triplicate with 10 ng of template cDNA per reaction using a CFX96™ Real-Time PCR Detection System and the iQ™ SYBR® Green Supermix (Bio-Rad). PCR of the TATA binding protein (TBP) coding sequence was used as an internal control and relative expression was quantified via double delta C_T analysis.

Primers used for RT-qPCR are as follows:

INS-F: 5'-AAGAGGCCATCAAGCAGATCA

INS-R: 5'-CAGGAGGCGCATCCACA

GCG-F: 5'-AAGCATTTACTTTGTGGCTGGATT

GCG-R: 5'-TGATCTGGATTTCTCCTCTGTGTCT

SST-F*:* 5'-CCCCAGACTCCGTCAGTTTC

SST-R: 5'-TCCGTCTGGTTGGGTTCAG

NGN3-F: 5'-ACTGTCCAAGTGACCCGTGA

NGN3-R: 5'-TCAGTGCCAACTCGCTCTTAG

TBP-F: 5'-ATTAAGGGAGGGAGTGGCAC

TBP-R: 5'-GCTTTGCTTCCCTTTCCCAA

FIGURES

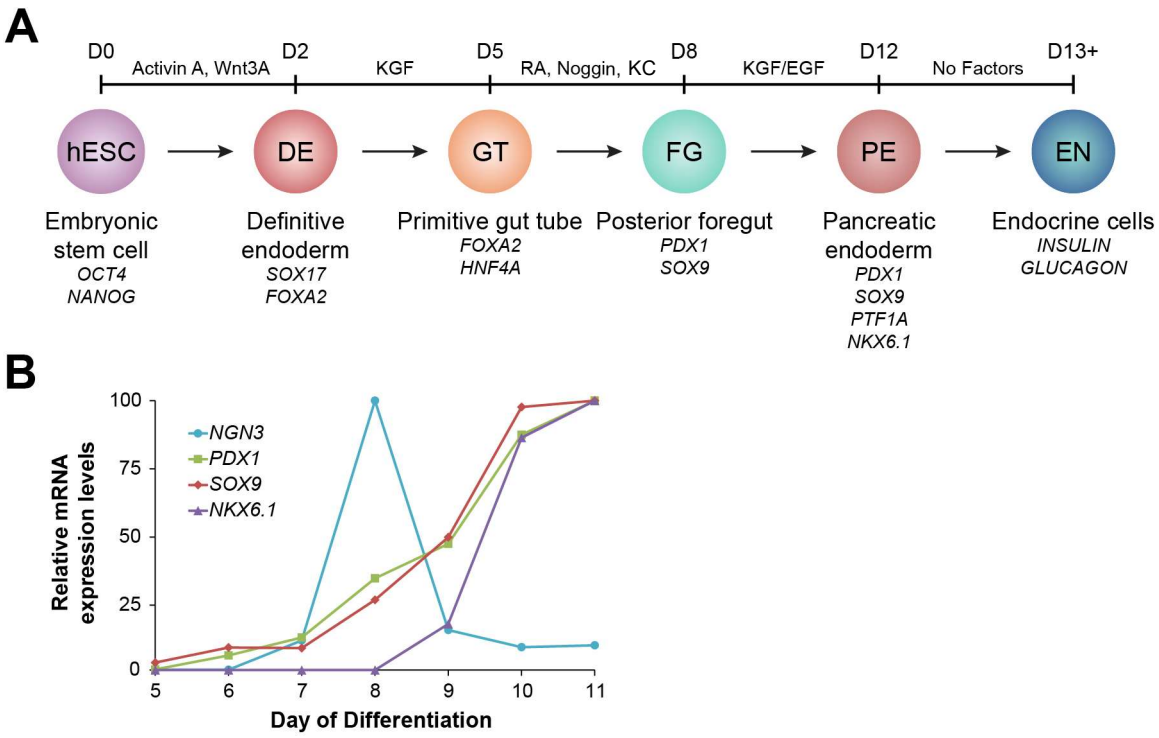

Figure 7. Pancreatic Differentiation of hESCs. (**A**) Schematic of directed differentiation protocol from human embryonic stem cells (hESCs), through lineage intermediates, to hormone$^+$ cells. Timing of expression for key stage-specific protein markers shown below stage names. Exogenous differentiation factors added to media are listed for the appropriate stages. (**B**) Relative mRNA levels during differentiation show peak activation of *NGN3* before that of the trunk progenitor markers *NKX6.1*, *PDX1* and *SOX9*. Relative expression values shown as percentages (0 – 100) of each gene's maximum expression across the differentiation time course.

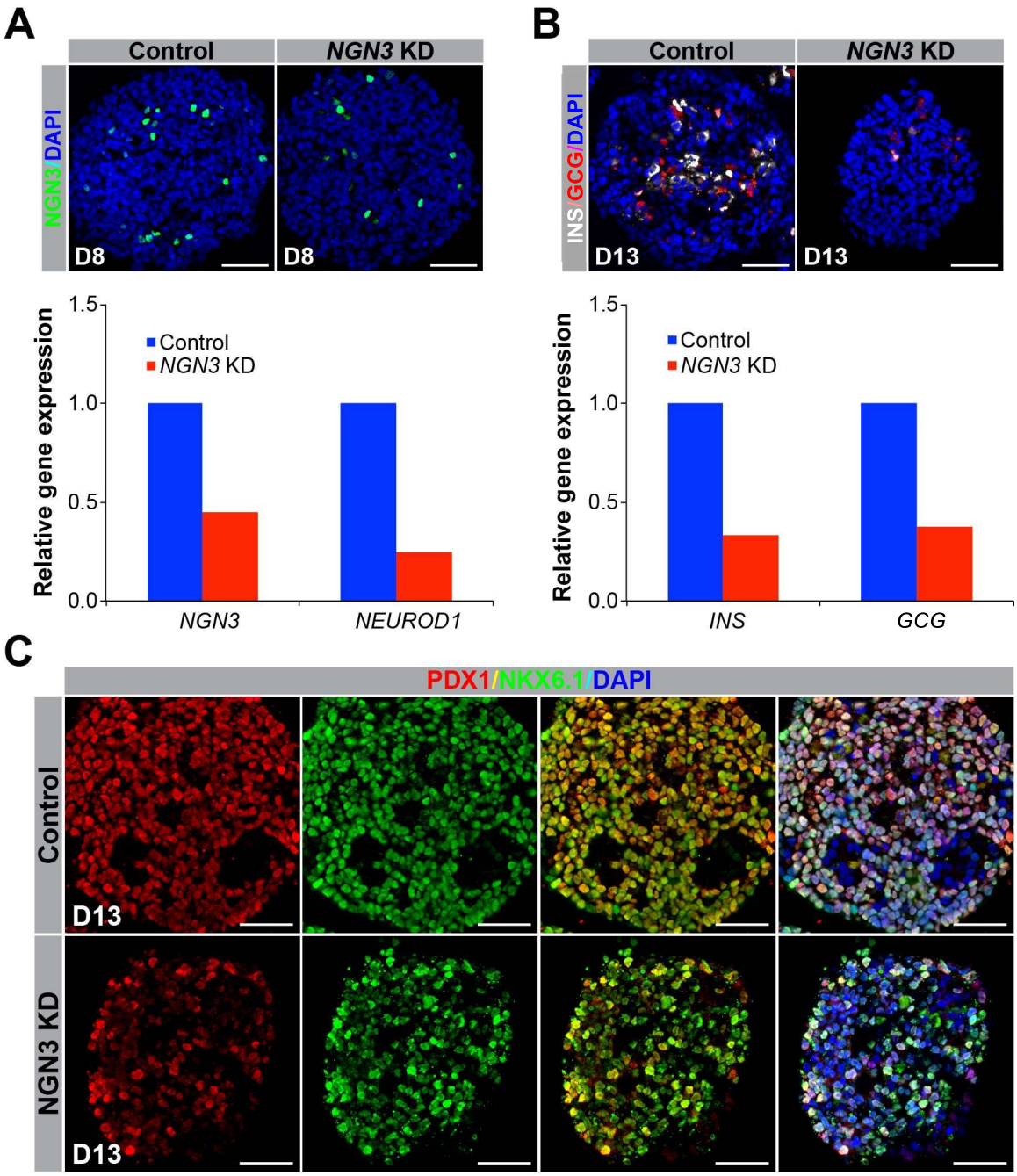

Figure 8. Knockdown of *NGN3* Prevents Formation of hESC-derived Pancreatic Endocrine Cells. (**A**) Immunofluorescence analysis for NGN3 expression (top) and RT-qPCR analysis of mRNA levels for *NGN3* and its downstream target, *NEUROD1* at D8 of differentiation. (**B**) End-stage analysis for insulin and glucagon show diminished expression of both hormones in NGN3 KD cells. (**C**) NGN3 KD cells still express the pancreatic trunk progenitor markers NKX6.1 and PDX1. Scale bars, 50 μM.

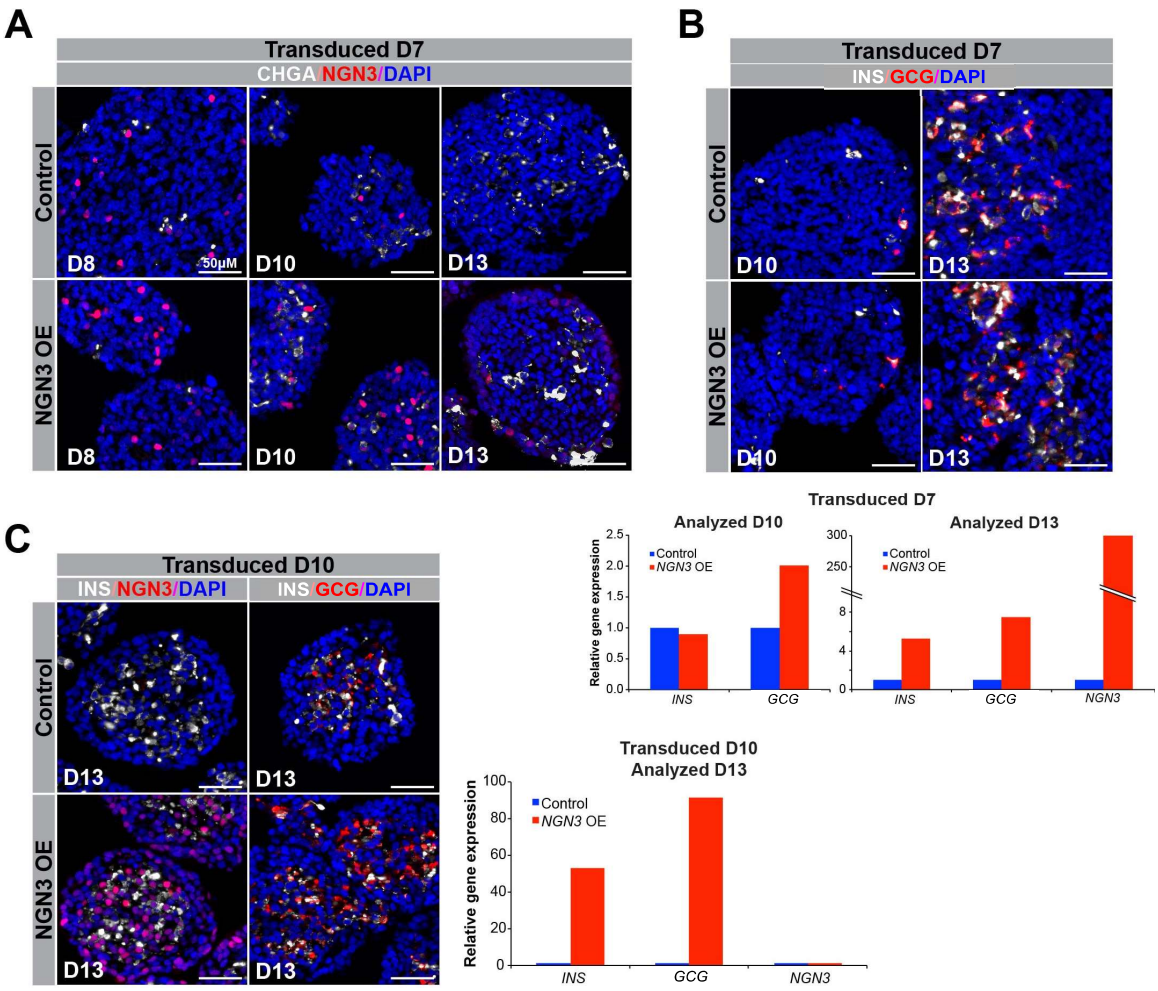

Figure 9. Overexpression of NGN3 at Different Times During Pancreatic Differentiation of hESCs. (**A**) Immunofluorescence analysis for NGN3 and chromogranin A (CHGA) 1, 3 and 5 days after D7 transduction of NGN3 OE. (**B**) Immunofluorescence (above) and RT-qPCR (below) analysis for insulin and glucagon 3 and 6 days after D7 transduction. End-stage RT-qPCR analysis for *NGN3* also shown (below). (**C**) Immunofluorescence (left) and RT-qPCR (right) analysis for NGN3, insulin and glucagon 3 days after D10 transduction. End-stage RT-qPCR analysis for NGN3 also shown (right). Scale bars, 50 μM.

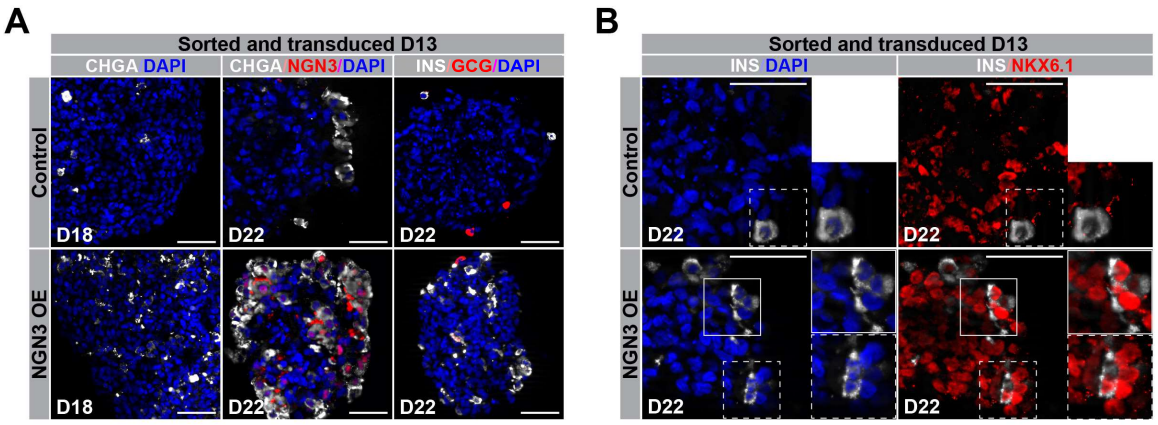

Figure 10. Overexpression of NGN3 in Magnetically Sorted CD142⁺ Pancreatic Progenitors. (**A**) Immunofluorescence analysis for CHGA, NGN3, insulin and glucagon 5 and 9 days after transduction of NGN3 OE in CD142⁺ D13 progenitors isolated by MACS. (**B**) Immunofluorescence analysis for insulin and NKX6.1 9 days after transduction of NGN3 OE in CD142⁺ D13 progenitors. Individual insulin⁺ cells highlighted (white boxes) and magnified. Scale bars, 50 μM.

ACKNOWLEDGEMENTS

Chapter 2 includes material of which the dissertation author was the primary investigator and author. This work was supported by funds granted to MS from the National Institutes of Health, Pediatrics Diabetes Research Consortium and the California Institute for Regenerative Medicine. In addition to these sources, NKV was also supported, in part, by the UCSD institutional Cancer Cell Biology training grant, from the National Institutes of Health.

CONCLUSION

From neurons and heart muscle to liver and pancreas and everything in between, each of these specialized cell types stems from pluripotent cells containing genomes identical to one another. How then can these highly distinct cell types arise from cells that all contain the exact same genes? This is one of the most important, unanswered questions of developmental biology . Research into this question has identified that modulation of the three-dimensional structure of DNA within the nucleus as a major component influencing gene expression (Shogren-Knaak, Ishii et al. 2006, Martino, Kueng et al. 2009). The reshaping of chromatin in a cell type-specific manner instills different developmental competencies in different cells, allowing them to navigate through various lineage intermediates of their respective cell fates even while exposed to the same inductive cues (Xie, Everett et al. 2013, Wang, Yue et al. 2015).

While in vivo animal studies have provided incredible insights into development and disease, and still serve as important models, hPSC-based in vitro differentiation systems provide the unique ability to dissect such developmental mechanisms, on a molecular level often not feasible in animal models. Indeed, the shear amount of cellular material required for certain assays like mapping the chromatin landscape throughout embryonic development would require a staggering number animal sacrifices and the associated costs quickly make these kinds of studies in animals impractical. Fortunately, in vitro models like the hESC-based in vitro pancreatic differentiation system employed here, have provided us and others with the tools required for systematic and meticulous examination of the various mechanisms involved in cell differentiation and development.

REFERENCES

Adamo, A., B. Sese, S. Boue, J. Castano, I. Paramonov, M. J. Barrero and J. C. Izpisua Belmonte (2011). "LSD1 regulates the balance between self-renewal and differentiation in human embryonic stem cells." Nat Cell Biol **13**(6): 652-659.

Ali, F., C. Hindley, G. McDowell, R. Deibler, A. Jones, M. Kirschner, F. Guillemot and A. Philpott (2011). "Cell cycle-regulated multi-site phosphorylation of Neurogenin 2 coordinates cell cycling with differentiation during neurogenesis." Development **138**(19): 4267-4277.

Andrews, S. (2010). "FastQC: a quality control tool for high throughput sequence data. Available online at: http://www.bioinformatics.babraham.ac.uk/projects/fastqc."

Annunziato, A. T. (2008). "DNA Packaging: Nucleosomes and Chromatin." Nature Education **1(1):26**.

Apelqvist, A., H. Li, L. Sommer, P. Beatus, D. J. Anderson, T. Honjo, M. Hrabe de Angelis, U. Lendahl and H. Edlund (1999). "Notch signalling controls pancreatic cell differentiation." Nature **400**(6747): 877-881.

Arda, H. E., C. M. Benitez and S. K. Kim (2013). "Gene regulatory networks governing pancreas development." Dev Cell **25**(1): 5-13.

Avantaggiato, V., D. Acampora, F. Tuorto and A. Simeone (1996). "Retinoic acid induces stage-specific repatterning of the rostral central nervous system." Dev Biol **175**(2): 347-357.

Avior, Y., I. Sagi and N. Benvenisty (2016). "Pluripotent stem cells in disease modelling and drug discovery." Nat Rev Mol Cell Biol **17**(3): 170-182.

Balmer, J. E. and R. Blomhoff (2002). "Gene expression regulation by retinoic acid." J Lipid Res **43**(11): 1773-1808.

Balmer, J. E. and R. Blomhoff (2005). "A robust characterization of retinoic acid response elements based on a comparison of sites in three species." J Steroid Biochem Mol Biol **96**(5): 347-354.

Bernstein, B. E., T. S. Mikkelsen, X. Xie, M. Kamal, D. J. Huebert, J. Cuff, B. Fry, A. Meissner, M. Wernig, K. Plath, R. Jaenisch, A. Wagschal, R. Feil, S. L. Schreiber and E. S. Lander (2006). "A bivalent chromatin structure marks key developmental genes in embryonic stem cells." Cell **125**(2): 315-326.

Bibel, M., J. Richter, K. Schrenk, K. L. Tucker, V. Staiger, M. Korte, M. Goetz and Y. A. Barde (2004). "Differentiation of mouse embryonic stem cells into a defined neuronal lineage." Nat Neurosci **7**(9): 1003-1009.

Campbell-Thompson, M., C. Wasserfall, J. Kaddis, A. Albanese-O'Neill, T. Staeva, C. Nierras, J. Moraski, P. Rowe, R. Gianani, G. Eisenbarth, J. Crawford, D. Schatz, A. Pugliese and M. Atkinson (2012). "Network for Pancreatic Organ Donors with Diabetes (nPOD): developing a tissue biobank for type 1 diabetes." Diabetes Metab Res Rev **28**(7): 608-617.

Chen, Y., F. C. Pan, N. Brandes, S. Afelik, M. Solter and T. Pieler (2004). "Retinoic acid signaling is essential for pancreas development and promotes endocrine at the expense of exocrine cell differentiation in Xenopus." Dev Biol **271**(1): 144-160.

Creyghton, M. P., A. W. Cheng, G. G. Welstead, T. Kooistra, B. W. Carey, E. J. Steine, J. Hanna, M. A. Lodato, G. M. Frampton, P. A. Sharp, L. A. Boyer, R. A. Young and R. Jaenisch (2010). "Histone H3K27ac separates active from poised enhancers and predicts developmental state." Proc Natl Acad Sci U S A **107**(50): 21931-21936.

Cunningham, T. J. and G. Duester (2015). "Mechanisms of retinoic acid signalling and its roles in organ and limb development." Nat Rev Mol Cell Biol **16**(2): 110-123.

D'Amour, K. A., A. G. Bang, S. Eliazer, O. G. Kelly, A. D. Agulnick, N. G. Smart, M. A. Moorman, E. Kroon, M. K. Carpenter and E. E. Baetge (2006). "Production of pancreatic hormone-expressing endocrine cells from human embryonic stem cells." Nat Biotechnol **24**(11): 1392-1401.

Dobin, A., C. A. Davis, F. Schlesinger, J. Drenkow, C. Zaleski, S. Jha, P. Batut, M. Chaisson and T. R. Gingeras (2013). "STAR: ultrafast universal RNA-seq aligner." Bioinformatics **29**(1): 15-21.

Durston, A. J., J. P. Timmermans, W. J. Hage, H. F. Hendriks, N. J. de Vries, M. Heideveld and P. D. Nieuwkoop (1989). "Retinoic acid causes an anteroposterior transformation in the developing central nervous system." Nature **340**(6229): 140-144.

Duteil, D., M. Tosic, F. Lausecker, H. Z. Nenseth, J. M. Muller, S. Urban, D. Willmann, K. Petroll, N. Messaddeq, L. Arrigoni, T. Manke, J. W. Kornfeld, J. C. Bruning, V. Zagoriy, M. Meret, J. Dengjel, T. Kanouni and R. Schule (2016). "Lsd1 Ablation Triggers Metabolic Reprogramming of Brown Adipose Tissue." Cell Rep **17**(4): 1008-1021.

Encode Project Consortium (2012). "An integrated encyclopedia of DNA elements in the human genome." Nature **489**(7414): 57-74.

Ernst, J., P. Kheradpour, T. S. Mikkelsen, N. Shoresh, L. D. Ward, C. B. Epstein, X. Zhang, L. Wang, R. Issner, M. Coyne, M. Ku, T. Durham, M. Kellis and B. E. Bernstein (2011). "Mapping and analysis of chromatin state dynamics in nine human cell types." Nature **473**(7345): 43-49.

Forneris, F., C. Binda, A. Dall'Aglio, M. W. Fraaije, E. Battaglioli and A. Mattevi (2006). "A highly specific mechanism of histone H3-K4 recognition by histone demethylase LSD1." J Biol Chem **281**(46): 35289-35295.

Foster, C. T., O. M. Dovey, L. Lezina, J. L. Luo, T. W. Gant, N. Barlev, A. Bradley and S. M. Cowley (2010). "Lysine-specific demethylase 1 regulates the embryonic transcriptome and CoREST stability." Mol Cell Biol **30**(20): 4851-4863.

Garcia-Ramirez, M., C. Rocchini and J. Ausio (1995). "Modulation of chromatin folding by histone acetylation." J Biol Chem **270**(30): 17923-17928.

Gasa, R., C. Mrejen, N. Leachman, M. Otten, M. Barnes, J. Wang, S. Chakrabarti, R. Mirmira and M. German (2004). "Proendocrine genes coordinate the pancreatic islet differentiation program in vitro." Proc Natl Acad Sci U S A **101**(36): 13245-13250.

Gradwohl, G., A. Dierich, M. LeMeur and F. Guillemot (2000). "neurogenin3 is required for the development of the four endocrine cell lineages of the pancreas." Proc Natl Acad Sci U S A **97**(4): 1607-1611.

Grunstein, M. (1997). "Histone acetylation in chromatin structure and transcription." Nature **389**(6649): 349-352.

Gu, G., J. Dubauskaite and D. A. Melton (2002). "Direct evidence for the pancreatic lineage: NGN3+ cells are islet progenitors and are distinct from duct progenitors." Development **129**(10): 2447-2457.

Hanna, J. H., K. Saha and R. Jaenisch (2010). "Pluripotency and cellular reprogramming: facts, hypotheses, unresolved issues." Cell **143**(4): 508-525.

Head, S. R., H. K. Komori, S. A. LaMere, T. Whisenant, F. Van Nieuwerburgh, D. R. Salomon and P. Ordoukhanian (2014). "Library construction for next-generation sequencing: overviews and challenges." Biotechniques **56**(2): 61-64, 66, 68, passim.

Heintzman, N. D., G. C. Hon, R. D. Hawkins, P. Kheradpour, A. Stark, L. F. Harp, Z. Ye, L. K. Lee, R. K. Stuart, C. W. Ching, K. A. Ching, J. E. Antosiewicz-Bourget, H. Liu, X. Zhang, R. D. Green, V. V. Lobanenkov, R. Stewart, J. A. Thomson, G. E. Crawford, M. Kellis and B. Ren (2009). "Histone modifications at human enhancers reflect global cell-type-specific gene expression." Nature **459**(7243): 108-112.

Heinz, S., C. Benner, N. Spann, E. Bertolino, Y. C. Lin, P. Laslo, J. X. Cheng, C. Murre, H. Singh and C. K. Glass (2010). "Simple combinations of lineage-determining transcription factors prime cis-regulatory elements required for macrophage and B cell identities." Mol Cell **38**(4): 576-589.

Heinz, S. and C. K. Glass (2012). "Roles of lineage-determining transcription factors in establishing open chromatin: lessons from high-throughput studies." Curr Top Microbiol Immunol **356**: 1-15.

Heinz, S., C. E. Romanoski, C. Benner and C. K. Glass (2015). "The selection and function of cell type-specific enhancers." Nat Rev Mol Cell Biol **16**(3): 144-154.

Hindley, C., F. Ali, G. McDowell, K. Cheng, A. Jones, F. Guillemot and A. Philpott (2012). "Post-translational modification of Ngn2 differentially affects transcription of distinct targets to regulate the balance between progenitor maintenance and differentiation." Development **139**(10): 1718-1723.

Hockemeyer, D. and R. Jaenisch (2016). "Induced Pluripotent Stem Cells Meet Genome Editing." Cell Stem Cell **18**(5): 573-586.

Jaenisch, R. and R. Young (2008). "Stem cells, the molecular circuitry of pluripotency and nuclear reprogramming." Cell **132**(4): 567-582.

Johansson, K. A., U. Dursun, N. Jordan, G. Gu, F. Beermann, G. Gradwohl and A. Grapin-Botton (2007). "Temporal control of neurogenin3 activity in pancreas progenitors reveals competence windows for the generation of different endocrine cell types." Dev Cell **12**(3): 457-465.

Kaikkonen, M. U., N. J. Spann, S. Heinz, C. E. Romanoski, K. A. Allison, J. D. Stender, H. B. Chun, D. F. Tough, R. K. Prinjha, C. Benner and C. K. Glass (2013). "Remodeling of the enhancer landscape during macrophage activation is coupled to enhancer transcription." Mol Cell **51**(3): 310-325.

Kam, R. K., W. Shi, S. O. Chan, Y. Chen, G. Xu, C. B. Lau, K. P. Fung, W. Y. Chan and H. Zhao (2013). "Dhrs3 protein attenuates retinoic acid signaling and is required for early embryonic patterning." J Biol Chem **288**(44): 31477-31487.

Keller, G. (2005). "Embryonic stem cell differentiation: emergence of a new era in biology and medicine." Genes Dev **19**(10): 1129-1155.

Kelly, O. G., M. Y. Chan, L. A. Martinson, K. Kadoya, T. M. Ostertag, K. G. Ross, M. Richardson, M. K. Carpenter, K. A. D'Amour, E. Kroon, M. Moorman, E. E. Baetge and A. G. Bang (2011). "Cell-surface markers for the isolation of pancreatic cell types derived from human embryonic stem cells." Nat Biotechnol **29**(8): 750-756.

Kent, W. J., C. W. Sugnet, T. S. Furey, K. M. Roskin, T. H. Pringle, A. M. Zahler and D. Haussler (2002). "The human genome browser at UCSC." Genome Res **12**(6): 996-1006.

Kerenyi, M. A., Z. Shao, Y. J. Hsu, G. Guo, S. Luc, K. O'Brien, Y. Fujiwara, C. Peng, M. Nguyen and S. H. Orkin (2013). "Histone demethylase Lsd1 represses hematopoietic stem and progenitor cell signatures during blood cell maturation." Elife **2**: e00633.

Kim, T. K. and R. Shiekhattar (2015). "Architectural and Functional Commonalities between Enhancers and Promoters." Cell **162**(5): 948-959.

Koch, C. M., R. M. Andrews, P. Flicek, S. C. Dillon, U. Karaoz, G. K. Clelland, S. Wilcox, D. M. Beare, J. C. Fowler, P. Couttet, K. D. James, G. C. Lefebvre, A. W. Bruce, O. M. Dovey, P. D. Ellis, P. Dhami, C. F. Langford, Z. Weng, E. Birney, N. P. Carter, D. Vetrie and I. Dunham (2007). "The landscape of histone modifications across 1% of the human genome in five human cell lines." Genome Res **17**(6): 691-707.

Kroon, E., L. A. Martinson, K. Kadoya, A. G. Bang, O. G. Kelly, S. Eliazer, H. Young, M. Richardson, N. G. Smart, J. Cunningham, A. D. Agulnick, K. A. D'Amour, M. K. Carpenter and E. E. Baetge (2008). "Pancreatic endoderm derived from human embryonic stem cells generates glucose-responsive insulin-secreting cells in vivo." Nat Biotechnol **26**(4): 443-452.

Langmead, B. and S. L. Salzberg (2012). "Fast gapped-read alignment with Bowtie 2." Nat Methods **9**(4): 357-359.

Laurent, B., L. Ruitu, J. Murn, K. Hempel, R. Ferrao, Y. Xiang, S. Liu, B. A. Garcia, H. Wu, F. Wu, H. Steen and Y. Shi (2015). "A specific LSD1/KDM1A isoform regulates neuronal differentiation through H3K9 demethylation." Mol Cell **57**(6): 957-970.

Lee, D. Y., J. J. Hayes, D. Pruss and A. P. Wolffe (1993). "A positive role for histone acetylation in transcription factor access to nucleosomal DNA." Cell **72**(1): 73-84.

Li, A., Y. Sun, C. Dou, J. Chen and J. Zhang (2012). "Lysine-specific demethylase 1 expression in zebrafish during the early stages of neuronal development." Neural Regen Res **7**(34): 2719-2726.

Li, H., B. Handsaker, A. Wysoker, T. Fennell, J. Ruan, N. Homer, G. Marth, G. Abecasis, R. Durbin and S. Genome Project Data Processing (2009). "The Sequence Alignment/Map format and SAMtools." Bioinformatics **25**(16): 2078-2079.

Linker, C. and C. D. Stern (2004). "Neural induction requires BMP inhibition only as a late step, and involves signals other than FGF and Wnt antagonists." Development **131**(22): 5671-5681.

Love, M. I., W. Huber and S. Anders (2014). "Moderated estimation of fold change and dispersion for RNA-seq data with DESeq2." Genome Biol **15**(12): 550.

Mahony, S., E. O. Mazzoni, S. McCuine, R. A. Young, H. Wichterle and D. K. Gifford (2011). "Ligand-dependent dynamics of retinoic acid receptor binding during early neurogenesis." Genome Biol **12**(1): R2.

Mark, M., N. B. Ghyselinck and P. Chambon (2009). "Function of retinoic acid receptors during embryonic development." Nucl Recept Signal **7**: e002.

Martin, M., J. Gallego-Llamas, V. Ribes, M. Kedinger, K. Niederreither, P. Chambon, P. Dolle and G. Gradwohl (2005). "Dorsal pancreas agenesis in retinoic acid-deficient Raldh2 mutant mice." Dev Biol **284**(2): 399-411.

Martino, F., S. Kueng, P. Robinson, M. Tsai-Pflugfelder, F. van Leeuwen, M. Ziegler, F. Cubizolles, M. M. Cockell, D. Rhodes and S. M. Gasser (2009). "Reconstitution of yeast silent chromatin: multiple contact sites and O-AADPR binding load SIR complexes onto nucleosomes in vitro." Mol Cell **33**(3): 323-334.

McCarthy, D. J., Y. Chen and G. K. Smyth (2012). "Differential expression analysis of multifactor RNA-Seq experiments with respect to biological variation." Nucleic Acids Res **40**(10): 4288-4297.

McDowell, G. S., R. Kucerova and A. Philpott (2010). "Non-canonical ubiquitylation of the proneural protein Ngn2 occurs in both Xenopus embryos and mammalian cells." Biochem Biophys Res Commun **400**(4): 655-660.

McGrath, P. S., C. L. Watson, C. Ingram, M. A. Helmrath and J. M. Wells (2015). "The Basic Helix-Loop-Helix Transcription Factor NEUROG3 Is Required for Development of the Human Endocrine Pancreas." Diabetes **64**(7): 2497-2505.

McLean, C. Y., D. Bristor, M. Hiller, S. L. Clarke, B. T. Schaar, C. B. Lowe, A. M. Wenger and G. Bejerano (2010). "GREAT improves functional interpretation of cis-regulatory regions." Nat Biotechnol **28**(5): 495-501.

Mercer, E. M., Y. C. Lin, C. Benner, S. Jhunjhunwala, J. Dutkowski, M. Flores, M. Sigvardsson, T. Ideker, C. K. Glass and C. Murre (2011). "Multilineage priming of enhancer repertoires precedes commitment to the B and myeloid cell lineages in hematopoietic progenitors." Immunity **35**(3): 413-425.

Metzger, E., M. Wissmann, N. Yin, J. M. Muller, R. Schneider, A. H. Peters, T. Gunther, R. Buettner and R. Schule (2005). "LSD1 demethylates repressive histone marks to promote androgen-receptor-dependent transcription." Nature **437**(7057): 436-439.

Molotkov, A., N. Molotkova and G. Duester (2005). "Retinoic acid generated by Raldh2 in mesoderm is required for mouse dorsal endodermal pancreas development." Dev Dyn **232**(4): 950-957.

Morton, N. E. (1991). "Parameters of the human genome." Proc Natl Acad Sci U S A **88**(17): 7474-7476.

Motte, E., E. Szepessy, K. Suenens, G. Stange, M. Bomans, D. Jacobs-Tulleneers-Thevissen, Z. Ling, E. Kroon, D. Pipeleers and E.-F. Beta Cell Therapy Consortium (2014). "Composition and function of macroencapsulated human embryonic stem cell-derived implants: comparison with clinical human islet cell grafts." Am J Physiol Endocrinol Metab **307**(9): E838-846.

Nair, V. D., Y. Ge, N. Balasubramaniyan, J. Kim, Y. Okawa, M. Chikina, O. Troyanskaya and S. C. Sealfon (2012). "Involvement of histone demethylase LSD1 in short-time-scale gene expression changes during cell cycle progression in embryonic stem cells." Mol Cell Biol **32**(23): 4861-4876.

Nakamura, E., M. T. Nguyen and S. Mackem (2006). "Kinetics of tamoxifen-regulated Cre activity in mice using a cartilage-specific CreER(T) to assay temporal activity windows along the proximodistal limb skeleton." Dev Dyn **235**(9): 2603-2612.

O'Geen, H., L. Echipare and P. J. Farnham (2011). "Using ChIP-seq technology to generate high-resolution profiles of histone modifications." Methods Mol Biol **791**: 265-286.

Pagliuca, F. W., J. R. Millman, M. Gurtler, M. Segel, A. Van Dervort, J. H. Ryu, Q. P. Peterson, D. Greiner and D. A. Melton (2014). "Generation of functional human pancreatic beta cells in vitro." Cell **159**(2): 428-439.

Papp, B. and K. Plath (2013). "Epigenetics of reprogramming to induced pluripotency." Cell **152**(6): 1324-1343.

Peng, Y. B., M. Yerle and B. Liu (2009). "Mapping and expression analyses during porcine foetal muscle development of 12 genes involved in histone modifications." Anim Genet **40**(2): 242-246.

Pham, T. H., J. Minderjahn, C. Schmidl, H. Hoffmeister, S. Schmidhofer, W. Chen, G. Langst, C. Benner and M. Rehli (2013). "Mechanisms of in vivo binding site selection of the hematopoietic master transcription factor PU.1." Nucleic Acids Res **41**(13): 6391-6402.

Plachta, N., M. Bibel, K. L. Tucker and Y. A. Barde (2004). "Developmental potential of defined neural progenitors derived from mouse embryonic stem cells." Development **131**(21): 5449-5456.

Quinlan, A. R. and I. M. Hall (2010). "BEDTools: a flexible suite of utilities for comparing genomic features." Bioinformatics **26**(6): 841-842.

Rada-Iglesias, A., R. Bajpai, T. Swigut, S. A. Brugmann, R. A. Flynn and J. Wysocka (2011). "A unique chromatin signature uncovers early developmental enhancers in humans." Nature **470**(7333): 279-283.

Rada-Iglesias, A. and J. Wysocka (2011). "Epigenomics of human embryonic stem cells and induced pluripotent stem cells: insights into pluripotency and implications for disease." Genome Med **3**(6): 36.

Rezania, A., J. E. Bruin, P. Arora, A. Rubin, I. Batushansky, A. Asadi, S. O'Dwyer, N. Quiskamp, M. Mojibian, T. Albrecht, Y. H. Yang, J. D. Johnson and T. J. Kieffer (2014). "Reversal of diabetes with insulin-producing cells derived in vitro from human pluripotent stem cells." Nat Biotechnol **32**(11): 1121-1133.

Rhinn, M. and P. Dolle (2012). "Retinoic acid signalling during development." Development **139**(5): 843-858.

Robinson, M. D., D. J. McCarthy and G. K. Smyth (2010). "edgeR: a Bioconductor package for differential expression analysis of digital gene expression data." Bioinformatics **26**(1): 139-140.

Rodriguez-Diaz, R., R. Dando, M. C. Jacques-Silva, A. Fachado, J. Molina, M. H. Abdulreda, C. Ricordi, S. D. Roper, P. O. Berggren and A. Caicedo (2011). "Alpha cells secrete acetylcholine as a non-neuronal paracrine signal priming beta cell function in humans." Nat Med **17**(7): 888-892.

Romanoski, C. E., V. M. Link, S. Heinz and C. K. Glass (2015). "Exploiting genomics and natural genetic variation to decode macrophage enhancers." Trends Immunol **36**(9): 507-518.

Rossetto, D., N. Avvakumov and J. Cote (2012). "Histone phosphorylation: a chromatin modification involved in diverse nuclear events." Epigenetics **7**(10): 1098-1108.

Rukstalis, J. M. and J. F. Habener (2009). "Neurogenin3 A master regulator of pancreatic islet differentiation and regeneration." Islets **1**(3): 177-184.

Russ, H. A., E. Sintov, L. Anker-Kitai, O. Friedman, A. Lenz, G. Toren, C. Farhy, M. Pasmanik-Chor, V. Oron-Karni, P. Ravassard and S. Efrat (2011). "Insulin-producing cells generated from dedifferentiated human pancreatic beta cells expanded in vitro." PLoS One **6**(9): e25566.

Sander, M., L. Sussel, J. Conners, D. Scheel, J. Kalamaras, F. Dela Cruz, V. Schwitzgebel, A. Hayes-Jordan and M. German (2000). "Homeobox gene Nkx6.1 lies downstream of Nkx2.2 in the major pathway of beta-cell formation in the pancreas." Development **127**(24): 5533-5540.

Schaffer, A. E., K. K. Freude, S. B. Nelson and M. Sander (2010). "Nkx6 transcription factors and Ptf1a function as antagonistic lineage determinants in multipotent pancreatic progenitors." Dev Cell **18**(6): 1022-1029.

Schuldiner, M., O. Yanuka, J. Itskovitz-Eldor, D. A. Melton and N. Benvenisty (2000). "Effects of eight growth factors on the differentiation of cells derived from human embryonic stem cells." Proc Natl Acad Sci U S A **97**(21): 11307-11312.

Schulz, T. C. (2015). "Concise Review: Manufacturing of Pancreatic Endoderm Cells for Clinical Trials in Type 1 Diabetes." Stem Cells Transl Med **4**(8): 927-931.

Schulz, T. C., H. Y. Young, A. D. Agulnick, M. J. Babin, E. E. Baetge, A. G. Bang, A. Bhoumik, I. Cepa, R. M. Cesario, C. Haakmeester, K. Kadoya, J. R. Kelly, J. Kerr, L. A. Martinson, A. B. McLean, M. A. Moorman, J. K. Payne, M. Richardson, K. G. Ross, E. S. Sherrer, X. Song, A. Z. Wilson, E. P. Brandon, C. E. Green, E. J. Kroon, O. G. Kelly, K. A. D'Amour and A. J. Robins (2012). "A scalable system for production of functional pancreatic progenitors from human embryonic stem cells." PLoS One **7**(5): e37004.

Schwitzgebel, V. M., D. W. Scheel, J. R. Conners, J. Kalamaras, J. E. Lee, D. J. Anderson, L. Sussel, J. D. Johnson and M. S. German (2000). "Expression of neurogenin3 reveals an islet cell precursor population in the pancreas." Development **127**(16): 3533-3542.

Seymour, P. A. and M. Sander (2011). "Historical Perspective: Beginnings of the beta-Cell Current Perspectives in beta-Cell Development." Diabetes **60**(2): 364-376.

Seymour, P. A. and M. Sander (2011). "Historical perspective: beginnings of the beta-cell: current perspectives in beta-cell development." Diabetes **60**(2): 364-376.

Shapiro, A. M., C. Ricordi, B. J. Hering, H. Auchincloss, R. Lindblad, R. P. Robertson, A. Secchi, M. D. Brendel, T. Berney, D. C. Brennan, E. Cagliero, R. Alejandro, E. A. Ryan, B. DiMercurio, P. Morel, K. S. Polonsky, J. A. Reems, R. G. Bretzel, F. Bertuzzi, T. Froud, R. Kandaswamy, D. E. Sutherland, G. Eisenbarth, M. Segal, J. Preiksaitis, G. S. Korbutt, F. B. Barton, L. Viviano, V. Seyfert-Margolis, J. Bluestone and J. R. Lakey (2006). "International trial of the Edmonton protocol for islet transplantation." N Engl J Med **355**(13): 1318-1330.

Shen, Y., F. Yue, D. F. McCleary, Z. Ye, L. Edsall, S. Kuan, U. Wagner, J. Dixon, L. Lee, V. V. Lobanenkov and B. Ren (2012). "A map of the cis-regulatory sequences in the mouse genome." Nature **488**(7409): 116-120.

Shi, Y., F. Lan, C. Matson, P. Mulligan, J. R. Whetstine, P. A. Cole, R. A. Casero and Y. Shi (2004). "Histone demethylation mediated by the nuclear amine oxidase homolog LSD1." Cell **119**(7): 941-953.

Shih, H. P., A. Wang and M. Sander (2013). "Pancreas organogenesis: from lineage determination to morphogenesis." Annu Rev Cell Dev Biol **29**: 81-105.

Shlyueva, D., G. Stampfel and A. Stark (2014). "Transcriptional enhancers: from properties to genome-wide predictions." Nat Rev Genet **15**(4): 272-286.

Shogren-Knaak, M., H. Ishii, J. M. Sun, M. J. Pazin, J. R. Davie and C. L. Peterson (2006). "Histone H4-K16 acetylation controls chromatin structure and protein interactions." Science **311**(5762): 844-847.

Simandi, Z., B. L. Balint, S. Poliska, R. Ruhl and L. Nagy (2010). "Activation of retinoic acid receptor signaling coordinates lineage commitment of spontaneously differentiating mouse embryonic stem cells in embryoid bodies." FEBS Lett **584**(14): 3123-3130.

Storvall, H., D. Ramskold and R. Sandberg (2013). "Efficient and comprehensive representation of uniqueness for next-generation sequencing by minimum unique length analyses." PLoS One **8**(1): e53822.

Su, S. T., H. Y. Ying, Y. K. Chiu, F. R. Lin, M. Y. Chen and K. I. Lin (2009). "Involvement of histone demethylase LSD1 in Blimp-1-mediated gene repression during plasma cell differentiation." Mol Cell Biol **29**(6): 1421-1431.

Sun, G., K. Alzayady, R. Stewart, P. Ye, S. Yang, W. Li and Y. Shi (2010). "Histone demethylase LSD1 regulates neural stem cell proliferation." Mol Cell Biol **30**(8): 1997-2005.

Takahashi, K. and S. Yamanaka (2006). "Induction of pluripotent stem cells from mouse embryonic and adult fibroblast cultures by defined factors." Cell **126**(4): 663-676.

Tan, M., H. Luo, S. Lee, F. Jin, J. S. Yang, E. Montellier, T. Buchou, Z. Cheng, S. Rousseaux, N. Rajagopal, Z. Lu, Z. Ye, Q. Zhu, J. Wysocka, Y. Ye, S. Khochbin, B. Ren and Y. Zhao (2011). "Identification of 67 histone marks and histone lysine crotonylation as a new type of histone modification." Cell **146**(6): 1016-1028.

Taylor, B. L., F. F. Liu and M. Sander (2013). "Nkx6.1 is essential for maintaining the functional state of pancreatic beta cells." Cell Rep **4**(6): 1262-1275.

Thurman, R. E., E. Rynes, R. Humbert, J. Vierstra, M. T. Maurano, E. Haugen, N. C. Sheffield, A. B. Stergachis, H. Wang, B. Vernot, K. Garg, S. John, R. Sandstrom, D. Bates, L. Boatman, T. K. Canfield, M. Diegel, D. Dunn, A. K. Ebersol, T. Frum, E. Giste, A. K. Johnson, E. M. Johnson, T. Kutyavin, B. Lajoie, B. K. Lee, K. Lee, D. London, D. Lotakis, S. Neph, F. Neri, E. D. Nguyen, H. Qu, A. P. Reynolds, V. Roach, A. Safi, M. E. Sanchez, A. Sanyal, A. Shafer, J. M. Simon, L. Song, S. Vong, M. Weaver, Y. Yan, Z. Zhang, Z. Zhang, B. Lenhard, M. Tewari, M. O. Dorschner, R. S. Hansen, P. A. Navas, G. Stamatoyannopoulos, V. R. Iyer, J. D. Lieb, S. R. Sunyaev, J. M. Akey, P. J. Sabo, R. Kaul, T. S. Furey, J. Dekker, G. E. Crawford and J. A. Stamatoyannopoulos (2012). "The accessible chromatin landscape of the human genome." Nature **489**(7414): 75-82.

Trounson, A. and N. D. DeWitt (2016). "Pluripotent stem cells progressing to the clinic." Nat Rev Mol Cell Biol **17**(3): 194-200.

Vosper, J. M., G. S. McDowell, C. J. Hindley, C. S. Fiore-Heriche, R. Kucerova, I. Horan and A. Philpott (2009). "Ubiquitylation on canonical and non-canonical sites targets the transcription factor neurogenin for ubiquitin-mediated proteolysis." J Biol Chem **284**(23): 15458-15468.

Vosper, J. M. D., C. S. Fiore-Heriche, I. Horan, K. Wilson, H. Wise and A. Philpott (2007). "Regulation of neurogenin stability by ubiquitin-mediated proteolysis." Biochemical Journal **407**: 277-284.

Wang, A., F. Yue, Y. Li, R. Xie, T. Harper, N. A. Patel, K. Muth, J. Palmer, Y. Qiu, J. Wang, D. K. Lam, J. C. Raum, D. A. Stoffers, B. Ren and M. Sander (2015). "Epigenetic priming of enhancers predicts developmental competence of hESC-derived endodermal lineage intermediates." Cell Stem Cell **16**(4): 386-399.

Wang, J., S. Hevi, J. K. Kurash, H. Lei, F. Gay, J. Bajko, H. Su, W. Sun, H. Chang, G. Xu, F. Gaudet, E. Li and T. Chen (2009). "The lysine demethylase LSD1 (KDM1) is required for maintenance of global DNA methylation." Nat Genet **41**(1): 125-129.

Wang, J., F. Lu, Q. Ren, H. Sun, Z. Xu, R. Lan, Y. Liu, D. Ward, J. Quan, T. Ye and H. Zhang (2011). "Novel histone demethylase LSD1 inhibitors selectively target cancer cells with pluripotent stem cell properties." Cancer Res **71**(23): 7238-7249.

Wang, J., K. Scully, X. Zhu, L. Cai, J. Zhang, G. G. Prefontaine, A. Krones, K. A. Ohgi, P. Zhu, I. Garcia-Bassets, F. Liu, H. Taylor, J. Lozach, F. L. Jayes, K. S. Korach, C. K. Glass, X. D. Fu and M. G. Rosenfeld (2007). "Opposing LSD1 complexes function in developmental gene activation and repression programmes." Nature **446**(7138): 882-887.

Whyte, W. A., S. Bilodeau, D. A. Orlando, H. A. Hoke, G. M. Frampton, C. T. Foster, S. M. Cowley and R. A. Young (2012). "Enhancer decommissioning by LSD1 during embryonic stem cell differentiation." Nature **482**(7384): 221-225.

Wissmann, M., N. Yin, J. M. Muller, H. Greschik, B. D. Fodor, T. Jenuwein, C. Vogler, R. Schneider, T. Gunther, R. Buettner, E. Metzger and R. Schule (2007). "Cooperative demethylation by JMJD2C and LSD1 promotes androgen receptor-dependent gene expression." Nat Cell Biol **9**(3): 347-353.

Wolffe, A. (2000). Chromatin (Third Edition). Chromatin (Third Edition). London, Academic Press.

Wolffe, A. P. and D. Pruss (1996). "Targeting chromatin disruption: Transcription regulators that acetylate histones." Cell **84**(6): 817-819.

Xie, F., L. Ye, J. Chang, A. Beyer, J. Wang, M. Muench and Y. Kan (2014). "Seamless gene correction of β-thalassemia mutations in patient-specific iPSCs using CRISPR/Cas9 and piggyBac." Genome Research **24**(9): 1526-1533.

Xie, R., L. J. Everett, H. W. Lim, N. A. Patel, J. Schug, E. Kroon, O. G. Kelly, A. Wang, K. A. D'Amour, A. J. Robins, K. J. Won, K. H. Kaestner and M. Sander (2013). "Dynamic chromatin remodeling mediated by polycomb proteins orchestrates pancreatic differentiation of human embryonic stem cells." Cell Stem Cell **12**(2): 224-237.

Xiong, Y., E. Wang, Y. Huang, X. Guo, Y. Yu, Q. Du, X. Ding and Y. Sun (2016). "Inhibition of Lysine-Specific Demethylase-1 (LSD1/KDM1A) Promotes the Adipogenic Differentiation of hESCs Through H3K4 Methylation." Stem Cell Rev **12**(3): 298-304.

Yamanaka, S. (2007). "Strategies and new developments in the generation of patient-specific pluripotent stem cells." Cell Stem Cell **1**(1): 39-49.

Yamanaka, S. and H. M. Blau (2010). "Nuclear reprogramming to a pluripotent state by three approaches." Nature **465**(7299): 704-712.

Zentner, G. E. and P. C. Scacheri (2012). "The chromatin fingerprint of gene enhancer elements." J Biol Chem **287**(37): 30888-30896.

Zentner, G. E., P. J. Tesar and P. C. Scacheri (2011). "Epigenetic signatures distinguish multiple classes of enhancers with distinct cellular functions." Genome Res **21**(8): 1273-1283.

Zhang, Y., B. Schmid, N. K. Nikolaisen, M. A. Rasmussen, B. I. Aldana, M. Agger, K. Calloe, T. C. Stummann, H. M. Larsen, T. T. Nielsen, J. Huang, F. Xu, X. Liu, L. Bolund, M. Meyer, L. K. Bak, H. S. Waagepetersen, Y. Luo, J. E. Nielsen, F. R. Consortium, B. Holst, C. Clausen, P. Hyttel and K. K. Freude (2017). "Patient iPSC-Derived Neurons for Disease Modeling of Frontotemporal Dementia with Mutation in CHMP2B." Stem Cell Reports.

Zibetti, C., A. Adamo, C. Binda, F. Forneris, E. Toffolo, C. Verpelli, E. Ginelli, A. Mattevi, C. Sala and E. Battaglioli (2010). "Alternative splicing of the histone demethylase LSD1/KDM1 contributes to the modulation of neurite morphogenesis in the mammalian nervous system." J Neurosci **30**(7): 2521-2532.

Chapter 15
Pancreatic Differentiation from Human Pluripotent Stem Cells

Nicholas Vinckier, Jinzhao Wang, and Maike Sander

Abstract The ability to produce human pancreatic cells *in vitro* would open new possibilities for developing improved therapies through cell transplantation, disease modeling, and drug screening. Of particular medical importance are the insulin-producing beta cells of the pancreas, which are lost or dysfunctional in diabetes. Furthermore, an *in vitro* model of human exocrine cells could help devise new therapies for pancreatic exocrine disease, most notably pancreatic cancer. In the past decade much progress has been made in developing protocols to generate multipotent pancreatic progenitor cells from human pluripotent stem cells (hPSCs) that are capable of differentiating into both endocrine and exocrine cells. The sole approach that has proven successful is to reproduce essential steps of *in vivo* development *in vitro* through directed step-wise differentiation of hPSCs. The directed differentiation entails sequential exposure of hPSCs to different signaling factors, thereby moving cells through several developmental intermediates towards the pancreatic fate. Upon implantation into mice, hPSC-derived pancreatic progenitor cells spontaneously differentiate into endocrine and exocrine cells. Here, we describe a detailed protocol for the generation of pancreatic progenitor cells from hPSCs. We provide methods for the directed differentiation as well as the characterization of pancreatic progenitor cells and lineage intermediates by immunofluorescence staining and flow cytometry. With recently developed protocols, these pancreatic progenitor cells can be further differentiated *in vitro* into beta-like cells that functionally resemble immature human beta cells.

Keywords Human pluripotent stem cell (hPSC) • Human embryonic stem cell (hESC) • Definitive endoderm (DE) • Gut tube (GT) • Posterior foregut (FG) • Pancreatic endoderm (PE) • SOX17 • HNF4A • PDX1 • SOX9

N. Vinckier • J. Wang
Departments of Pediatrics and Cellular and Molecular Medicine, Pediatric Diabetes Research Center, University of California San Diego, La Jolla, CA 92093, USA

M. Sander (✉)
Departments of Pediatrics and Cellular and Molecular Medicine, Pediatric Diabetes Research Center, University of California San Diego, La Jolla, CA 92093, USA

Sanford Consortium for Regenerative Medicine,
2880 Torrey Pines Scenic Dr. – Room 3006, La Jolla, CA 92093, USA
e-mail: masander@ucsd.edu

15.1 Introduction

The development of protocols for deriving mature cell types from hPSCs has opened opportunities for modeling human disease *ex vivo* as well as for discovery of novel drugs (Merkle and Eggan 2013). In addition, functional cell types derived from hPSCs could provide an unlimited source to replace tissue cells lost in disease through cell transplantation. hPSC-based cell models are particularly promising in the context of diseases where a single cell type is affected. One such example is diabetes, which is characterized by loss or dysfunction of the insulin-producing beta cells in the pancreas (Nathan 2015). There are two major forms of diabetes, type 1 and type 2 diabetes. While the causes of both types of diabetes are distinct, the manifestation is similar: insufficient production of insulin results in inadequate glucose uptake by peripheral tissues, which in turn leads to elevated blood glucose levels. Type 1 diabetes is caused by autoimmune-mediated beta cell destruction and comprises 5 % of diabetes cases (Cnop et al. 2005). The remaining 95 % of diabetes cases are classified as type 2, and arise due to a combination of insufficient insulin production by the beta cells and insulin resistance of insulin target tissues (Johnson and Luciani 2010; Kahn et al. 2006; Stumvoll et al. 2005). Because both type 1 and type 2 diabetes eventually result in beta cell loss, transplantation of beta cells produced *in vitro* from hPSCs could help normalize blood glucose levels in patients with diabetes. In the pancreas, beta cells reside in so-called islets of Langerhans, where beta cells form functional units with other hormone-producing cells involved in blood glucose regulation, most notably the glucagon-producing alpha cells and somatostatin-producing delta cells. Since there is paracrine signaling between the endocrine cell types within the islet (Caicedo 2013), transplantation of functional islets might be clinically more beneficial than transplanting beta cells alone. There is already precedence that transplantation of cadaveric islets can be curative for diabetes, at least in the short term (Meloche 2007; Robertson et al. 2000). hPSC-derived beta cells or islets could obviate both the limited supply of cadaveric islets and the need for immunosuppression owing to the allogeneic origin of cadaveric islets. In fact, the first clinical trial to determine the safety and efficacy of a hPSC-based islet cell replacement therapy is currently ongoing (ViaCyte 2014). The current clinical trial involves encapsulation of human embryonic stem cell (hESC)-derived multipotent pancreatic progenitor cells in small devices that are implanted subcutaneously. Animal studies have provided proof-of principle that these pancreatic progenitor cells will further differentiate into islet-like structures containing all endocrine cell types when implanted under the skin (Kelly et al. 2011; Kroon et al. 2008; Nostro et al. 2015; Rezania et al. 2012; Schulz et al. 2012; Xie et al. 2013).

While beta cell loss is the hallmark of type 1 diabetes, type 2 diabetes, at least in its early stages, is characterized by beta cell dysfunction rather than destruction. Type 2 diabetes has a strong genetic component; yet how genetic risk factors cause beta cell dysfunction remains largely unknown. While mouse models have provided important insight into the regulation of insulin production and secretion, comparisons between mouse models of diabetes and the human disease have also revealed species differences. One condition that exemplifies such differences is a monogenetic

form of type 2 diabetes, called maturity onset diabetes of the young (MODY). In humans, inheritance of one mutant allele is sufficient to cause MODY, whereas mice carrying the same heterozygous mutation do not acquire the disease (Haumaitre et al. 2006; Lee et al. 1998; Mayer et al. 2008; Yamagata et al. 1996). *In vitro*-generated beta cells and their precursors would provide a powerful model to study how MODY-associated gene mutations cause diabetes. With recent breakthroughs in genome editing technologies, known mutations, like those seen in MODY, could be introduced into hPSCs and beta cell differentiation and function could be analyzed *in vitro*. Alternatively, induced hPSCs could be derived from MODY patients to create patient-specific disease models. Similar strategies could be implemented to determine how genetic variants, identified via genome-wide association studies, affect beta cell development and/or function and cause disease.

A scalable differentiation system for human beta cells or islets would also provide an ideal drug-screening platform. In addition to enabling new drug discovery, such a system could help customize diabetes treatment in a patient-specific manner. It is known that not all patients with type 2 diabetes respond similarly to existing anti-diabetic drugs (Standl and Fuchtenbusch 2003). Responsiveness to different drugs could be tested by deriving induced hPSCs from patients and producing patient-specific beta cells or islets *in vitro*. In the long term, the collective data from such experiments might allow us to predict drug responsiveness based on the absence or presence of specific genetic markers, as already used to predict responsiveness to cancer therapy.

The past decade has seen remarkable progress in the development of protocols to generate pancreatic cells from hPSCs (Mfopou et al. 2010; Pagliuca and Melton 2013). Multiple differentiation protocols aimed at deriving pancreatic progenitors and beta cells have been published with mounting levels of success. The underlying principle of all successful approaches is to closely mimic embryonic development *in vitro*. Efficacious protocols have taken a step-wise approach in which cells are guided through defined developmental stages by sequential exposure to the growth factors that are also relevant during *in vivo* development. Earlier protocols yielded insulin-expressing cells *in vitro* that were not functional, expressed multiple hormones, and failed to restore blood glucose levels when implanted into diabetic mice (D'Amour et al. 2006; Kelly et al. 2011; Kroon et al. 2008; Nostro et al. 2011; Rezania et al. 2012). In contrast, when pancreatic progenitor cells were implanted into mice, the implants rescued diabetes within ~16 weeks after implantation (Kroon et al. 2008; Nostro et al. 2015; Rezania et al. 2012; Schulz et al. 2012). During this time, the progenitors differentiate into islet-like structures, containing mature functional beta cells as well as other endocrine cell types. A small fraction of pancreatic progenitors also differentiates into exocrine acinar and ductal cells after implantation (Kroon et al. 2008; Xie et al. 2013).

Here, we present a step-wise protocol for the generation of pancreatic progenitor cells by directed differentiation of hESCs. The protocol was adapted from several previously published protocols (Schulz et al. 2012; Rezania et al. 2013, 2014). The protocol is optimized for the H1 hESC line from WiCell (WiCell Research Institute, WA01) and employs a planar culture system in which the cells are adhered to Matrigel-coated tissue culture plates throughout differentiation. Recently, protocols have been published

that report strategies to further differentiate hPSC-derived pancreatic progenitor cells into functional beta-like cells entirely *in vitro* (Pagliuca et al. 2014; Rezania et al. 2014; Russ et al. 2015). After implantation into diabetic mice, these beta-like cells lead to normalization of blood glucose levels within 2 weeks.

15.2 Materials

15.2.1 Cell Culture Supplies and Equipment

- Biological safety cabinet.
- CO_2 incubator capable of maintaining 5 % CO_2 and >95 % humidity at 37 °C.
- 37 °C water bath.
- Sterile plastic tissue culture treated cell culture dishes:
  - 6-Well plate; 9.5 cm^2 cell growth area (Corning, Cat. No. 3516).
  - 12-Well plate; 3.8 cm^2 cell growth area (Corning, Cat. No. 3513).
  - 10 cm plate; 56.5 cm^2 cell growth area (Corning, Cat. No. 351029).
- Sterile ultra-low attachment 6-well plates (Corning, Cat. No. 3471), for alternative suspension culture (see *Sect. 15.3.5* and ***Note 5***).
- Cell lifter/scraper (VWR, Cat. No. 3008).
- Hemocytometer or other cell counting tool.
- Sterile 15 ml conical tubes.
- Benchtop centrifuge capable of spinning 15 ml conical tubes.
- Sterile 1.5 ml microcentrifuge tubes.
- Benchtop microcentrifuge capable of spinning 1.5 ml microcentrifuge tubes.
- Serological pipette controller and 10 ml sterile pipettes.
- 2, 20, 200, and 1000 µl pipettes and accompanying sterile pipette tips.
- Stericup-GP, 0.22 µm, polyethersulfone, 500 ml, radio-sterilized vacuum filters (Millipore, SCGPU05RE).
- Falcon 5 ml round bottom polystyrene test tube with cell strainer snap cap (Corning, Cat. No. 352235).
- Inverted light microscope (Zeiss Axio Vert or equivalent).
- Inverted fluorescence microscope (Zeiss Axio Observer or equivalent).
- Flow cytometer (BD FACSCanto™ or equivalent).

15.2.2 Reagents

- Matrigel Growth Factor Reduced Basement Membrane Matrix (Corning, Cat. No. 356231).
- RHO/ROCK Pathway Inhibitor Y-27632 (StemCell, Cat. No. 72307).
- TrypLE™ Express Enzyme (Life Technologies, Cat. No. 12604-021).

- Accutase (eBioscience, Cat. No. 00-4555-56).
- Sterile DPBS (Dulbecco's Phosphate Buffered Saline) without Ca^{2+} and Mg^{2+} (VWR, Cat. No. 45000-434).
- DMEM/F12 50:50 mix without glutamine (VWR, Cat. No. 45000-346).
- Bovine Serum Albumin (BSA) Fraction V (7.5 % solution) (Life Technologies, Cat. No. 15260-037), for alternative suspension culture (see *Sect. 15.3.5* and ***Note 6***).
- Reagent Grade BSA—pH 7.0, >98 % purity (Lampire Biological Laboratories, Cat. No. 7500804), for use in differentiation media.
- H1 hESC line (WiCell Research Institute, WA01). Other hPSC lines may be used, but may require further optimization.
- Essential 8 (E8) pluripotency maintenance medium (Life Technologies, Cat. No. A1517001). The E8 culture medium is a xeno-free pluripotency maintenance medium (Chen et al. 2011) used here for feeder-free growth and expansion of hESCs.
- MCDB 131 cell culture medium (Life Technologies, Cat. No. 10372-019). The MCDB 131 medium is used here as the base medium throughout differentiation and is supplemented with different components and factors depending on the stage of differentiation. See *Sect. 15.2.3* for proper stage-specific base-medium formulations and Table 15.1 for additional factors to be added on each day of differentiation.
- Supplements and factors used for endocrine differentiation:
  - Sodium bicarbonate ($NaHCO_3$) (Sigma, Cat. No. S6297).
  - Recombinant Activin A (AA) (R&D Systems, Cat. No. 338-AC/CF).
  - Recombinant Wnt-3a (R&D Systems, Cat. No. 1324-WN/CF).
  - GlutaMAX (Life Technologies, Cat. No. 35050061).
  - BSA (Fisher, Cat. No. 7500804).
  - L-Ascorbic Acid (Vitamin C, VIT-C) (Sigma, Cat. No. A4544).
  - Recombinant KGF/FGF-7 (R&D Systems, Cat. No. 251-KG/CF).
  - D-Glucose (Fisher Scientific, Cat. No. D161).
  - Retinoic Acid (RA) (Sigma, Cat. No. R2625).
  - LDN193189 (Stemgent, Cat. No. 04-0074).
  - ITS-X (Life Technologies, Cat. No. 51500056).
  - SANT-1 (Sigma, Cat. No. S4572).
  - TPB (EMD Millipore, Cat. No. 565740).
- Cell fixation solution for immunofluorescence (IF) analysis: 4 % paraformaldehyde (PFA) (96 % extra pure, Acros Organics, Cat. No. 41678) in DPBS.
- Cell permeabilization and blocking buffer for IF analysis: 0.15 % Triton X-100 (Fisher, Cat. No. BP151) and 1 % donkey serum (Gemini Bio-Products, Cat. No. 100-151) in DPBS.
- Superfrost Plus microscope slides (Fisher Scientific, Cat. No. 12-550-15).
- VECTASHIELD Antifade mounting medium (Vector Laboratories, Cat. No. H-1000).
- FACS buffer: 0.2 % (w/v) BSA (Lampire, Cat. No. 7500804) in DPBS, keep at 2–8 °C.
- BD fixation/permeabilization solution (BD Biosciences, Cat. No. 554714) for flow cytometry analysis, keep at 2–8 °C.

Table 15.1 Medium formulations used for each day of differentiation. See *Sect. 15.2.3* for stage-specific base-medium formulations

Day	Base medium	Added factors
1	Stage 1 medium	100 ng/ml activin A 25 ng/ml Wnt-3a
2–3	Stage 1 medium	100 ng/ml activin A
4–5	Stage 2 medium	0.25 mM VIT-C 50 ng/ml FGF7
6–7	Stage 3 medium	0.25 mM VIT-C 50 ng/ml FGF7 0.25 μM SANT-1 1 μM retinoic acid 100 nM LDN193189 1:200 ITS-X 200 nM TPB
8–10	Stage 4 medium	0.25 mM VIT-C 2 ng/μl FGF7 0.25 μM SANT-1 0.1 μM retinoic acid 200 nM LDN193189 1:200 ITS-X 100 nM TPB

The same base media formulations and factors are used for either adherent cultures or suspension cultures

- BD perm/wash buffer (BD Biosciences, Cat. No. 554723) for flow cytometry analysis, keep at 2–8 °C.

15.2.3 Stage-Specific Medium Formulations

The supplements listed below are stable in the MCDB 131 medium for 1 month if kept at 2–8 °C. Because sodium bicarbonate ($NaHCO_3$) and BSA are supplied as a non-sterile powder, the medium must be sterile filtered (0.22 μm vacuum filter) after $NaHCO_3$ and BSA are added.

Stage 1 Medium

- MCDB 131 medium.
- 1.5 g/l $NaHCO_3$.
- 1× GlutaMAX.
- 10 mM D-Glucose (final concentration; MCDB 131 already contains 5.55 mM).
- 0.5 % BSA.

Stage 2 Medium

- MCDB 131 medium.
- 1.5 g/l $NaHCO_3$.
- 1× GlutaMAX.
- 10 mM D-Glucose (final concentration; MCDB 131 already contains 5.55 mM).
- 0.5 % BSA.

Stage 3/4 Medium

- MCDB 131 medium.
- 2.5 g/l $NaHCO_3$.
- 1× GlutaMAX.
- 10 mM D-glucose (final concentration; MCDB 131 already contains 5.55 mM).
- 2 % BSA.

15.2.4 Antibodies Used for Cell Characterization

Primary Antibodies for Flow Cytometry

- Mouse anti-SOX17-PE (1:20, BD Biosciences, Cat. No. 561591).
- Mouse anti-PDX1-PE (1:20, BD Biosciences, Cat. No. 562161).
- Mouse anti-NKX6.1-Alexa Fluor 647 (1:20, BD Biosciences, Cat. No. 563338).
- Rabbit anti-SOX9 (1:50, Millipore, Cat. No. AB5535).
- Mouse anti-IgG1, κ-PE isotype control (1:20, BD Biosciences, Cat. No. 556650).
- Mouse anti-IgG1, κ-Alexa Fluor 647 isotype control (1:20, BD Biosciences, Cat. No. 557732).

Secondary Antibodies for Flow Cytometry

- Donkey anti-rabbit IgG-PE (1:20, eBioscience, Cat. No. 12-4739-81).

Primary Antibodies for Immunofluorescence

- Goat anti-SOX17 (1:1000, R&D Systems, Cat. No. AF1924).
- Rabbit anti-OCT4 (1:1000, Cell Signaling Technology, Cat. No. 2840).
- Rabbit anti-HNF4A (1:500, Santa Cruz, Cat. No. SC-6556).
- Rabbit anti-SOX9 (1:1000, Millipore, Cat. No. AB5535).
- Goat anti-PDX1 (1:500, Abcam, Cat. No. ab47383).
- Mouse anti-NKX6.1 (1:300, Developmental Studies Hybridoma Bank, Cat. No. F55A10).

Secondary Antibodies for Immunofluorescence

- Donkey anti-goat Cy3 (1:1000, Jackson Immuno, Cat. No. 705-165-147).
- Donkey anti-rabbit Cy3 (1:1000, Jackson Immuno, Cat. No. 711-165-152).
- Donkey anti-goat Alexa Fluor 488 (1:1000, Jackson Immuno, Cat. No. 705-545-147).

15.3 Methods

Cell culture and passaging of hESCs

Proper handling and preparation of hESCs is important to ensure successful and efficient differentiation. The protocol is optimized for H1 cells, which can be obtained from WiCell Research Institute (WA01). Below are the recommended methods for proper culture and expansion of H1 cells prior to differentiation.

15.3.1 Preparation of Matrigel-Coated Tissue Culture Dishes

Expansion is performed in 6-well plates and differentiation in 12-well plates. If different sizes of culture dishes are desired, adjust volumes as necessary.

1. Thaw Matrigel on ice and keep cold at all times;
2. Following the manufacturer's instructions dilute Matrigel in the appropriate volume of cold DMEM/F12 medium and keep on ice. The dilution used in this protocol is 1:100, but may vary from lot to lot. Unused diluted Matrigel can be stored at 2–8 °C, but should be used within 2 weeks from the time of dilution;
3. Load diluted Matrigel into each well of the tissue culture plate to be used. Ensure there is sufficient volume to completely cover the entire well surface (~2 ml per well of a 6-well plate and ~1 ml per well of a 12-well plate);
4. Incubate the plate at 37 °C for 30 min before use.

15.3.2 Culturing hESCs

1. Aspirate excess Matrigel from pre-coated plates before seeding cells;
2. Thaw frozen cells in 37 °C water bath until just a small amount of ice is left in the vial;
3. Wash cells by resuspending in ~5 ml of E8 medium and spin at $200 \times g$ for 4 min at room temperature;
4. Aspirate supernatant carefully to not disrupt the cell pellet;
5. Resuspend cells in E8 medium ($\sim 5 \times 10^5$ cells/ml) containing freshly added ROCK inhibitor (10 μM);
6. Add 2 ml cell suspension per well of the Matrigel-coated 6-well plate and place in a 37 °C incubator at 5 % CO_2;
7. Replace medium with fresh E8 medium (w/o ROCK inhibitor) every 24 h;
8. Cells are passaged at ~80 % confluency.

15.3.3 Passaging hESCs with TrypLE

1. Aspirate medium from wells and wash with DPBS without Ca^{2+} and Mg^{2+};
2. Aspirate DPBS and load 0.5–1 ml of room temperature TrypLE in each well and incubate at 37 °C for 1 min;

3. After 1 min examine cells under a microscope to ensure sufficient detachment from plate. Cells should appear balled up at the edges of colonies, but not free-floating. If more time is required for cell detachment, place cells back in 37 °C and examine under microscope every 1 min until cells are sufficiently detached (see ***Note 1***);
4. Stop enzymatic reaction by adding 4 volumes of E8 medium;
5. Use a cell scraper to lift cell clusters off plate;
6. Use a serological pipette to transfer the cell suspension into sterile 15 ml conical tubes;
7. Centrifuge for 4 min at 200 × *g* to pellet cells;
8. Aspirate media and resuspend cells in appropriate volume of E8 medium containing 10 μM ROCK inhibitor (Y-27632) to achieve desired dilution (see ***Note 2***);
9. Add 2 ml of cell suspension per well of a Matrigel-coated 6-well plate;
10. Replace medium with fresh E8 medium (w/o ROCK inhibitor) every 24 h.

15.3.4 Cell Differentiation

We describe a step-wise protocol for the directed differentiation of H1 hESCs into pancreatic progenitor cells, which we refer to as pancreatic endoderm (Fig. 15.1). During *in vitro* differentiation, the cells progress through different lineage intermediates, resembling cell populations found in the developing embryo. The first step is the differentiation to definitive endoderm, from which endodermal organs, such as liver, lungs, thymus, intestine, and pancreas are derived (Wells and Melton 1999). In subsequent steps, definitive endoderm cells are directed to acquire primitive gut tube, posterior foregut, and finally pancreatic endoderm identity. Expression of early pancreatic transcription factors, such as PDX1 and SOX9, is observed as early as the end of the

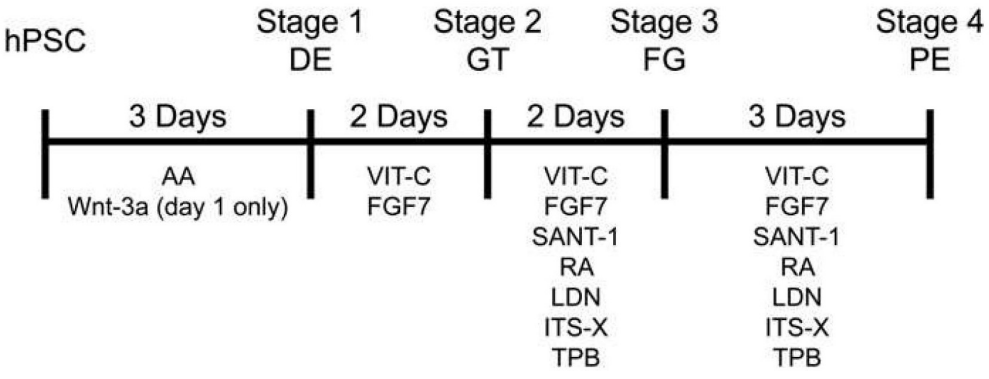

Fig. 15.1 Schematic outlining the protocol for differentiation of human pluripotent stem cells into pancreatic progenitor cells (pancreatic endoderm). The duration of each differentiation step and the required factors are depicted. Exact concentrations of factors and medium composition can be found in *Sects. 15.2.2* and *15.2.3*. *hPSC* human pluripotent stem cell, *DE* definitive endoderm, *GT* primitive gut tube, *FG* posterior foregut, *PE* pancreatic endoderm, *AA* activin A, *VIT-C* vitamin C, *RA* retinoic acid

posterior foregut stage. When implanted subcutaneously or under the kidney capsule into mice, pancreatic endoderm differentiates into fully functional beta cells, other endocrine cell types, as well as a small percentage of pancreatic ductal cells (Kelly et al. 2011; Kroon et al. 2008; Rezania et al. 2013; Schulz et al. 2012; Xie et al. 2013). The *in vivo* differentiation and maturation process of implanted pancreatic endoderm takes ~16 weeks, regardless of the protocol and cell line used to generate pancreatic endoderm. Although the application of the protocol we describe is not limited to H1 hESCs, when other hPSC lines are used, the protocol needs to be adapted to achieve similar differentiation efficiencies as observed with H1 hESCs. Key variables include the concentration of the factors and the duration of each differentiation step.

15.3.4.1 Preparation of Coverslips for Culturing hESCs

Optional: If analysis will be performed later, it is necessary to load coverslips into the culture dish wells prior to coating with Matrigel. To prepare coverslips for culturing hESCs follow the procedure below, otherwise continue with the next Section.

1. Put coverslips into a sterile 10 cm petri dish with lid;
2. Pour enough 70 % ethanol into the dish to completely submerge all coverslips and place the lid on the petri dish;
3. Allow coverslips to soak in 70 % ethanol overnight;
4. The following day, aspirate 70 % ethanol and replace it with 100 % ethanol, ensuring all coverslips are submerged;
5. Allow coverslips to soak for 5 min;
6. Aspirate 100 % ethanol and replace it with fresh 100 % ethanol, again submerging all coverslips;
7. Allow coverslips to soak for 5 min;
8. Place petri dish lid upside down inside the biological safety cabinet;
9. Using sterilized tweezers, remove coverslips from 100 % ethanol and place inside the inverted lid;
10. Lean each coverslip against the inside wall of the lid at an angle so that both sides of the coverslip are exposed to air;
11. Allow the coverslips to dry completely;
12. Once coverslips have dried, using sterilized tweezers, place one coverslip on the bottom of each well of the 12-well culture dish;
13. Proceed to coat the now sterilized coverslips with Matrigel as previously explained.

15.3.4.2 Seeding hESCs for Differentiation

H1 cells must be plated at an appropriate density before beginning *in vitro* differentiation. Proper starting density will ensure efficient and reproducible differentiations. After expanding cells to reach the desired cell numbers, the cells are passaged

and plated on Matrigel-coated 12-well plates. To allow for accurate counting, the cells must be dissociated into a single cell suspension before seeding wells to prepare for the *in vitro* differentiation.

1. Aspirate medium from wells and rinse with DPBS without Ca^{2+} and Mg^{2+} (~2 ml);
2. Place 0.5–1 ml of room temperature TrypLE in each well and incubate at 37 °C for 3–5 min;
3. After the first 2 min, examine cells under a microscope to ensure sufficient detachment from plate (see ***Note 3***);
4. Continue to incubate cells at 37 °C and examine under microscope every 1 min until cells appear balled and many are free-floating;
5. Stop enzymatic reaction by adding 4 volumes of E8 medium;
6. Use a 1 ml pipette to triturate the detached cells several times to break up remaining clumps, leaving a single-cell suspension (see ***Note 4***);
7. Use a serological pipette to transfer the cell suspension into sterile 15 ml conical tubes;
8. Reserve a small aliquot of cell suspension for cell counting;
9. Centrifuge for 4 min at $200 \times g$ to pellet cells and count cells during centrifugation;
10. Aspirate media and resuspend cells in E8 medium (~3×10^5 cells/ml) containing freshly added ROCK inhibitor (10 μM);
11. Add 1.5 ml of cell suspension per well of a Matrigel-coated 12-well plate;
12. After 24–48 h cells should be roughly 90% confluent and ready to begin *in vitro* differentiation.

15.3.5 Differentiation to Pancreatic Endoderm (Adherent Culture)

Figure 15.1 outlines the step-wise differentiation process and key factors contained in the differentiation medium at each stage of differentiation. Once cells have reached 90% confluency (Fig. 15.2a), the differentiation process can be started. Figure 15.2b shows an example of cells that need to be expanded further before differentiation can be initiated. Stage-specific base-media are stable at 2–8 °C for up to 1 month and can therefore be mixed ahead of time. The formulations for stage-specific base-media are listed in *Sect. 15.2.3*. Table 15.1 shows the final concentrations of the added factors at each day of differentiation. *These factors are not stable at 2–8 °C for long periods of time and must be added to stage-specific base-medium immediately prior to warming the medium on each day of differentiation.*

Described here is a method in which the cells are adhered to 12-well plates in planar culture. However, this protocol can also be performed in suspension culture (Fig. 15.2c), as previously described in detail (Schulz et al. 2012). Suspension culture requires scaling up medium volumes and cell numbers, as well as orbital rotation (see ***Notes 5*** and ***6***).

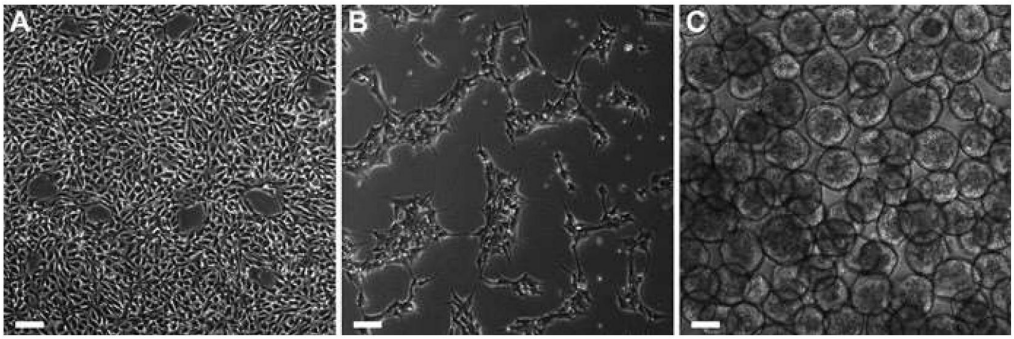

Fig. 15.2 Brightfield images of H1 human embryonic stem cells. H1 cells cultured under adherent conditions (**A**, **B**) or as suspension aggregates (**C**). (**A**) Image showing adherent H1 cells at the correct density to initiate *in vitro* differentiation. (**B**) Image showing cells that are of insufficient density to initiate differentiation. (**C**) Image showing aggregated H1 cells prior to induction of directed differentiation. Scale bars = 50 μM in **A**, **B** and 100 μM in **C**

- **Day 1:** Aspirate E8 medium and wash cells with DPBS without Ca^{2+} and Mg^{2+}.
- To each well add 1.5 ml of prewarmed Stage 1 Medium with freshly added Activin A (100 ng/ml) and Wnt-3a (25 ng/ml);
- **Day 2:** Aspirate medium and replace with 1.5 ml of prewarmed Stage 1 Medium with freshly added Activin A (100 ng/ml);
- **Day 3:** Repeat the previous step. At this point (or the following day) it is recommended to analyze the cells for differentiation efficiency to the definitive endoderm (DE) stage. The success of downstream differentiation is largely dependent upon highly efficient DE induction. Figure 15.3a provides an example of efficient DE induction (data generated using protocols in *Sect. 15.3.6.1*);
- **Day 4:** Aspirate Stage 1 Medium and wash cells with MCDB 131 base medium without added supplements or factors. To each well add 1.5 ml of prewarmed Stage 2 Medium with freshly added L-Ascorbic Acid (VIT-C) (0.25 mM) and FGF7 (50 ng/ml);
- **Day 5:** Repeat the previous step;
- **Day 6:** Aspirate medium and replace with 1.5 ml of fresh, prewarmed Stage 3 Medium with freshly added L-Ascorbic Acid (VIT-C) (0.25 mM), FGF7 (50 ng/ml), SANT-1 (0.25 μM), Retinoic Acid (1 μM), LDN193189 (100 nM), ITS-X (1:200) and TPB (200 nM);
- **Day 7:** Repeat the previous step;
- **Day 8:** Aspirate medium and replace with 1.5 ml of fresh, prewarmed Stage 4 Medium with freshly added L-Ascorbic Acid (VIT-C) (0.25 mM), FGF7 (2 ng/ml), SANT-1 (0.25 μM), Retinoic Acid (0.1 μM), LDN193189 (200 nM), ITS-X (1:200) and TPB (100 nM);
- **Day 9:** Repeat the previous step;
- **Day 10:** Repeat the previous step (same as *Day 8*).

At the end of the differentiation protocol the cells have adopted characteristics of pancreatic progenitor cells. A recent report by Rezania et al. describes a method to further differentiate these H1-derived pancreatic endoderm cells into beta-like cells *in vitro* (Rezania et al. 2014). The method involves culturing the cells in a liquid-air interface after the pancreatic endoderm stage. An alternative method to the liquid-air interface culture is to perform the differentiation into beta-like cells in suspension culture. However, the differentiation efficiency is reported to be lower in suspension culture than in liquid-air interface culture (Rezania et al. 2014). Two other recent reports utilized suspension culture methods to derive beta-like cells, similar to the ones reported by Rezania et al. from hPSC-derived pancreatic endoderm (Pagliuca et al. 2014; Russ et al. 2015).

15.3.6 Cell Characterization

15.3.6.1 Characterization of Cells by Flow Cytometry and Immunofluorescence Analysis

To ensure efficient differentiation, it is important to characterize the cells at various stages throughout the differentiation. Flow cytometry analysis and IF staining for stage-specific proteins are the hallmark methods to assess differentiation efficiencies. Figure 15.3 shows example images of IF analysis as well as flow cytometry plots of stage-specific markers from a successful differentiation. For a complete list of antibodies used for flow cytometry and IF analysis see *Sect. 15.2.4*. Below are recommended protocols for both flow cytometry and IF analysis.

Flow cytometry analysis protocol

1. Thaw Accutase at room temperature or 2–8 °C prior to use;
2. Aspirate medium from each well to be analyzed;
3. Wash cells with DPBS (~1.5 ml per well of 12-well plate) and aspirate;
4. Add enough Accutase® to cover the surface of each well (0.3–0.5 ml per well of 12-well plate);
5. Incubate at 37 °C for 5 min, then check briefly under microscope to ensure cells appear balled up and many are detached. If needed, place back at 37 °C and check every 1 min for good detachment (see ***Note 7***);
6. Add ~1 ml cold FACS buffer (0.2 % BSA in DPBS) to each well (final volume ~1.5 ml) to stop Accutase activity;
7. Using a 1000 µl pipette triturate cells to break up any clumps and obtain a single cell suspension;
8. Label a 5 ml polystyrene tube with cell strainer cap for each sample and add ~250 µl FACS buffer to each cap to pre-wet the cell strainer. Ensure the buffer flows through the cap into the tube;
9. Load each sample into the cap of the appropriately labeled tube and allow the entire suspension to flow through the cell strainer. This will ensure good cell

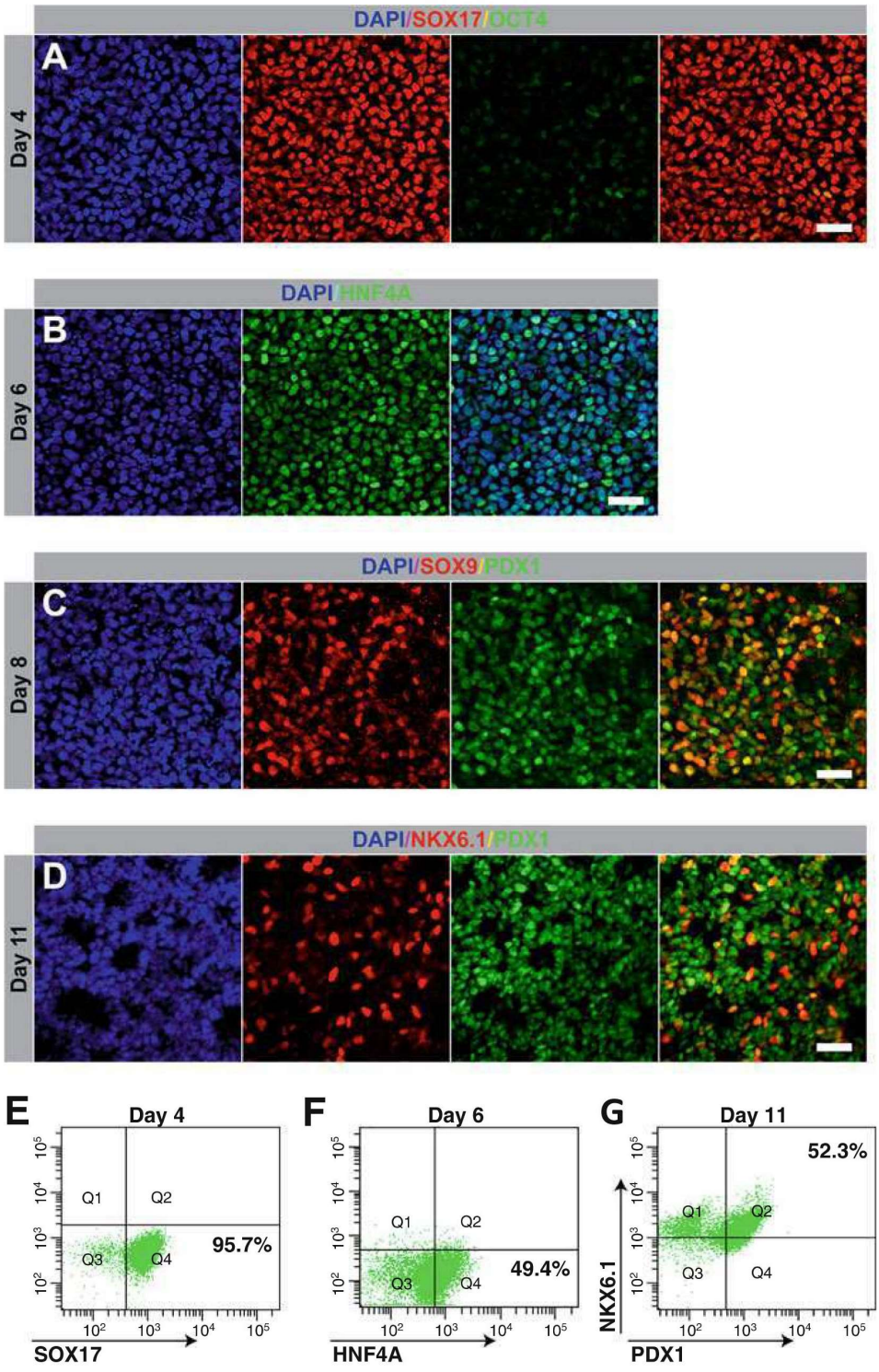

Fig. 15.3 Immunofluorescence staining and flow cytometry analysis of H1 cells throughout pancreatic differentiation. Immunofluorescent staining (**A**–**D**) or flow cytometry analysis (**E**–**G**) for stage-restricted transcription factors in H1 cells at different days of differentiation toward pancreatic endoderm. Day 4 represents definitive endoderm; day 6 primitive gut tube; day 8 posterior foregut; and day 11 pancreatic endoderm. Scale bars = 50 μm

separation, which will provide better flow cytometry results. If the suspension does not easily flow through the cell strainer it may be necessary to pull the sample through. To do so, place the tip of a 1000 µl pipette on the underside of the cell strainer cap containing the sample. Slowly release the pipette plunger to gently pull the sample through the filter top. Carefully eject the sample from the 1000 µl pipette into the bottom of the tube;
10. Transfer the strained cells into new 1.5 ml microcentrifuge tubes and centrifuge at room temperature and 200×*g* for 5 min;
11. Resuspend each cell pellet with cold BD fixation/permeabilization solution (300 µl per tube);
12. Incubate cells for 20 min at 2–8 °C (i.e. refrigerate—*do not place on ice*);
13. Wash cells by adding ~1.1 ml cold 1× BD Perm/Wash™ Buffer to each tube following fixation/permeabilization (1.5 ml per well of 12-well plate) and centrifuge at 10 °C and 200×*g* for 5 min;
14. Aspirate supernatant and repeat *step 11*;
15. Aspirate supernatant and resuspend cells in 50 µl cold 1× BD Perm/Wash Buffer for each staining and isotype control to be used (e.g. add 150 µl total for two different staining samples and one isotype control sample);
16. Aliquot 50 µl of cell suspension into separate microcentrifuge tubes for each individual reaction. Co-staining with PE and AlexaFluor 647 conjugated antibodies can be performed together in one 50 µl aliquot;
17. For analysis of SOX17 expression (DE marker) load 2.5 µl SOX17-PE antibody into one 50 µl cell suspension aliquot. Load 2.5 µl PE isotype into a separate 50 µl cell suspension aliquot to serve as a control;
18. For analysis of PDX1 expression (pancreatic endoderm marker) load 2.5 µl PDX1-PE antibody into one 50 µl cell suspension aliquot. Load 2.5 µl PE isotype into a separate 50 µl cell suspension aliquot to serve as a control;
19. For analysis of NKX6.1 expression (pancreatic endoderm marker) load 2.5 µl NKX6.1-AlexaFluor 647 antibody into one 50 µl cell suspension aliquot. Load 2.5 µl AlexaFluor 647 isotype into a separate 50 µl cell suspension aliquot to serve as a control;
20. After the antibodies and matching isotypes have been loaded into cell suspensions, incubate cells in the dark for 1 h at 2–8 °C (i.e. refrigerate—*do not place on ice*);
21. Wash cells by adding 1.25 ml cold 1× BD Wash Buffer to each tube and centrifuge at room temperature and 200×*g* for 5 min;
22. Aspirate supernatant and resuspend each sample in 300 µl cold FACS buffer;
23. The samples are now stained and ready for analysis on a flow cytometer, such as the FACSCanto used to generate the plots in Fig. 15.3.

Immunofluorescence analysis protocol

1. Aspirate medium from each well to be analyzed;
2. Wash cells with DPBS (~1.5 ml per well of 12-well plate) and aspirate;
3. Repeat *step 2*;
4. Add 1 ml of 4 % PFA to each well and incubate at 2–8 °C overnight;
5. The following day, aspirate PFA and wash with DPBS (~1.5 ml per well of 12-well plate);

6. Aspirate DPBS and add 1 ml of blocking buffer (0.15% Triton X-100, 1% normal donkey serum in DPBS) and incubate at room temperature for 1 h;
7. Prepare primary antibody solutions by mixing appropriate volumes of each antibody in blocking buffer (1 ml per well of a 12 well plate) and vortex gently. See *Sect. 15.2.4* for appropriate working dilutions. For example, to analyze SOX17 expression, add 1 µl of goat anti-SOX17 antibody to 1 ml of blocking buffer;
8. Aspirate buffer from each well and load 1 ml of pre-mixed primary antibody solution to the appropriate wells and incubate at 2–8 °C overnight;
9. The following day, aspirate antibody solution and wash with DPBS (~1.5 ml per well of 12-well plate);
10. Aspirate DPBS and repeat *step 9* three times;
11. Prepare secondary antibody solutions by mixing appropriate volumes of each antibody in blocking buffer (1 ml per well of 12 well plate) and vortex gently. See *Sect. 15.2.4* for appropriate working dilutions;
12. Aspirate DPBS from each well and add 1 ml of pre-mixed secondary antibody solution to the appropriate wells and incubate at room temperature for 1 h in the dark;
13. Aspirate antibody solution and wash with DPBS (~1.5 ml per well of 12-well plate);
14. Prepare nuclear staining solution by mixing Hoescht 33342 in DPBS (1:3000, 1 ml per well of 12-well plate);
15. Aspirate DPBS from each well and add 1 ml of nuclear staining solution and incubate at room temperature for 5 min in the dark;
16. Aspirate nuclear staining solution and wash with DPBS (~1.5 ml per well of 12-well plate);
17. Aspirate DPBS and wash once more with DPBS (~1.5 ml per well of 12-well plate);
18. The coverslips containing stained cells are now ready to be mounted on slides. Gently remove coverslips with tweezers and rinse by briefly dipping each coverslip into distilled water;
19. Allow fluid to run off the coverslip and remove excess fluid by blotting the edge of the coverslip with a paper towel. Capillary action should help remove the excess;
20. Place one drop of VECTASHIELD Antifade Mounting Medium (or desired mounting solution) on the coverslip on the side containing the cells;
21. Gently invert coverslip while placing it cell side down on a slide. Be careful to avoid any air bubbles between the slide and coverslip;
22. Seal the edges of the coverslip to the slide with clear nail polish and allow it to fully dry in the dark before analyzing the slides. The nail polish prevents the slides from drying out if stored for extended periods of time;
23. The slide containing the coverslip with the stained cells is now ready to be analyzed on an inverted fluorescent microscope, such as the Zeiss Axio Observer used to generate the images in Fig. 15.3;
24. Slides can be stored at 4 °C for short periods of time and at −20 °C for extended periods of time.

15.4 Notes

1. During expansion of H1 cells it is better to passage cells as clusters rather than as a single cell suspension. This will enhance health and survival of the cells.
2. Typical passaging dilutions for expanding H1 cells is 1:6 (i.e. 1 well split into 6 wells).
3. Avoid incubating with TrypLE for longer than necessary as this can reduce cell viability.
4. Avoid excessive pipetting as this can reduce cell viability.
5. *Performing differentiation in suspension culture*—To culture cells in suspension, use ultra-low attachment 6-well plates and rotate on an orbital shaker at 100 rpm. This ensures proper cell aggregation, which is necessary for cell survival and differentiation (Fig. 15.2c). The culture volume is 5.5 ml/well and base media formulations and concentrations of factors are the same as used for differentiation in adherent cultures (Table 15.1). Following expansion and dissociation of hESCs with TrypLE, seed wells with 1×10^6 cells/ml, which is a total of 5.5×10^6 cells/well. Add 10 μM ROCK inhibitor to medium when seeding cells to promote cell survival and aggregation. 48 h following cell seeding the now aggregated cells (Fig. 15.2c) are ready to initiate the *in vitro* differentiation. The differentiation protocol is the same as described for adherent culture, but the volume of culture medium has to be adjusted.
6. *Handling cell aggregates in suspension culture*—A solution of 0.2 % BSA in DPBS should be used to coat pipettes in order to prevent aggregates from adhering to plastic surfaces during medium exchanges. To properly exchange culture medium, draw PBS/BSA solution into the pipette and eject the solution. Swirl the 6-well plate in a circular motion to bring all aggregates to the center. Tilt the plate and draw medium off the side of each well with the pre-coated pipette, removing most of the medium. Leave a very small amount of medium to ensure no aggregates are removed. Load each well with 5.5 ml of the appropriate culture medium for that day. Place the plate back on the orbital shaker at 100 rpm inside a 37 °C incubator.
7. Avoid prolonged exposure to Accutase. Detachment of monolayer H1 cells should occur after 5 min, however if the Accutase has started to become inactive, more time may be necessary. To ensure swift cell detachment use freshly thawed Accutase.

Acknowledgements The authors would like to thank Andrea Carrano and Allen Wang for comments. This work was supported by National Institutes of Health grants (U01-DK089567 and UC4-DK104202), California Institute for Regenerative Medicine grants (RB5-07236 and RB4-06144), and Helmsley Charitable Trust grant 2012PG-T1D074 to M.S. N.V. was supported by the National Cancer Institute Cancer Cell Biology training grant 5T32 CA067754.

References

Caicedo A (2013) Paracrine and autocrine interactions in the human islet: more than meets the eye. Semin Cell Dev Biol 24:11–21

Chen G, Gulbranson DR, Hou Z, Bolin JM, Ruotti V, Probasco MD, Smuga-Otto K, Howden SE, Diol NR, Propson NE et al (2011) Chemically defined conditions for human iPSC derivation and culture. Nat Methods 8:424–429

Cnop M, Welsh N, Jonas JC, Jorns A, Lenzen S, Eizirik DL (2005) Mechanisms of pancreatic beta-cell death in type 1 and type 2 diabetes: many differences, few similarities. Diabetes 54(Suppl 2):S97–S107

D'Amour KA, Bang AG, Eliazer S, Kelly OG, Agulnick AD, Smart NG, Moorman MA, Kroon E, Carpenter MK, Baetge EE (2006) Production of pancreatic hormone-expressing endocrine cells from human embryonic stem cells. Nat Biotechnol 24:1392–1401

Haumaitre C, Fabre M, Cormier S, Baumann C, Delezoide AL, Cereghini S (2006) Severe pancreas hypoplasia and multicystic renal dysplasia in two human fetuses carrying novel HNF1beta/MODY5 mutations. Hum Mol Genet 15:2363–2375

Johnson JD, Luciani DS (2010) Mechanisms of pancreatic beta-cell apoptosis in diabetes and its therapies. Adv Exp Med Biol 654:447–462

Kahn SE, Hull RL, Utzschneider KM (2006) Mechanisms linking obesity to insulin resistance and type 2 diabetes. Nature 444:840–846

Kelly OG, Chan MY, Martinson LA, Kadoya K, Ostertag TM, Ross KG, Richardson M, Carpenter MK, D'Amour KA, Kroon E et al (2011) Cell-surface markers for the isolation of pancreatic cell types derived from human embryonic stem cells. Nat Biotechnol 29:750–756

Kroon E, Martinson LA, Kadoya K, Bang AG, Kelly OG, Eliazer S, Young H, Richardson M, Smart NG, Cunningham J et al (2008) Pancreatic endoderm derived from human embryonic stem cells generates glucose-responsive insulin-secreting cells in vivo. Nat Biotechnol 26:443–452

Lee YH, Sauer B, Gonzalez FJ (1998) Laron dwarfism and non-insulin-dependent diabetes mellitus in the Hnf-1alpha knockout mouse. Mol Cell Biol 18:3059–3068

Mayer C, Bottcher Y, Kovacs P, Halbritter J, Stumvoll M (2008) Phenotype of a patient with a de novo mutation in the hepatocyte nuclear factor 1beta/maturity-onset diabetes of the young type 5 gene. Metabolism 57:416–420

Meloche RM (2007) Transplantation for the treatment of type 1 diabetes. World J Gastroenterol 13:6347–6355

Merkle FT, Eggan K (2013) Modeling human disease with pluripotent stem cells: from genome association to function. Cell Stem Cell 12:656–668

Mfopou JK, Chen B, Sui L, Sermon K, Bouwens L (2010) Recent advances and prospects in the differentiation of pancreatic cells from human embryonic stem cells. Diabetes 59:2094–2101

Nathan DM (2015) Diabetes: advances in diagnosis and treatment. JAMA 314:1052–1062

Nostro MC, Sarangi F, Ogawa S, Holtzinger A, Corneo B, Li X, Micallef SJ, Park IH, Basford C, Wheeler MB et al (2011) Stage-specific signaling through TGFbeta family members and WNT regulates patterning and pancreatic specification of human pluripotent stem cells. Development 138:861–871

Nostro MC, Sarangi F, Yang C, Holland A, Elefanty AG, Stanley EG, Greiner DL, Keller G (2015) Efficient generation of NKX6-1+ pancreatic progenitors from multiple human pluripotent stem cell lines. Stem Cell Rep 4:591–604

Pagliuca FW, Melton DA (2013) How to make a functional beta-cell. Development 140:2472–2483

Pagliuca FW, Millman JR, Gurtler M, Segel M, Van Dervort A, Ryu JH, Peterson QP, Greiner D, Melton DA (2014) Generation of functional human pancreatic beta cells in vitro. Cell 159:428–439

Rezania A, Bruin JE, Riedel MJ, Mojibian M, Asadi A, Xu J, Gauvin R, Narayan K, Karanu F, O'Neil JJ et al (2012) Maturation of human embryonic stem cell-derived pancreatic progenitors

into functional islets capable of treating pre-existing diabetes in mice. Diabetes 61:2016–2029

Rezania A, Bruin JE, Xu J, Narayan K, Fox JK, O'Neil JJ, Kieffer TJ (2013) Enrichment of human embryonic stem cell-derived NKX6.1-expressing pancreatic progenitor cells accelerates the maturation of insulin-secreting cells in vivo. Stem Cells 31:2432–2442

Rezania A, Bruin JE, Arora P, Rubin A, Batushansky I, Asadi A, O'Dwyer S, Quiskamp N, Mojibian M, Albrecht T et al (2014) Reversal of diabetes with insulin-producing cells derived in vitro from human pluripotent stem cells. Nat Biotechnol 32:1121–1133

Robertson RP, Davis C, Larsen J, Stratta R, Sutherland DE (2000) Pancreas and islet transplantation for patients with diabetes. Diabetes Care 23:112–116

Russ HA, Parent AV, Ringler JJ, Hennings TG, Nair GG, Shveygert M, Guo T, Puri S, Haataja L, Cirulli V et al (2015) Controlled induction of human pancreatic progenitors produces functional beta-like cells in vitro. EMBO J 34:1759–1772

Schulz TC, Young HY, Agulnick AD, Babin MJ, Baetge EE, Bang AG, Bhoumik A, Cepa I, Cesario RM, Haakmeester C et al (2012) A scalable system for production of functional pancreatic progenitors from human embryonic stem cells. PLoS One 7:e37004

Standl E, Fuchtenbusch M (2003) The role of oral antidiabetic agents: why and when to use an early-phase insulin secretion agent in Type II diabetes mellitus. Diabetologia 46(Suppl 1):M30–M36

Stumvoll M, Goldstein BJ, van Haeften TW (2005) Type 2 diabetes: principles of pathogenesis and therapy. Lancet 365:1333–1346

ViaCyte I (2014) ViaCyte, Inc. Announces FDA acceptance of IND to commence clinical trial of VC-01™ candidate cell replacement therapy for type 1 diabetes. [Press release online] http://viacyte.com/press-releases/viacyte-inc-announces-fda-acceptance-of-ind-to-commence-clinical-trial-of-vc-01-candidate-cell-replacement-therapy-for-type-1-diabetes/

Wells JM, Melton DA (1999) Vertebrate endoderm development. Annu Rev Cell Dev Biol 15:393–410

Xie R, Everett LJ, Lim HW, Patel NA, Schug J, Kroon E, Kelly OG, Wang A, D'Amour KA, Robins AJ et al (2013) Dynamic chomatin remodeling mediated by polycomb proteins orchestrates pancreatic differentiation of human embryonic stem cells. Cell Stem Cell 12:224–237

Yamagata K, Furuta H, Oda N, Kaisaki PJ, Menzel S, Cox NJ, Fajans SS, Signorini S, Stoffel M, Bell GI (1996) Mutations in the hepatocyte nuclear factor-4alpha gene in maturity-onset diabetes of the young (MODY1). Nature 384:458–460

ACKNOWLEDGEMENTS

Appendix, in full, is a reprint of material as it appears in Vinckier, Nicholas; Jinzhao, Wang and Sander, Maike. "Pancreatic Differentiation from Human Pluripotent Stem Cells." *Working with Stem Cells*. Ed. Henning Ulrich, Ed. Priscilla Davidson Negraes. Switzerland: Springer International Publishing, 2016. 257-275. The dissertation author was the primary investigator and author of this material.